



University of  
Massachusetts  
Amherst

## Prediction of Emulsion Drop Size Distributions with Population Balance Equation Models to Enable Emulsified Product Design

Item Type	Dissertation (Open Access)
Authors	Maindarkar, Shashank
DOI	<a href="https://doi.org/10.7275/6247197.0">10.7275/6247197.0</a>
Download date	2026-06-09 00:22:05
Link to Item	<a href="https://hdl.handle.net/20.500.14394/19514">https://hdl.handle.net/20.500.14394/19514</a>

**PREDICTION OF EMULSION DROP SIZE  
DISTRIBUTIONS WITH POPULATION BALANCE  
EQUATION MODELS TO ENABLE EMULSIFIED  
PRODUCT DESIGN**

A Dissertation Presented

by

SHASHANK N. MAINDARKAR

Submitted to the Graduate School of the  
University of Massachusetts Amherst in partial fulfillment  
of the requirements for the degree of

DOCTOR OF PHILOSOPHY

February 2015

Chemical Engineering

© Copyright by Shashank N. Maindarkar 2015

All Rights Reserved

**PREDICTION OF EMULSION DROP SIZE  
DISTRIBUTIONS WITH POPULATION BALANCE  
EQUATION MODELS TO ENABLE EMULSIFIED  
PRODUCT DESIGN**

A Dissertation Presented

by

SHASHANK N. MAINDARKAR

Approved as to style and content by:

---

Michael A. Henson, Chair

---

Surita Bhatia, Member

---

David J. McClements, Member

---

John Collura, Interim Department Head  
Chemical Engineering

*To my family.*

## ACKNOWLEDGMENTS

I would like to thank my advisor Michael A. Henson for providing me with the opportunity to work on this project. His valuable advice, guidance, and motivation helped me throughout my work. I would like to thank David J. McClements for his help and insights on the problem and also for allowing me to use instruments in his laboratory. I would also like to thank Surita Bhatia for serving on my committee and for the use her laboratory instruments. I will never forget the help, guidance, and the opportunity of collaboration given by Peter Bongers, who sadly passed away in June 2012. I will always be thankful for our shared memories. I would like to thank Hans Hoogland for actively collaborating with me on this project and for giving me the opportunity to visit Unilever R&D as a graduate research intern.

Family support is the most important even though it is from a distance. My mother and father have been source of motivation for me throughout my studies. I am also grateful to all my friends without whom my stay in Amherst would not have been a fun experience. Special thanks to Neha, Dwaipayana and Harshwardhan who have always helped and supported me whenever I needed. I would also like to thank all my group members, classmates and other members of the chemical engineering department for their support and help in times of difficulties. I am also grateful to Arend Dubbelboer, who made my internship in Vlaardingen, Netherlands a fun learning experience.

I dedicate my thesis to my family. I am here because of them and they will always remain my source of inspiration.

## ABSTRACT

# PREDICTION OF EMULSION DROP SIZE DISTRIBUTIONS WITH POPULATION BALANCE EQUATION MODELS TO ENABLE EMULSIFIED PRODUCT DESIGN

FEBRUARY 2015

SHASHANK N. MAINDARKAR

B.Chem Engg, UNIVERSITY INSTITUTE OF CHEMICAL TECHNOLOGY,  
MUMBAI

Ph.D., UNIVERSITY OF MASSACHUSETTS AMHERST

Directed by: Professor Michael A. Henson

Oil-in-water emulsions are ubiquitous dispersed phase systems with diverse applications in consumer products, processed foods, and the pharmaceutical industry. Emulsion formulation variables and process operating conditions both impact the drop size distribution, a key property that influences emulsion rheology, stability, texture, and appearance. A typical emulsified product requires the drop size distribution to be maintained within acceptable limits. Due to a lack of quantitative understanding, emulsified products are currently manufactured by combining a broad knowledge of previous product formulations with empirical scientific experimentation.

An alternative to trial-and-error experimentation is to utilize a suitable mathematical model to predict the drop size distribution. The population balance equation (PBE) modeling framework particularly is well suited for this problem as size dis-

tribution dynamics can be captured using mechanistic functions for drop breakage and coalescence phenomena which occur during emulsification. This thesis presents a PBE modeling framework for high intensity emulsification processes including high pressure homogenizers and colloid mills. It is demonstrated that by incorporating coalescence phenomenon into PBE model with only breakage functions significantly improves model predictions of emulsion drop size distributions at high oil-to-surfactant ratios. To make the model more realistic, the effect of surface coverage of surfactant molecules is added to the coalescence function which improves the extensibility of the model over different surfactant types. To extend model predictability over a large range of surfactant and oil concentrations, a new drop breakage model is formulated; and to capture the change in emulsion viscosity due to changes in oil and surfactant concentrations, the PBE model is coupled with an experimentally fitted emulsion viscosity model. Furthermore, it is demonstrated that use of a dynamic surface coverage model over an equilibrium model, improves the predictions of drop size distribution in both surfactant rich and surfactant limited regimes.

In this thesis, the PBE model is also utilized to optimally achieve target emulsion drop size distributions by controlling the number of homogenization passes and the pressure of each pass. The model predictions are successfully validated by performing homogenization experiments using the optimal formulation and homogenization variables. Apart from developing models for the high pressure homogenization, this thesis presents a new model for emulsification in colloid mill obtained by formulating new mechanistic breakage frequency and daughter drop distribution functions. The predictions of the new model are significantly better than predictions obtained using models with conventional daughter drop distribution functions.

# TABLE OF CONTENTS

	Page
ACKNOWLEDGMENTS .....	v
ABSTRACT .....	vi
LIST OF TABLES .....	xii
LIST OF FIGURES .....	xiv
 <b>CHAPTER</b>	
<b>1. INTRODUCTION .....</b>	<b>1</b>
1.1 Emulsification .....	2
1.1.1 High Pressure Homogenizer .....	2
1.1.2 Colloid Mills .....	3
1.2 Drop Size Distribution .....	6
1.3 Modeling of Emulsion Formation .....	8
<b>2. INCORPORATING EMULSION DROP COALESCENCE     INTO POPULATION BALANCE EQUATION MODEL OF     HIGH PRESSURE HOMOGENIZATION .....</b>	<b>12</b>
2.1 Introduction .....	12
2.2 Experimental Methods .....	13
2.2.1 Materials .....	13
2.2.2 Emulsion Preparation .....	13
2.2.3 Emulsion Characterization .....	14
2.3 Theory .....	15
2.3.1 Population Balance Equation Model .....	15
2.3.2 PBE Functions .....	16

2.3.3	Dynamic Simulation and Parameter Estimation .....	19
2.4	Results and Discussion .....	20
2.4.1	Parameter Estimation for Base Case Conditions .....	20
2.4.2	Parameter Estimation for Different Pressures and Surfactant Concentrations.....	22
2.4.3	Model Extensibility.....	22
2.4.3.1	Homogenization Pressure.....	23
2.4.3.2	Surfactant Concentration.....	25
2.4.3.3	Surfactant Type .....	27
2.5	Conclusions.....	32
<b>3.</b>	<b>PREDICTING THE EFFECTS OF SURFACTANT     COVERAGE ON DROP SIZE DISTRIBUTIONS OF     HOMOGENIZED EMULSIONS .....</b>	<b>33</b>
3.1	Introduction .....	33
3.2	Experimental Methods .....	34
3.2.1	Materials.....	34
3.2.2	Emulsion Preparation.....	34
3.2.3	Emulsion Characterization.....	34
3.3	Theory.....	35
3.3.1	Population Balance Equation (PBE) .....	35
3.3.1.1	PBE Functions .....	37
3.3.2	Extended PBE Model.....	39
3.3.3	Dynamic Simulation and Parameter Estimation .....	40
3.4	Results and Discussion .....	43
3.4.1	Extensibility for the Surfactant Concentration.....	43
3.4.1.1	Extensibility for the Surfactant Type .....	45
3.5	Conclusions.....	53
<b>4.</b>	<b>PREDICTING THE COMBINED EFFECTS OF OIL AND     SURFACTANT CONCENTRATIONS ON THE DROP SIZE     DISTRIBUTIONS OF HOMOGENIZED EMULSIONS .....</b>	<b>58</b>

4.1	Introduction .....	58
4.2	Experimental Methods .....	59
	4.2.1 Materials.....	59
	4.2.2 Emulsion Preparation and Characterization .....	59
4.3	Theory .....	59
	4.3.1 Population Balance Equation (PBE) .....	59
	4.3.2 Model 1.....	61
	4.3.3 Model 2.....	63
	4.3.4 Model 3.....	67
	4.3.5 Dynamic Simulation and Parameter Estimation .....	69
4.4	Results and Discussion .....	71
	4.4.1 Experimental Results .....	71
	4.4.2 Estimating Surfactant Properties .....	71
	4.4.3 Model Predictions .....	74
	4.4.4 Effect of Oil Concentration .....	77
	4.4.5 Effect of Surfactant Concentration .....	78
4.5	Conclusions .....	80
<b>5.</b>	<b>PREDICTION OF EMULSION DROP SIZE DISTRIBUTIONS</b>	
	<b>IN COLLOID MILLS .....</b>	<b>82</b>
5.1	Introduction .....	82
5.2	Experimental Methods .....	82
	5.2.1 Materials.....	82
	5.2.2 Emulsion Preparation.....	83
	5.2.3 Emulsion Characterization.....	83
5.3	Theory .....	84
	5.3.1 Population Balance Equation (PBE) .....	84
	5.3.2 PBE Functions .....	85
	5.3.3 Emulsion Viscosity Model .....	90
	5.3.4 Dynamic Simulation and Parameter Estimation .....	91
5.4	Results and Discussion .....	93
	5.4.1 Prediction of Emulsion Viscosity .....	93
	5.4.2 Evaluation of Daughter Drop Distribution Functions .....	94
	5.4.3 Effect of Oil Volume Fraction .....	96
	5.4.4 Effect of Flow Rate.....	98

5.4.5	Effect of Rotor Speed .....	100
5.5	Conclusions .....	101
<b>6.</b>	<b>ACHIEVING TARGET EMULSION DROP SIZE DISTRIBUTIONS USING POPULATION BALANCE EQUATION MODELS OF HIGH PRESSURE HOMOGENIZATION .....</b>	<b>104</b>
6.1	Introduction .....	104
6.2	PBE Model Development .....	104
6.2.1	Model Formulation .....	104
6.2.2	Emulsification Experiments .....	108
6.2.3	Parameter Estimation and Model Extensibility .....	108
6.3	Model-Based Design of Homogenizer Operating Conditions .....	111
6.3.1	Optimization Methodology .....	111
6.3.2	Results .....	113
6.4	Conclusions .....	114
<b>7.</b>	<b>CONCLUSIONS AND FUTURE WORK .....</b>	<b>117</b>
7.1	Summary .....	117
7.2	Future work .....	118
 <b>APPENDICES</b>		
<b>A.</b>	<b>COLINEARITY OF THE ADJUSTABLE BREAKAGE AND COALESCENCE PARAMETERS .....</b>	<b>120</b>
<b>B.</b>	<b>DERIVATION OF EQUATIONS OF ADSORBED AND FREE SURFACTANT CONCENTRATION .....</b>	<b>123</b>
 <b>BIBLIOGRAPHY .....</b>		
		<b>126</b>

## LIST OF TABLES

Table	Page
2.1	Base case emulsion formulation and homogenization conditions . . . . . 14
2.2	Minimized objective function values for emulsions consisting of 50wt% oil and 1wt% Pluronic F-68 homogenized at different pressures . . . . . 23
2.3	Minimized objective function values for emulsions homogenized at 800 bar with different oil to surfactant ratios . . . . . 23
2.4	Objective function values at different pressures using optimal parameters $K_1 - K_6$ obtained at one pressure for emulsions consisting of 50wt% oil and 1wt% Pluronic F-68 . . . . . 25
2.5	Objective function values at different pressures using optimal parameters $K_1 - K_6$ obtained at two pressures for emulsions consisting of 50wt% oil and 1wt% Pluronic F-68 . . . . . 25
2.6	Objective function values at different oil to surfactant ratios using optimal parameters $K_1 - K_6$ obtained at one oil to surfactant ratio for emulsions homogenized at 800 bar . . . . . 27
2.7	Objective function values at different oil to surfactant ratios using optimal parameters $K_1 - K_6$ obtained for one surfactant at 50wt% oil and 1wt% surfactant for emulsions homogenized at 800 bar . . . . . 29
3.1	Bulk properties of the emulsion system . . . . . 42
3.2	Surfactant adsorption parameters . . . . . 43
3.3	Summary of model results at different oil-PF68 ratios . . . . . 45
3.4	Summary of model results at different oil-P127 ratios . . . . . 49
3.5	Summary of model results at different oil-PF108 ratios . . . . . 53
3.6	Summary of model results at different oil-PF87 ratios . . . . . 55

4.1	Model equations used for size independent and dependent surfactant adsorption dynamics.....	68
4.2	Bulk properties of the emulsion system.....	70
4.3	Objective function values obtained with the three different PBE models .....	75
5.1	Base case emulsion formulation and homogenization conditions .....	83
5.2	Reynolds numbers for emulsions prepared with different oil weight fractions.....	87
5.3	Daughter drop distribution functions .....	88
6.1	Minimized objective function values at different pressures .....	111
6.2	Model predicted and experimental results for the target $d_{32} = 0.3$ and $PD = 2$ .....	113
6.3	Model predicted and experimental results for the target $\mu = 0.5$ and $\sigma^2 = 0.8$ .....	114
6.4	Model predicted and experimental results for the target $\mu = 0.8$ and $\sigma^2 = 0.8$ .....	115
A.1	Optimized parameters obtained using base model.....	122
A.2	Parameter sensitivity coefficients and measure of parameter colinearity.....	122

## LIST OF FIGURES

Figure	Page
1.1 Schematic representation of (a) high pressure homogenization, (b) drop breakage due to turbulent inertia, (c) drop breakage due to turbulent shear stress. . . . .	4
1.2 (a) Schematic representation of a colloid mill. (b) Different regions of drop breakage (taken from [93]); Region A: end pinching, Region B: bimodal distribution, Region C: uni-modal distribution. Colored lines denote the capillary numbers of emulsions with different oil fractions used in this study. (c) Drop breakage at different viscosity ratios. . . . .	5
1.3 Effect of surfactant concentration and homogenization pressure in: (a),(b) the surfactant limited regime; (c),(d) the energy rich regime; and (e),(f) the transitional regime. P1–P6 and S1–S6 represent increasing homogenization pressures and surfactant concentration, respectively. . . . .	7
2.1 Experimental and model predicted results for the emulsion formulation with 50wt% oil, 1wt% PF-68 homogenized at 800 bar (a)Drop size distributions using PBE model with breakage function only ( $\Psi = 0.1348$ ); (b)Sauter mean diameter using PBE model with breakage function only; (c)Drop size distribution using PBE model with breakage and coalescence functions ( $\Psi = 0.0254$ ); (d)Sauter mean diameter using PBE model with breakage and coalescence functions . . . . .	21
2.2 Experimental and model predicted results for the emulsion formulation with 50wt% oil, 5wt% PF-68 homogenized at 800 bar (a)Drop size distributions using PBE model with breakage function only ( $\Psi = 0.1354$ ); (b)Sauter mean diameter using PBE model with breakage function only; (c)Drop size distribution using PBE model with breakage and coalescence functions ( $\Psi = 0.0325$ ); (d)Sauter mean diameter using PBE model with breakage and coalescence functions . . . . .	24

2.3	Experimental and model predicted drop size distributions, obtained using optimized parameters for the case of 50wt% oil, 1wt% Pluronic F-68 homogenized at 600 bar using PBE model with breakage and coalescence functions, at different pressures (a)200 bar ( $\Psi = 1.284$ ), (b)400 bar ( $\Psi = 0.383$ ), (c)600 bar ( $\Psi = 0.032$ ), (d)800 bar ( $\Psi = 0.236$ ) . . . . .	26
2.4	Experimental and model predicted drop size distributions, obtained using optimized parameters for the base case formulation using PBE model with breakage and coalescence functions, at different oil-surfactant ratios (a)50-0.5 wt% ( $\Psi = 0.4575$ ), (b)50-1wt% ( $\Psi = 0.0254$ ), (c)50-2wt% ( $\Psi = 0.4834$ ), (d)50-5wt% ( $\Psi = 0.2051$ ) . . . . .	28
2.5	Interfacial tension values for different surfactants . . . . .	29
2.6	Experimental and model predicted drop size distributions, obtained using optimized parameters for the case of 50wt% oil, 1wt% Pluronic F127 homogenized at 800 bar using PBE model with breakage and coalescence functions, at different oil-surfactant ratios (a)50-0.5 wt% ( $\Psi = 0.2283$ ), (b)50-1wt% ( $\Psi = 0.0127$ ), (c)50-2wt% ( $\Psi = 0.0530$ ), (d)50-5wt% ( $\Psi = 0.5387$ ) . . . . .	30
2.7	Experimental and model predicted drop size distributions, obtained using optimized parameters for the case of 50wt% oil, 1wt% Tween 60 homogenized at 800 bar using PBE model with breakage and coalescence functions, at different oil-surfactant ratios (a)50-0.5 wt% ( $\Psi = 0.7497$ ), (b)50-1wt% ( $\Psi = 0.0308$ ), (c)50-2wt% ( $\Psi = 0.2539$ ), (d)50-5wt% ( $\Psi = 0.2550$ ) . . . . .	31
3.1	(a) Interfacial tension values (symbols) and model fits (solid lines) for four Pluronic surfactants; and (b) experimental Sauter mean diameters of fifth pass homogenized emulsions obtained with the four surfactants. . . . .	44
3.2	Experimental and model predicted drop size distributions obtained using optimized parameters found at different oil-PF68 ratios with the base model: (a) 50 wt% oil, 0.5 wt% PF68 ( $\Psi = 0.0454$ ), (b) 50 wt% oil, 1.0 wt% PF68 ( $\Psi = 0.0254$ ), (c) 50 wt% oil, 2.0 wt% PF68 ( $\Psi = 0.0376$ ), e(d) Experimental $d_{32}$ values (symbols) and model predicted $d_{32}$ values (solid lines). . . . .	46

3.3	Experimental and model predicted drop size distributions obtained using optimized parameters found at 50 wt% oil, 1 wt% PF68 with the base model: (a) 50 wt% oil, 0.5 wt% PF68 ( $\Psi = 0.4575$ ), (b) 50 wt% oil, 1.0 wt% PF68 ( $\Psi = 0.0254$ ), (c) 50 wt% oil, 2.0 wt% PF68 ( $\Psi = 0.4834$ ), (d) Experimental $d_{32}$ values (symbols) and model predicted $d_{32}$ values (solid lines). . . . .	47
3.4	Experimental and model predicted drop size distributions obtained using optimized parameters found at 50 wt% oil, 1 wt% PF68 with the extended model: (a) 50 wt% oil, 0.5 wt% PF68 ( $\Psi = 0.5434$ ), (b) 50 wt% oil, 1.0 wt% PF68 ( $\Psi = 0.0286$ ), (c) 50 wt% oil, 2.0 wt% PF68 ( $\Psi = 0.4946$ ), (d) Experimental $d_{32}$ values (symbols) and model predicted $d_{32}$ values (solid lines). . . . .	48
3.5	Experimental and model predicted drop size distributions obtained using optimized parameters found at 50 wt% oil, 1 wt% PF127 with the extended model: (a) 50 wt% oil, 0.5 wt% PF127 ( $\Psi = 0.2749$ ), (b) 50 wt% oil, 1.0 wt% PF127 ( $\Psi = 0.0145$ ), (c) 50 wt% oil, 2.0 wt% PF127 ( $\Psi = 0.0768$ ), (d) Experimental $d_{32}$ values (symbols) and model predicted $d_{32}$ values (solid lines). . . . .	50
3.6	Experimental and model predicted drop size distributions obtained using optimized parameters found at 50 wt% oil, 1 wt% PF68 with the base model: (a) 50 wt% oil, 0.5 wt% PF127 ( $\Psi = 2.6046$ ), (b) 50 wt% oil, 1.0 wt% PF127 ( $\Psi = 2.6126$ ), (c) 50 wt% oil, 2.0 wt% PF127 ( $\Psi = 3.4692$ ), (d) Experimental $d_{32}$ values (symbols) and model predicted $d_{32}$ values (solid lines). . . . .	51
3.7	Experimental and model predicted drop size distributions obtained using optimized parameters found at 50 wt% oil, 1 wt% PF68 with the extended model: (a) 50 wt% oil, 0.5 wt% PF127 ( $\Psi = 0.5567$ ), (b) 50 wt% oil, 1.0 wt% PF127 ( $\Psi = 0.1486$ ), (c) 50 wt% oil, 2.0 wt% PF127 ( $\Psi = 0.2824$ ), (d) Experimental $d_{32}$ values (symbols) and model predicted $d_{32}$ values (solid lines). . . . .	52
3.8	Extended model variables as a function of dimensionless time for a dynamic simulation of five homogenizer passes with 50 wt% oil, 1 wt% PF127 using optimized parameters found at 50 wt% oil, 1 wt% PF68: (a) free surfactant concentration and interfacial tension, (b) dimensionless surface coverage $\frac{\Gamma}{\Gamma_{\infty}}$ and coalescence efficiency factor ( $\eta$ ). . . . .	53

3.9	Experimental and model predicted drop size distributions obtained using optimized parameters found at 50 wt% oil, 1 wt% PF68 with the extended model: (a) 50 wt% oil, 0.5 wt% PF108 ( $\Psi = 1.5758$ ), (b) 50 wt% oil, 1.0 wt% PF108 ( $\Psi = 0.6452$ ), (c) 50 wt% oil, 2.0 wt% PF108 ( $\Psi = 0.5477$ ), (d) Experimental $d_{32}$ values (symbols) and model predicted $d_{32}$ values (solid lines). . . . .	54
3.10	Experimental and model predicted drop size distributions obtained using optimized parameters found at 50 wt% oil, 1 wt% PF68 with the extended model: (a) 50 wt% oil, 0.5 wt% PF87 ( $\Psi = 1.2477$ ), (b) 50 wt% oil, 1.0 wt% PF87 ( $\Psi = 0.4425$ ), (c) 50 wt% oil, 2.0 wt% PF87 ( $\Psi = 0.3424$ ), (d) Experimental $d_{32}$ values (symbols) and model predicted $d_{32}$ values (solid lines). . . . .	56
4.1	Experimental results: (a) DSDs for 30 wt% oil and 2 wt% PF68 for five homogenization passes; (b) fifth pass DSDs for 30 wt% oil and different surfactant concentrations; (c) fifth pass $d_{32}$ for different oil and surfactant concentrations; and (d) fifth pass $d_{43}$ for different oil and surfactant concentrations. . . . .	72
4.2	(a) Fifth pass DSDs with 10 wt% oil and different surfactant concentrations; and (b) free surfactant concentrations calculated with different maximum surface coverage values assuming all drops were fully covered. . . . .	73
4.3	Model 1: Comparison of experimental and predicted (a) $d_{32}$ and (b) $d_{43}$ values calculated from fifth pass DSDs. . . . .	74
4.4	Predicted emulsion viscosity at high shear rates. The dashed line represents the viscosity of water. . . . .	76
4.5	Models 2 and 3: Comparison of experimental and predicted mean drop sizes calculated from fifth pass DSDs. (a) $d_{32}$ and (b) $d_{43}$ values obtained using Model 2; and (c) $d_{32}$ and (d) $d_{43}$ values obtained using Model 3. . . . .	77
4.6	Effect of the oil fraction on model 2 predictions at 2 wt% PF682 wt% surfactant. (a) Breakage frequency functions; (b) premix (black), first (blue), third (green) and fifth (red) pass DSD predictions for 10 wt% oil; (c) premix (black), first (blue), third (green) and fifth (red) pass DSD predictions for 30 wt% oil; and (d) premix (black), first (blue), third (green) and fifth (red) pass DSD predictions for 50 wt% oil. . . . .	79

4.7	Effect of the oil fraction on model 2 predictions for all five passes at 30 wt% oil. (a) $d_{32}$ , (b) $d_{43}$ , (c) free surfactant concentration and (d) relative drop coverage for 0.1–2.0 wt% surfactant.....	80
5.1	Daughter drop distribution functions: (1) bell-shaped function; (2) U-shaped function; (3) beta function ( $p = 15$ );(4) new bimodal function ( $M_1 = 1, M_2 = 27; M_3 = 512$ ); (5) new unimodal function ( $M_4 = 2162, M_5 = 17.5$ ).....	90
5.2	Emulsion viscosity predictions at different oil volume fractions and shear rates with model parameters $K_\lambda = 19.5, k = 1900, m = 0.59, a_1 = 0.8, a_2 = 0.2$ and $a_3 = 0.01$ . ....	94
5.3	Drop volume distributions (—: first pass, —: second pass, —: third pass, —: forth pass) obtained using the (a) bell-shaped daughter distribution function ( $\Psi = 0.01335$ ), (b) u-shaped daughter distribution function ( $\Psi = 0.1475$ ), (c) beta daughter distribution function ( $p = 20, \Psi = 0.0071$ ), and (d) beta daughter distribution function ( $p = 200, \Psi = 0.0401$ ) for the base case conditions. ....	95
5.4	Number distributions (—: first pass, —: second pass, —: third pass, —: forth pass) obtained using the (a) bell-shaped daughter distribution function, (b) u-shaped daughter distribution function, (c) beta daughter distribution function ( $p = 20$ ), and (d) beta daughter distribution function ( $p = 200$ ) for the base case conditions.....	96
5.5	(a)Drop volume distributions (—: first pass, —: second pass, —: third pass, —: forth pass) ( $\Psi = 0.0048$ ), (b) number distributions, and (c) Sauter mean diameter obtained using the proposed bimodal daughter drop distribution function for base case conditions .....	97
5.6	Drop volume distribution predictions (—: first pass, —: second pass, —: third pass, —: forth pass) of emulsions with (a) 10 wt% oil ( $\Psi = 0.0050$ ), (b) 30 wt% oil ( $\Psi = 0.0048$ ), (c) 50 wt% oil ( $\Psi = 0.0118$ ), and (d) predicted and measured Sauter mean diameters obtained using the proposed bimodal daughter drop distribution function.....	99
5.7	(a) Drop volume distribution predictions (—: first pass, —: second pass) and (b) predicted and measured Sauter mean diameters of an emulsion with 70 wt% oil ( $\Psi = 0.059$ ) obtained using the proposed uni-modal daughter drop distribution function.....	100

5.8	Drop volume distributions (—: first pass, —: second pass, —: third pass, —: fourth pass) of emulsions with 50 wt% oil passed through the colloid mill at a flow rate of (a) 16 kg/hr ( $\Psi = 0.0207$ ), (b) 35 kg/hr ( $\Psi = 0.0543$ ), (c) 70 kg/hr ( $\Psi = 0.0765$ ); and (d) Sauter mean diameters at the different flow rates ( *: 16 kg/hr, *: 35 kg/hr, *: 70 kg/hr) using model parameters estimated from data collected at 16 kg/hr. ....	101
5.9	Drop volume distributions (—: first pass, —: second pass, —: third pass, —: fourth pass) of emulsions with (a) 10 wt% oil processed at 10000 RPM ( $\Psi = 0.007$ ), (b) 30 wt% oil processed at 10000 RPM ( $\Psi = 0.0325$ ), (c) 50 wt% oil processed at 10000 RPM ( $\Psi = 0.325$ ), and (d) 70 wt% oil processed at 8000 RPM ( $\Psi = 0.41$ ), .....	102
6.1	Experimental and model predicted results for homogenization with 50wt% oil, 1wt% PF-68 homogenized at 800 bar. (a) Drop volume distributions, (b) Sauter mean diameters. ....	110
6.2	Experimental and model predicted drop size distributions obtained using optimized parameters at 600 bar: (a) 200 bar, (b) 400 bar, (c) 800 bar. ....	112
6.3	Interpolated model parameters using $K_2$ (*) and $K_4$ ( $\Delta$ ) values obtained at four different pressures. ....	113
6.4	Model predicted and experimental distributions obtained with four optimized homogenization passes for the target $\mu = 0.5$ and $\sigma^2 = 0.8$ . ....	115
6.5	Model predicted and experimental distributions obtained with two optimized homogenization passes for the target $\mu = 0.8$ and $\sigma^2 = 0.8$ . ....	116

# CHAPTER 1

## INTRODUCTION

Emulsions are ubiquitous dispersed phase systems with diverse applications that include consumer products, processed foods, polishes, waxes, agricultural sprays and road surfacing materials [7, 11, 32]. Emulsions are also encountered in the petroleum industry with applications at many stages of petroleum recovery, transportation, and processing [7, 71]. Emulsifying heavy oils with an aqueous solution significantly reduces the viscosity and pumping power requirements and allows more economical transportation [68, 65, 90]. In the foods industry, emulsions constitute natural foods as well as numerous processed products such as milk, butter, margarine, ice cream, sauces and desserts. Food emulsions contain edible oils, water and biocompatible surfactants as the major ingredients and vitamins, minerals and/or flavors as minor ingredients [51]. These products exhibit a wide range of physicochemical and sensory characteristics based on the emulsion system formulation, which influence dispersed and continuous phase properties such as density, viscosity and dielectric constant. The surfactant plays a critical role in determining interfacial properties and surface charge as well as emulsion stability. Process operations such as mixing, homogenization and pasteurization also have a substantial effect on emulsified product properties, including appearance, taste, mouthfeel, odor and safety. Emulsion system formulation and processing operations both impact the drop size distribution, a key property that influences emulsion rheology, stability, texture and appearance. A typical processed food requires the drop size distribution to be maintained within acceptable limits, which includes achieving a prescribed mean drop size, maintaining small variations

about the mean and avoiding very small or large drops that adversely affect product properties such as texture and appearance.

## 1.1 Emulsification

Emulsions are usually prepared via a two step process. In the first step, a coarse emulsion or premix is prepared by thoroughly mixing the ingredients in a low shear device. The coarse emulsion is then passed through a high energy mechanical device such as a high pressure homogenizer or a colloid mill. High pressure homogenization is generally preferred for low viscosity emulsions [57] because sub-micron drops can be readily generated due to the high energy input. Colloid mills are the preferred technology for highly viscous emulsions ( $> 5000$  cp) commonly encountered in industry.

### 1.1.1 High Pressure Homogenizer

In high pressure homogenization, a coarse emulsion is passed through a small orifice under very high pressure (Fig. 1.1(a)). The fluid stream passes radially through the narrow gap formed between the piston and the valve seat at high velocity, creating a local environment of high turbulence and shear stress that causes drop deformation and breakage. The processed liquid exits the homogenizer at atmospheric pressure, and the pressure drop across the device is called the homogenization pressure. Several phenomenon occurring simultaneously in the homogenizer determine the resulting drop size distribution. Under turbulent conditions near valve exit, drops undergo breakage and coalescence. Turbulent inertial breakage and turbulent viscous breakage are the most dominant breakage mechanisms in high pressure homogenization [84, 85]. Drops larger than the smallest-scale eddies (Kolmogorov length scale eddies) break due to energy transfer from eddies (Fig. 1.1(b)). And drops smaller than the smallest-scale eddies break due to shearing inside eddies (Fig. 1.1(c)). A drop will

break only if energy dissipated from eddies is larger than surface energy of drop or if turbulent shear stress is larger the Laplace pressure of drop. Drop breakage leads to the creation of new interfacial area that must be stabilized by the surfactant. If newly formed drops are not sufficiently covered by surfactant, the drops will coalesce to form larger drops and produce corresponding increases in drop mean size and variability. Inability of the surfactant to achieve adequate drop coverage can be attributable to either insufficient free surfactant in solution or slow surfactant adsorption kinetics [6, 85]. Under typical industrial conditions where surfactant use is minimized to reduce manufacturing costs, drop coalescence is prevalent due to insufficient surfactant regardless of the adsorption kinetics. While drop breakage under laminar conditions has been extensively studied [21, 27], the problem of turbulent breakage and coalescence is less understood.

### 1.1.2 Colloid Mills

In colloid mill, an emulsion is passed through the narrow gap between the stator and the rotor rotating at high angular velocity (Fig. 3.1(a)). Emulsion drops tend to stretch due to the very high shear rate  $\dot{\gamma}$  ( $10^4$ – $10^6$  1/s). When the ratio of the viscous stress acting on the drop to the interfacial tension force surpasses some critical value, a mother drop breaks into two or more daughter drops. This ratio is called the capillary number  $Ca$  and is defined as [34],

$$Ca = \eta_c \dot{\gamma} d / 2\sigma \tag{1.1}$$

where  $\eta_c$  is continuous phase viscosity;  $d$  is the mother drop diameter; and  $\sigma$  is the interfacial tension. The critical value is called the critical capillary number  $Ca_{cr}$  and depends on type of flow and the viscosity ratio of the dispersed and continuous phases ( $\lambda = \eta_d / \eta_c$ ). The situation is more complicated in high oil emulsions because droplets interact with each other. In this case, the continuous phase viscosity  $\eta_c$  in

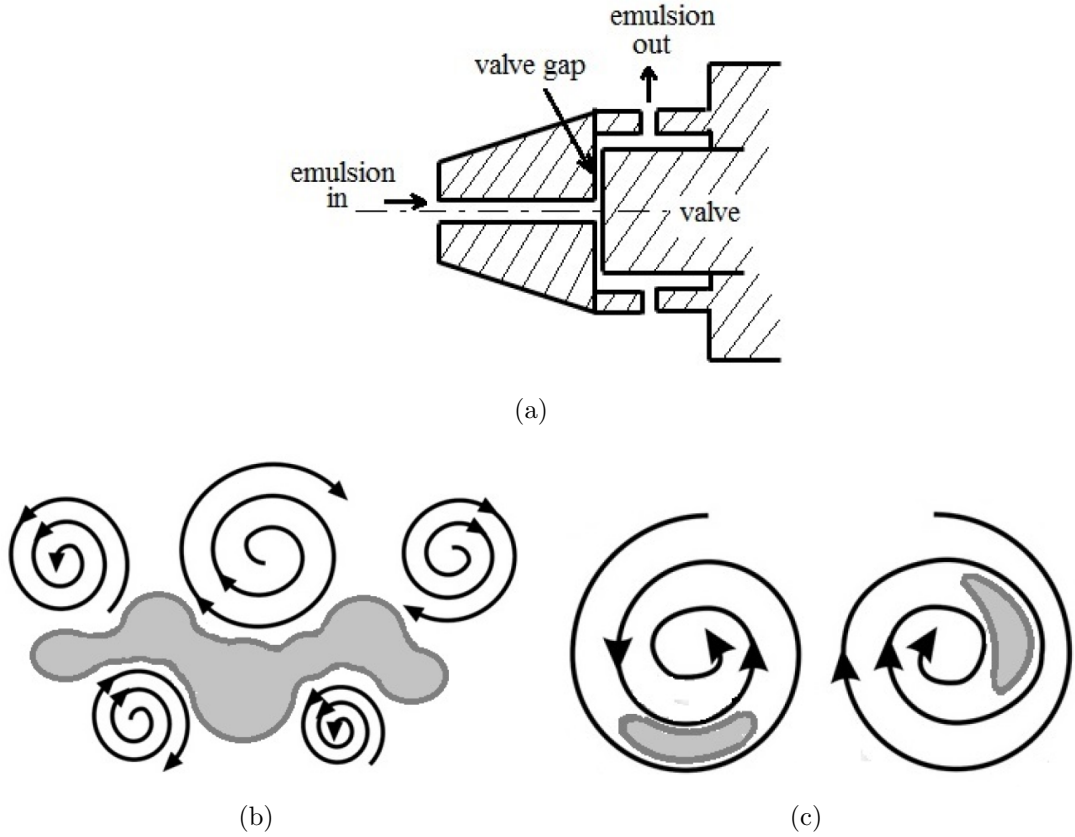


**Figure 1.1.** Schematic representation of (a) high pressure homogenization, (b) drop breakage due to turbulent inertia, (c) drop breakage due to turbulent shear stress.

the capillary number must be replaced by the apparent emulsion viscosity  $\eta_{em}$  and the viscosity ratio must be modified accordingly ( $\lambda = \eta_d/\eta_{em}$ ).

Drop breakage in laminar shear flow is known to be very complex. When the capillary number is just slightly larger than the critical value such that  $1 \leq \frac{Ca}{Ca_{cr}} \leq 2$ , a drop breaks into two nearly equally sized daughter drops by an end-pinching mechanism (Region A in Fig. 3.1(b)) [34, 88, 93]. When  $\frac{Ca}{Ca_{cr}} \gg 1$  and  $0.1 < \lambda < 1$ , a drop breaks into many nearly equally sized daughter drops by a capillary mechanism (Region C in Fig. 3.1(b), Fig. 2.1(c)). When  $\frac{Ca}{Ca_{cr}} \gg 1$  and  $\lambda > 1$ , a drop breaks into many unequally sized daughter or satellite drops (Region B in Fig. 3.1(b), Fig. 2.1(c)) [93, 17]. Adding to the complexity,  $Ca_{cr}$  is known to depend on the type of flow field in addition to the viscosity ratio. For example, drops with  $\lambda > 4$  will almost

never break in simple shear flow because  $Ca_{cr}$  is too large, but such drop can break in extensional shear flow as  $Ca_{cr}$  is much smaller. Furthermore, Taylor vortices can appear in the flow field when the Taylor number ( $Ta$ ) exceeds some critical value ( $Ta_{cr}$ ), which depends on the Reynolds number of flow. Taylor vortices have been experimentally observed for Reynolds number above 800 [42]. Simple calculations show that our emulsions prepared at 10 and 30 wt% oil will break due to Taylor vortices [1] and not due to shearing in simple shear flow (Fig. 3.1(b)).

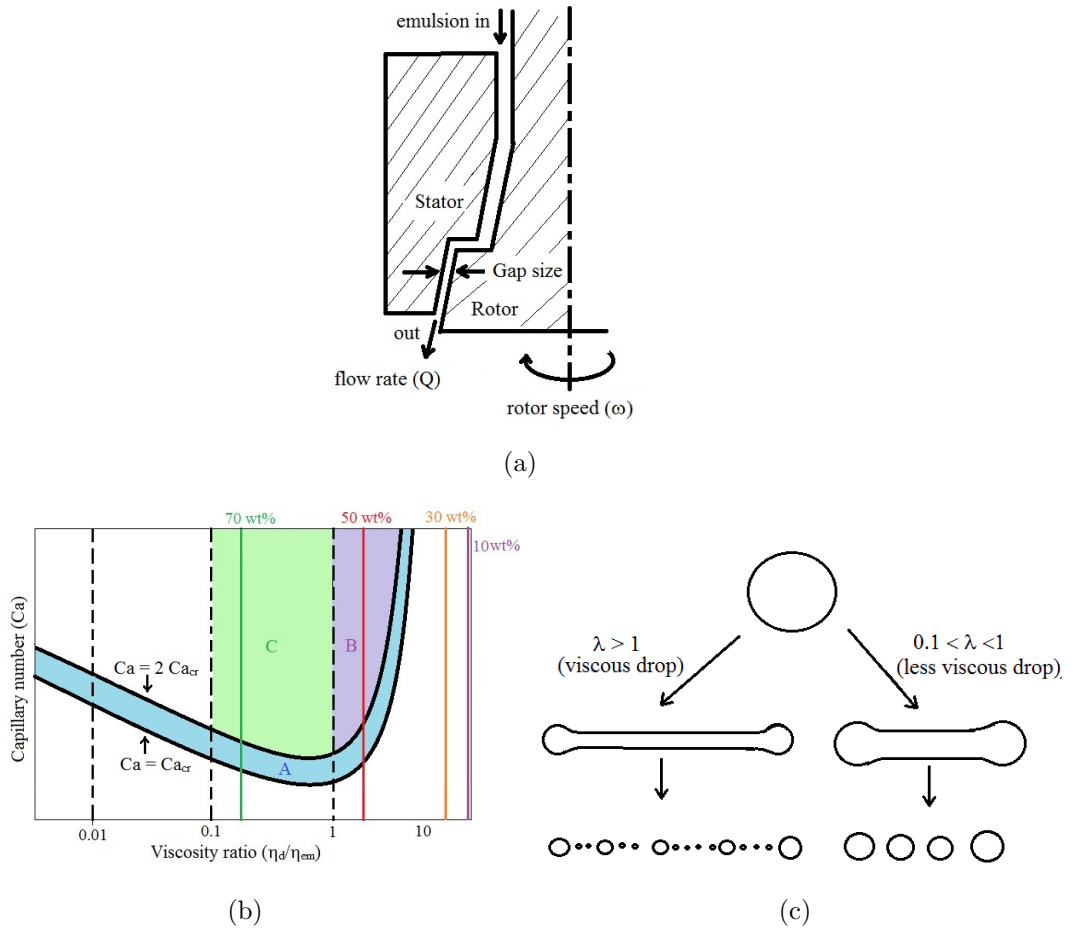


**Figure 1.2.** (a) Schematic representation of a colloid mill. (b) Different regions of drop breakage (taken from [93]); Region A: end pinching, Region B: bimodal distribution, Region C: uni-modal distribution. Colored lines denote the capillary numbers of emulsions with different oil fractions used in this study. (c) Drop breakage at different viscosity ratios.

## 1.2 Drop Size Distribution

The drop size distribution (DSD) of an emulsion is a crucial property that affects product stability, taste, appearance and rheology [51]. Achieving a desired DSD is a very challenging problem as the emulsion formulation (e.g. oil and surfactant concentrations) and processing conditions (e.g. operating pressure and numbers of passes through the homogenizer) combine to affect the DSD in a complex and often poorly understood manner [85]. At very high operating pressures, the mean drop size is expected to independent of pressure and depends only on surfactant concentration. Surfactant reduces the Laplace pressure of drops such that even small drops can be broken if sufficient free surfactant is present. Therefore, the mean drop size decreases with increasing surfactant concentration, and this regime is called “surfactant limited” (Fig. 1.3(a),1.3(b)). At very low operating pressures, small drops cannot be broken due to limited dissipated energy even if surfactant is available for drop stabilization. Therefore the mean drop size decreases with increasing pressure, and this regime is called “surfactant rich” or “energy limited” due to the negligible effect of the surfactant concentration (Fig. 1.3(c),1.3(d)). Furthermore, the location of the surfactant limited and surfactant rich regimes depend strongly on the oil content, with high oil concentrations demanding more surfactant for drop stabilization. Most emulsification conditions of practical interest represent a transitional regime between these two extremes (Fig. 1.3(e),1.3(f)). Consequently, accurately predicting the DSD as a function of the surfactant concentration, oil concentration and operating pressure is a problem of great practical significance.

The surfactant limited and surfactant rich regimes were experimentally demonstrated in high pressure homogenizers, and different empirical equations were used to predict the mean drop size in these regimes [79, 80]. For common surfactants such as Tween 20, the mean drop size has been shown to decrease with increasing surfactant concentration [58]. Correlations have been developed to predict the mean

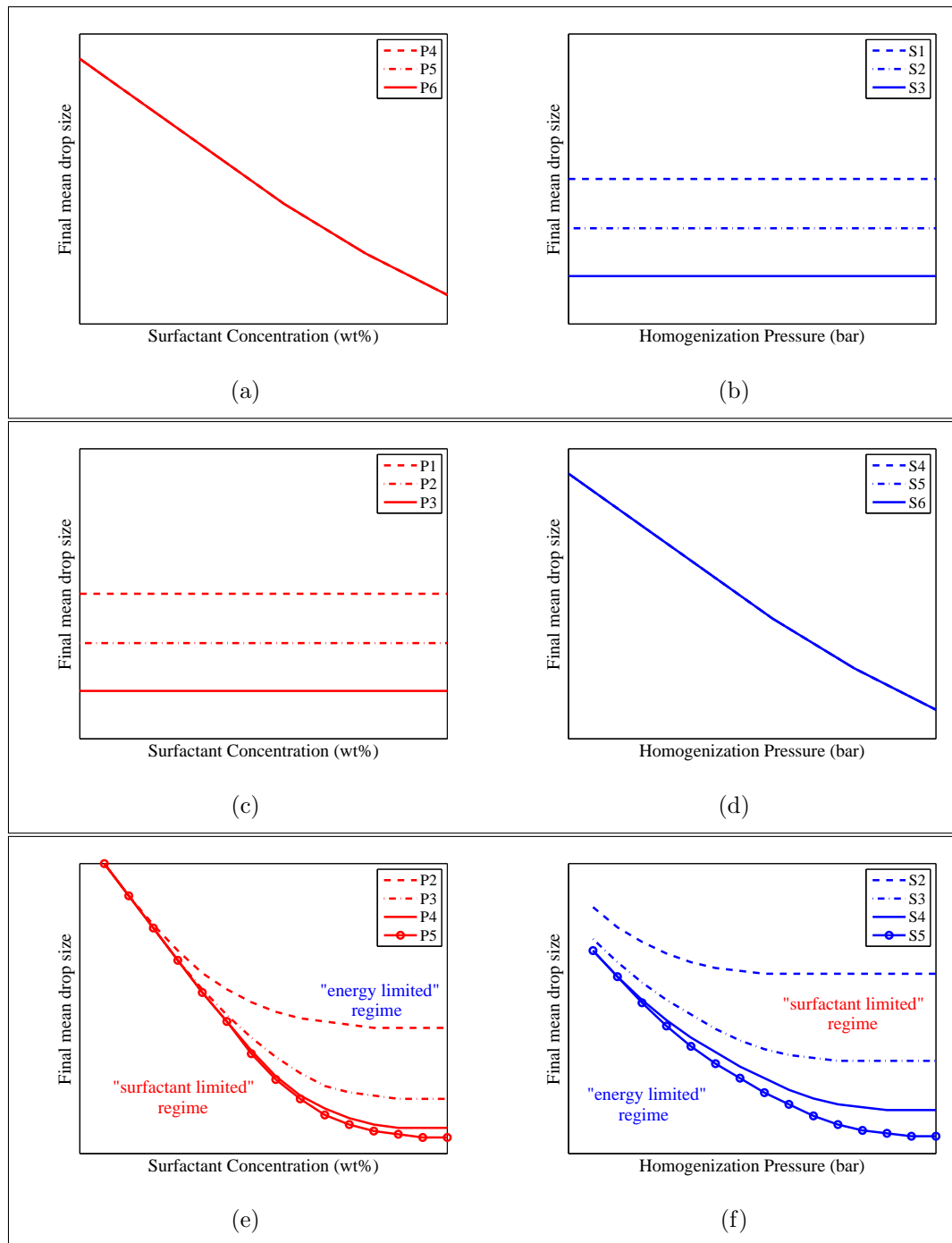


**Figure 1.3.** Effect of surfactant concentration and homogenization pressure in: (a),(b) the surfactant limited regime; (c),(d) the energy rich regime; and (e),(f) the transitional regime. P1–P6 and S1–S6 represent increasing homogenization pressures and surfactant concentration, respectively.

drop size as a function of the surfactant concentration, holdup fraction and impeller Weber number for mixer-settler-type extraction process [37]. A bivariate population balance equation (PBE) model has been developed to capture the effects of surfactant concentration and homogenization pressure on the DSD [30]. The bivariate PBE was reduced to two monivariate PBEs (one for drop volume and the other for the amount of adsorbed surfactant) assuming all drops of a certain size had same amount of adsorbed surfactant. However, model predictions were not compared to measured DSDs in this study. The effect of the oil volume fraction on homogenized DSDs also has been studied extensively [12, 20, 81]. For high pressure homogenizers, the mean drop size has been shown to increase with increasing dispersed phase volume fraction [81, 50]. The opposite trend has been observed with rotor-stator emulsification devices such as colloid mills, as the energy dissipation rate increases with increasing oil fraction due to increased emulsion viscosity [48].

### 1.3 Modeling of Emulsion Formation

Due to lack of quantitative understanding, new emulsified products are currently developed by combining a broad knowledge of previous product formulations with empirical scientific experimentation. Because this approach is intuitive and experimental, the progression of a formulation is generally unpredictable and a new product will often go through hundreds of prototype formulations in a laboratory or pilot plant before commercialization. Due to the very large number of possible formulation and processing combinations that need to be explored, the traditional trial-and-error approach requires significant time and resources.

An alternative to brute force experimentation is to utilize a suitable mathematical model to predict the drop size distribution for different emulsion formulations and processing conditions. The population balance equation (PBE) modeling framework [63] is particularly well suited for this problem as functions describing single

drop events such as breakage and coalescence can be incorporated within a fundamental number balance equation to predict the evolution of the drop size distribution. Ramkrishna et al. have used the population balance modeling to a number of dispersion systems such as lean liquid-liquid dispersions, microbial populations etc[40, 41, 47, 53, 52, 63, 62, 64, 70, 69]. PBE models have been developed for a wide variety of dispersed phase systems including continuously agitated liquid-liquid dispersions [2, 4, 3, 16, 39, 75, 76], liquid-liquid extractors [66, 67, 72], continuous flow screw-loop reactors [13] and bubble columns [87]. More recently, several investigators have developed PBE models of high pressure homogenizers with application to small vesicle formation [46, 74], intracellular product recovery [36] and food emulsion production [28, 29, 49, 50, 59]. Model formulation requires functions that capture the relevant drop breakage and coalescence mechanisms. Droplet breakage due to turbulent flow fields inside homogenizers has been studied extensively [67, 84, 73]. Although other mechanisms are possible, drops are mainly broken due to turbulent inertial forces and turbulent viscous shear [16, 84, 28]. Coualaloglou et al. [16] formulated a breakage frequency function for the turbulent inertial breakage mechanism which has been widely used in PBE models of dispersed systems. The distribution of drop volume between a mother droplet and the resulting daughter droplets in turbulent flows remains poorly understood, with a wide variety of functions proposed [44]. Mechanisms of drop coalescence in turbulent flows also have been studied [16, 54]. The collision frequency depends on the local flow field, while the coalescence efficiency depends on the ratio of the contact time between drops and the time required for drainage of the liquid film between the drops. The coalescence model formulated by Coualaloglou et al. [16] for turbulent flows remains widely used in PBE models. These breakage and coalescence functions depend on the emulsion formulation though bulk physical properties such as the continuous phase viscosity. For emulsions with very low oil fraction, the water/solvent viscosity is used as the continuous phase vis-

cosity. But for emulsions with high oil fraction, the water/solvent viscosity needs to be replaced with the apparent emulsion viscosity to account for the influence of surrounding drops [88].

Perhaps due to the focus on homogenization, very few PBE models have been presented for colloid mills despite their industrial significance. Wieringa et al. [88] developed a simple PBE model based on the assumption that the drop breakage frequency was the reciprocal of the breakage time, which in turn depended linearly on the drop size. An empirical equation for the number of daughter drops formed as a function of the capillary number was derived. Coalescence was completely neglected under the assumption that sufficient surfactant was available in solution for stabilization of newly formed drops. Also under the assumption of negligible coalescence, Almeida-Rivera et al. [1] modeled the frequency of binary drop breakage to be proportional to  $(d_i - d_{max})^n$ , where  $d_i$  is the drop diameter,  $d_{max}$  is the critical drop size below which drops cannot break, and  $n$  is an adjustable model parameter. In addition to providing few insights into the relevant drop breakage mechanisms, these PBE models of emulsification in colloid mills are not capable of accurate prediction due to their restrictive assumptions.

## Organization of the Thesis

In chapter 2, I have incorporated the coalescence frequency functions in previously built breakage-only PBE model for high pressure homogenization. I examined the model predictability for emulsions with high oil-to-surfactant ratios where drop coalescence can not be neglected due to insufficient surfactant to cover all drops. In chapter 3, I have incorporated the effect of surface coverage of surfactant molecules in PBE model. I have modified coalescence frequency as function of surface coverage of colliding drops and I have tested the model extensibility for surfactant concentration and type. In chapter 4, I have further extended the PBE model by 1) formulating

dynamic surface coverage model, 2) reformulating the drop breakage function to behave differently with respect to drop size, and 3) replacing the constant continuous phase viscosity with a calculated emulsion viscosity that increased strongly with oil content. I have tested model predictability in both “surfactant limited” and “surfactant rich” regimes. In chapter 5, I have developed PBE model of emulsification in colloid mill by formulating new mechanistic drop breakage frequency function and daughter drop distribution function. In chapter 6, I have utilized the built PBE model of high pressure homogenization for emulsion product design. I have developed the methodology for achieving target drop size distribution by controlling the number of homogenization passes and homogenization pressure at each pass.

## CHAPTER 2

# INCORPORATING EMULSION DROP COALESCENCE INTO POPULATION BALANCE EQUATION MODEL OF HIGH PRESSURE HOMOGENIZATION

### 2.1 Introduction

In this chapter, I develop population balance equation model for high pressure homogenization. In the previous work, breakage-only PBE models was developed for prediction of the drop volume distribution [60, 59]. It was shown that the system exhibited negligible coalescence for the low oil to surfactant ratio (5% oil, 1% surfactant) used through experimental and computational studies. The models included two mechanistic breakage rate functions that depended on the emulsion formulation through bulk physical properties (dispersed phase volume fraction, continuous phase viscosity, interfacial tension) and on the homogenization pressure through the energy dissipation rate. The distribution function was chosen such that the breakage of a single mother drop produced a large number of daughter drops under the assumption that the turbulent homogenization conditions would produce results similar to laminar flow experiments [61, 77, 94]. Nonlinear optimization was used to fit adjustable breakage rate parameters to measured drop volume distributions for a particular experimental condition, and then showed that the model produced reasonable predictions for different homogenization pressures and different surfactant concentrations that maintained the same oil to surfactant ratio.

In this study, I incorporate mechanistic drop coalescence functions into my research group's most recent breakage-only PBE model [59] to allow the drop volume distribution to be predicted over a much larger range of oil to surfactant ratios. In

addition to examining model extensibility for different surfactant concentrations and homogenization pressures, I investigate how the model could be adapted to different surfactants as a first step towards emulsion formulation design.

## **2.2 Experimental Methods**

### **2.2.1 Materials**

Oil-in-water emulsions were prepared using vegetable oil (Fisher Scientific) as the dispersed phase and water as the continuous phase. The base case emulsion consisted of 50 wt% oil, 1 wt% Pluronic F-68 surfactant with the remainder water (Table 3.2). The high oil-to-surfactant ratio of 50 wt%/ 1 wt% was chosen to promote homogenization conditions leading to coalescence. Extensibility experiments were performed at three other Pluronic F-68 concentrations (0.5, 2.0 and 5.0 wt%) . To examine model extensibility to other nonionic surfactants, Pluronic F-127 (Sigma) and Tween 60 (Sigma) were also used as the emulsifier.

### **2.2.2 Emulsion Preparation**

Emulsions were prepared using a two-step process. First approximately 400 ml of coarse pre-emulsion was prepared by mixing the ingredients in a stator-rotor device (Ultra-Turrax Model T25, Rose Scientific Ltd.) at 16000 rpm for 15 minute. About 100 ml of pre-emulsion was processed in a high-pressure homogenizer (Emulsiflex C-3, Avestin Inc.) to reduce the average drop size. The base case homogenization pressure was chosen as 800 bar to produce small drops likely to undergo coalescence. Multiple passes were performed by reprocessing the emulsion obtained from the previous homogenizer pass. Five passes were performed for each experiment, and after each pass approximately 2 ml of emulsion was sampled to analyze the drop size distribution. Extensibility experiments were performed at three lower pressures (200, 400 and 600 bar) .

### 2.2.3 Emulsion Characterization

Drop size distributions were measured using a light scattering device (Master-sizer S, Malvern Instruments). Densities, viscosities and the interfacial tension were measured prior to each homogenization experiment. Continuous and dispersed phase densities were measured using Bio-Rad 36XMX densitometer. Continuous and dispersed phase viscosities were measured using a Ubbelohde type capillary viscometer (Model CT-1000, Canon Instruments Company) at 25°C. The oil-water interfacial tension  $\sigma_{o/w}$  was measured by drop shape analysis (Model DSA-10 Tensiometer, KRUSS Instruments) at 25°C. The interfacial tension  $\sigma$  at surfactant concentration of  $c$  temperature  $T$  was calculated as,

$$\sigma = \sigma_{o/w} - RT\Gamma_{\infty} \ln \left( 1 + \frac{c}{c_{1/2}} \right) \quad (2.1)$$

where  $\Gamma_{\infty}$  is maximum surface coverage and  $c_{1/2}$  is the surfactant concentration corresponding to half of the maximum surface coverage. The constants  $\Gamma_{\infty}$  and  $c_{1/2}$  were found by plotting surface coverage  $\Gamma$  versus surfactant concentration  $c$  with  $\Gamma$  values calculated from the Gibb's adsorption isotherm (Eq. (2.2)),

$$\Gamma = -\frac{1}{RT} \frac{d\sigma}{d(\ln(c))} \quad (2.2)$$

**Table 2.1.** Base case emulsion formulation and homogenization conditions

Vegetable oil	50 wt%
Pluronic F-68 surfactant	1 wt%
Continuous phase density ( $\phi_c$ )	997 g/L
Dispersed phase density ( $\phi_d$ )	917 g/L
Interfacial tension ( $\sigma$ )	14.4 mN/m
Continuous phase viscosity ( $\eta_c$ )	1 cP
Premix speed and time	16000 rpm, 15 minutes
Homogenizer pressure ( $P$ )	800 bar
Number of passes	5

## 2.3 Theory

### 2.3.1 Population Balance Equation Model

The PBE is formally derived from a number balance on particles by accounting for the various rate processes such as breakage and coalescence that affect particle size [63]. In this study, a volume structured PBE was used because light scattering most directly measures drop volume. Under the assumption that drops are spherical, drop volume is readily converted into drop diameter. Although homogenizers have distinct zones where local shear forces can change dramatically [28], I treated the homogenizer as a well-mixed batch system to avoid the complexities associated with including spatial variations. In this case, the PBE can be written as [60, 16],

$$\begin{aligned} \frac{\partial n(v, t)}{\partial t} = & -g(v)n(v, t) + \int_v^\infty \beta(v, v')g(v')n(v', t)dv' \\ & -n(v, t) \int_0^\infty C(v, v')n(v', t)dv' + \frac{1}{2} \int_0^v C(v - v', v')n(v - v', t)n(v', t)dv' \end{aligned} \quad (2.3)$$

where  $v$  is the volume of the particle;  $n(v, t)dv$  is the number of drops with volume in the range  $[v, v + dv]$  per unit volume of dispersion at time  $t$ ;  $g(v)$  is the breakage rate representing the fraction of drops of volume  $v$  breaking per unit time;  $\beta(v, v')$  is the daughter drop distribution function representing the probability of forming a daughter drop of size  $v$  from breakage of a mother drop of size  $v'$ ; and  $C(v, v')$  is coalescence frequency representing the rate at which drops of size  $v$  and drops of size  $v'$  coalesce. The first and third terms on the right hand side of Eq. (6.1) account for disappearance of drops of size  $v$  due to breakage and coalescence, respectively, while the second and fourth terms account for the appearance of drops of size  $v$ . The model requires specification of the functions that describe the breakage and coalescence processes, namely  $g(v)$ ,  $\beta(v, v')$  and  $C(v, v')$ . The previous models [60, 59] have been based on the assumption of negligible coalescence, which is reasonable if the oil-to-surfactant

ratio is sufficiently small that the emulsion is not surfactant limited. In this case, the PBE can be simplified as [16, 13, 9, 60],

$$\frac{\partial n(v, t)}{\partial t} = -g(v)n(v, t) + \int_v^\infty \beta(v, v')g(v')n(v', t)dv' \quad (2.4)$$

The PBE (6.1) describes the evolution of the number density  $n(v, t)$ , while the particle analyzer provided measurements of the volume percent distribution  $n_p(v, t)$ . Under the standard assumption that drops are spherical, the two distributions are related as follows,

$$n(v, t) = \frac{V_{tot}n_p(v, t)}{v} \quad (2.5)$$

where  $V_{tot}$  is the conserved total volume of the drops. The PBE (6.1) was reformulated in terms of  $n_p(v, t)$  to yield,

$$\begin{aligned} \frac{\partial n_p(v, t)}{\partial t} = & -g(v)n_p(v, t) + v \int_v^\infty \frac{\beta(v, v')g(v')n_p(v', t)}{v'} dv' \\ & - n_p(v, t) \int_0^\infty \frac{C(v, v')n_p(v', t)V_{tot}}{v'} dv' \\ & + \frac{v}{2} \int_0^v \frac{C(v - v', v')n_p(v - v', t)n_p(v', t)V_{tot}}{v'(v - v')} dv' \end{aligned} \quad (2.6)$$

<sup>1</sup> The measured volume percent distribution of the coarse pre-emulsion was used as initial condition  $n_p(v, 0)$  for the first homogenizer pass. Each pass corresponded to one dimensionless time unit, and the initial condition for each subsequent pass was the predicted volume percent distribution from the previous pass.

### 2.3.2 PBE Functions

The PBE (6.1) contains three functions ( $g(v), \beta(v, v'), C(v, v')$ ) that must be specified to compute the drop size distribution. Following my research group's previous

---

<sup>1</sup>The equation is discretized by fixed pivot technique described in [40] which makes sure that the denominator in the last term does not go to zero as  $v'$  approaches  $v$ .

work [60], the breakage rate  $g(v)$  was assumed to be determined by turbulent breakage of drops by both inertial and viscous forces such that  $g(v) = g_1(v) + g_2(v)$ . The first breakage function  $g_1(v)$  was derived assuming drops break due to collision with turbulent eddies [16],

$$g_1(v) = K_1 v^{-2/9} \epsilon^{1/3} \left[ \exp - \left( \frac{K_2 \sigma (1 + \phi)^2}{\rho_d v^{5/9} \epsilon^{2/3}} \right) \right] \quad (2.7)$$

where  $K_1$  and  $K_2$  are adjustable constants. The second breakage rate function  $g_2(v)$  was derived assuming that drop breakage results from turbulent shear [60],

$$g_2(v) = K_3 \left( \frac{2}{\pi} \right)^{1/2} \left( \frac{\epsilon \rho_d}{\eta_d} \right)^{1/2} \left[ \exp \left( - \frac{K_4 \sigma^2 \lambda}{v^{2/3} \epsilon \eta_c} \right) \right] \quad (2.8)$$

where  $K_3$  and  $K_4$  are the adjustable constants. The two breakage rates depend on the homogenizer pressure  $P$  through the energy dissipation rate  $\epsilon$  (see below) and bulk emulsion properties including the dispersed phase volume fraction  $\phi$ , the interfacial tension  $\sigma$ , the dispersed phase density  $\rho_d$ , the continuous phase viscosity  $\eta_c$  and the dispersed phase viscosity  $\eta_d$  through the ratio  $\lambda = \frac{\eta_d}{\eta_c}$ . I have shown that these dependencies are necessary for the PBE model to be predictive over a range of formulation and homogenization conditions with a single set of constants  $K_1 - K_4$  [60, 59].

The breakage rate function was specialized to high-pressure homogenizers by using the following relation for the energy dissipation rate [84, 83],

$$\epsilon = \frac{\Delta P Q}{V_{diss}} \quad (2.9)$$

where  $\Delta P$  is the applied pressure,  $Q$  is the volumetric flow rate and  $V_{diss}$  is the valve gap volume which depends on valve gap distance  $h_{gap}$ . Equations for  $V_{diss}$  and  $h_{gap}$  can be found in the previous work [60]. As in the previous breakage-only PBE model [60], I used the power law product form of the generalized Hill-Ng distribution [31, 22, 91] as the daughter drop distribution function  $\beta(v, v')$  to model the breakage

of a mother drop into multiple daughter drops. The parameter  $q$  was chosen as unity to represent the uniform probability of daughter drops of any size ( $v < v'$ ) being formed due to breakage of a mother drop of size  $v'$ . In this case, the daughter drop distribution function has the form [60],

$$\beta(v, v') = (p - 1) \left(1 - \frac{v}{v'}\right)^{p-2} \quad (2.10)$$

where  $p \geq 2$  is the number of daughter drops formed from breakage of a single mother drop. Based on preliminary simulation results (not shown), I determined that the best fit of the base case drop volume distribution data was obtained for  $p = 80$ . While laminar flow experiments have established that a mother drop can break into numerous daughter drops [61, 77, 94], the assumption that turbulent homogenization conditions could produce as many as 80 daughter drops from a single mother drop would require experimental testing beyond the scope of this study.

The coalescence frequency  $C(v, v')$  of drops of size  $v$  and  $v'$  was modeled as the product of the drop collision frequency  $h(v, v')$  and the coalescence efficiency  $\lambda(v, v')$ :  $C(v, v') = h(v, v')\lambda(v, v')$ . While certainly not mechanistically correct, I followed the common practice of modeling the collision frequency assuming that drops in turbulent flow behave like gas molecules [16],

$$h(v, v') = \frac{K_5 \epsilon^{1/3}}{1 + \phi} (v^{2/3} + v'^{2/3})(v^{2/9} + v'^{2/9})^{1/2} \quad (2.11)$$

where  $K_5$  is an adjustable constant. The coalescence efficiency was modeled to depend on the contact time of droplets, with coalescence occurring if the contact time is greater than the time required for the liquid film between two drops to drain [16],

$$\lambda(v, v') = \exp \left[ \frac{-K_6 \eta_c \rho_c \epsilon}{\sigma^2 (1 + \phi)^3} \left( \frac{v^{1/3} v'^{1/3}}{v^{1/3} + v'^{1/3}} \right)^4 \right] \quad (2.12)$$

where  $K_6$  is an adjustable constant. Similar to the breakage rate, the coalescence frequency depends on the homogenizer pressure  $P$  through the energy dissipation rate  $\epsilon$  and bulk emulsion properties including the continuous phase density  $\rho_c$  and  $\phi$ ,  $\sigma$  and  $\eta_c$ .

### 2.3.3 Dynamic Simulation and Parameter Estimation

The PBE model (6.1) was solved numerically by approximating the integral expression using the fixed pivot technique [40] with 100 equally spaced node points. Increasing the number of node points produced very small changes in the solution but substantially increased the computational cost for simulation and optimization (see below). The discretized PBE model consisted of 100 nonlinear ordinary differential equations in which the independent variable was time and the dependent variables represented the volume percent distribution at each node point. The ODE system was solved with the Matlab integration code `ode45` using the measured premix distribution as the initial condition  $n_p(v, 0)$ .

The constants  $K_1 - K_4$  in the breakage rate function and  $K_5 - K_6$  in the coalescence frequency function were estimated from base case homogenization experiments. The data used for parameter estimation were the bulk emulsion properties ( $\phi$ ,  $\sigma$ ,  $\rho_c$ ,  $\rho_d$ ,  $\eta_c$ ,  $\eta_d$ ), the premix volume distribution  $n_p(v, 0)$  and measured drop volume distributions  $n_p(v, t)$  for five homogenization passes. The 100 ODEs obtained from spatial discretization of the PBE model were temporally discretized using orthogonal collocation with 15 finite elements and 2 internal collocation points per element to produce a large set of nonlinear algebraic equations. Each homogenizer pass corresponded to 3 finite elements. The algebraic equation system was posed as a set of equality constraints in the nonlinear optimization problem. I found that additional spatial node points, finite elements, and/or collocation points had little effect on the param-

eter estimates but increased the computational effort significantly. The least-squares objective function  $\Psi$  used for parameter estimation was,

$$\Psi = \sum_{i=1}^N \frac{\sum_{j=1}^n [\hat{n}_p(v_j, i) - n_p(v_j, i)]^2}{\sum_{j=1}^n [n_p(v_j, i)]^2} \quad (2.13)$$

where  $n_p(v_j, i)$  is the measured value of the drop volume distribution at drop volume  $v_j$  and homogenizer pass  $i$ ,  $\hat{n}_p(v_j, i)$  is the corresponding predicted value from the discretized PBE model,  $n$  is the total number of spatial node points, and  $N$  is the number of passes. The objective function was minimized subject to the large number of equality constraints representing the discretized model equations as well as continuity conditions across the finite elements. The optimization problem was formulated in AMPL [25] and solved using the nonlinear program solver CONOPT [23]. I found that the solution was relatively insensitive to the initial guess of the parameter values, so an acceptable solution could be found with only a small number of guesses. Values of the objective function  $\Psi$  were used to judge the quality of model predictions for different experiments.

## 2.4 Results and Discussion

### 2.4.1 Parameter Estimation for Base Case Conditions

The PBE models, Eqs.(5.3 and 6.1), contained adjustable parameters that were estimated from experimental data collected at the base case conditions (Table 3.2) to allow predictions for other emulsion formulations and homogenization conditions. More specifically, the constants  $K_1 - K_4$  in the breakage rate function and  $K_5 - K_6$  in the coalescence frequency function were estimated from bulk emulsion properties ( $\phi$ ,  $\sigma$ ,  $\rho_c$ ,  $\rho_d$ ,  $\eta_c$ ,  $\eta_d$ ), the premix volume distribution  $n_p(v, 0)$  and drop volume distributions  $n_p(v, t)$  for five homogenization passes. Parameter estimation was performed for both the breakage-only PBE model (5.3) and the full PBE model (6.1) to assess the value of including drop coalescence. The breakage-only model produced noticeable

errors in predicted volume distributions (Fig. 3.1(a)) and Sauter mean diameters (Fig. 3.1(b)) despite explicit fitting of the parameters for these conditions. By comparison, the full PBE model produced very accurate predictions (Figs. 2.1(c)) and 2.1(d)). The overall quality of prediction was quantified with the objective function value, which was  $\Psi = 0.1348$  for the breakage-only model and decreased by a factor of 5 for the full model ( $\Psi = 0.0254$ ). The full model generated much more accurate predictions because the base case conditions of a 50/1 oil-surfactant ratio and 800 bar homogenization pressure favored coalescence because inadequate surfactant was available to stabilize the small drops produced.

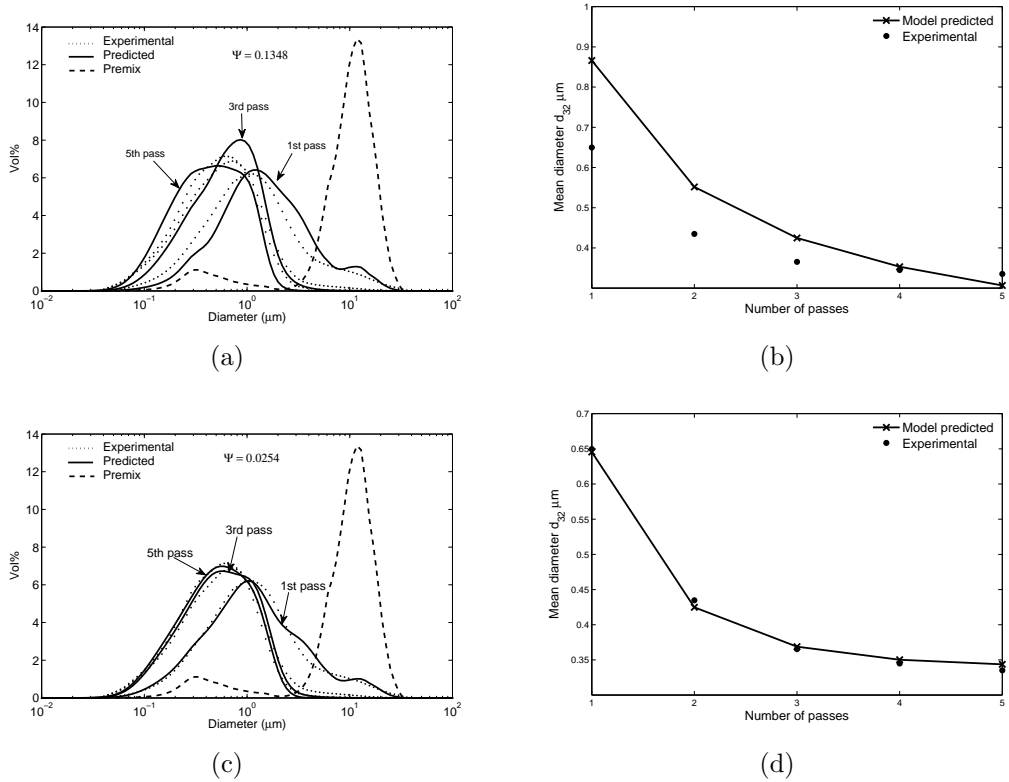


**Figure 2.1.** Experimental and model predicted results for the emulsion formulation with 50wt% oil, 1wt% PF-68 homogenized at 800 bar (a) Drop size distributions using PBE model with breakage function only ( $\Psi = 0.1348$ ); (b) Sauter mean diameter using PBE model with breakage function only; (c) Drop size distribution using PBE model with breakage and coalescence functions ( $\Psi = 0.0254$ ); (d) Sauter mean diameter using PBE model with breakage and coalescence functions

### 2.4.2 Parameter Estimation for Different Pressures and Surfactant Concentrations

The model parameters were re-estimated for different homogenization pressures and surfactant concentrations than the base case values to further access the impact of including coalescence in the model description. For each case, drop volume distributions measured following five homogenization passes were used to estimate the parameters in the breakage-only PBE model (5.3) and the full PBE model (6.1). The homogenization pressure was incorporated into the models through the energy dissipation rate. While the full model produced more accurate predictions for all four pressures considered, the relative improvement over the breakage-only model decreased as the pressure decreased (Table 3.3). These results can be attributed to the production of increasingly small drops, insufficient surfactant coverage and increased coalescence at higher pressures. The surfactant concentration was incorporated into the models by adjusting the interfacial tension  $\sigma$  (Figure 5.4) in breakage and coalescence rate functions. Unlike the pressure, the full model produced approximately equal improvement over the breakage-only model for the range of surfactant concentrations considered (Table 3.4). The full model even generated substantially improved volume distribution and Sauter mean diameter predictions as compared to the breakage-only model at 5% surfactant (Fig. 5.1), conditions under which minimal coalescence was expected. Therefore, I concluded that the full model with coalescence was superior over a wide range of conditions and did not consider the breakage-only model further in this study.

### 2.4.3 Model Extensibility

Parameter estimation at the base case conditions yielded a set of model parameters  $K_1 - K_6$  that provided excellent prediction of the measured drop volume distributions used for estimation (Figs. 2.1(c)) and 2.1(d)). To examine model extensibility to

**Table 2.2.** Minimized objective function values for emulsions consisting of 50wt% oil and 1wt% Pluronic F-68 homogenized at different pressures

Pressure (bar)	Model with breakage function only	Model with breakage and coalescence functions
200	0.117	0.0769
400	0.1303	0.0744
600	0.1028	0.0315
800	0.1348	0.0254

**Table 2.3.** Minimized objective function values for emulsions homogenized at 800 bar with different oil to surfactant ratios

Oil concentration (wt%)	Pluronic F68 concentration (wt%)	Model with breakage function only	Model with breakage, coalescence functions
50	0.5	0.1782	0.0454
50	1	0.1348	0.0254
50	2	0.1248	0.0376
50	5	0.1354	0.0325

other emulsification conditions, I investigated the ability of the PBE model to predict drop volume distributions over a range of homogenization pressures and surfactant concentrations with a single set of parameters. These predictions were generated by changing the pressure in the energy dissipation rate and the interfacial tension in breakage and coalescence rate functions. As a first step towards formulation design, I attempted to adapt the PBE model to two other nonionic surfactants by first adjusting the interfacial tension and then by re-estimating the model parameters for each surfactant.

#### 2.4.3.1 Homogenization Pressure

Homogenization experiments were performed at 50% oil, 1% surfactant and four pressures (200, 400, 600 and 800 bar). Drop volume distributions were measured for five passes at each pressure, and these data were used to estimate a different set of model parameters  $K_1 - K_6$  for each pressure. Then the model parameters found at each pressure were used to predict drop volume distributions at all four pressures, with the objective function  $\Psi$  providing a measure of prediction accuracy for each case.

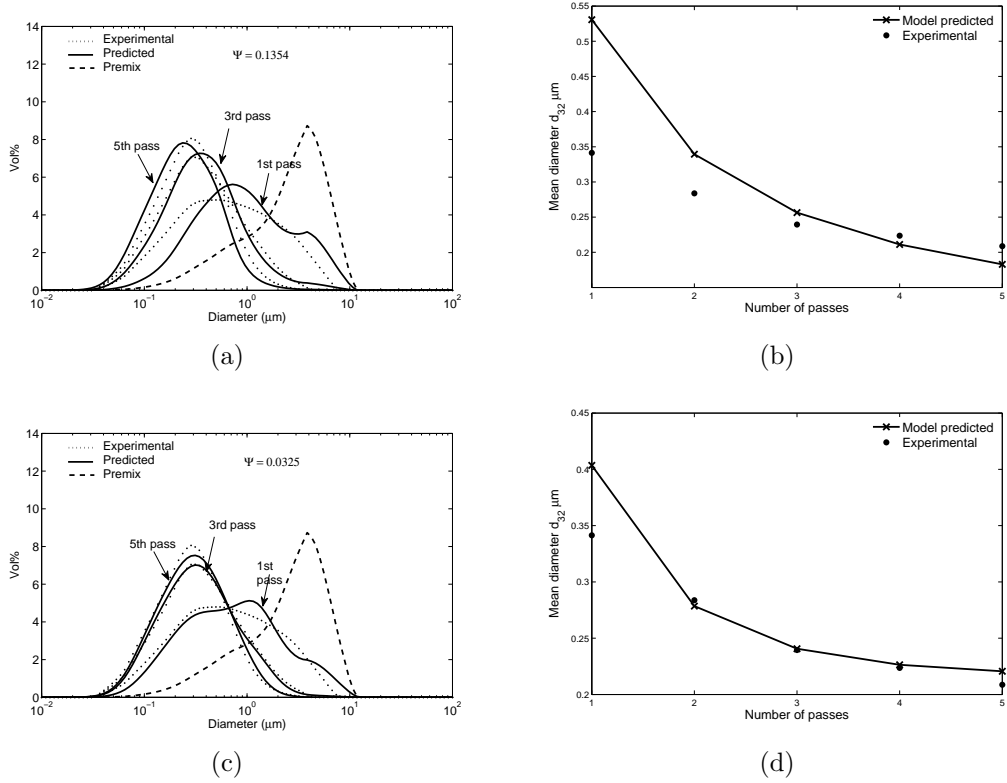


**Figure 2.2.** Experimental and model predicted results for the emulsion formulation with 50wt% oil, 5wt% PF-68 homogenized at 800 bar (a) Drop size distributions using PBE model with breakage function only ( $\Psi = 0.1354$ ); (b) Sauter mean diameter using PBE model with breakage function only; (c) Drop size distribution using PBE model with breakage and coalescence functions ( $\Psi = 0.0325$ ); (d) Sauter mean diameter using PBE model with breakage and coalescence functions

The results obtained show that parameters estimated at either pressure extreme (200 and 800 bar) generated relatively poor predictions at the other pressures (Table 3.5). Predictions with parameter estimated at 200 bar were particularly poor, most likely due to the large drops produced and limited coalescence occurring at this low pressure. Parameters estimated at intermediate pressures (400 and 600 bar) generated better predictions over the pressure range. The lowest total objective function value was obtained with the 600 bar parameters, which produced reasonable drop volume distribution predictions except at 200 bar where the breakage-coalescence balance was significantly underpredicted (Fig. 5.2). I also investigated the possible advan-

tage of using drop volume distributions collected at multiple pressures for parameter estimation. Due to limitations on optimization problem size, the computations were restricted to two pressures per dataset. The results obtained show that the two pressures chosen for estimation had little effect on prediction accuracy (Table 3.6) and that the inclusion of multiple pressures did not improve predictive capability relative to a single pressure (Table 3.5). Hence, I concluded that homogenization experiments performed at a single, intermediate pressure provided the best drop distribution data for parameter estimation.

**Table 2.4.** Objective function values at different pressures using optimal parameters  $K_1 - K_6$  obtained at one pressure for emulsions consisting of 50wt% oil and 1wt% Pluronic F-68

Pressure (bar)	Using parameters			
	at 200 bar	at 400 bar	at 600 bar	at 800 bar
200	0.07699	0.4987	1.2835	1.8954
400	0.7843	0.0485	0.3828	0.9771
600	3.1223	0.5011	0.0318	0.2421
800	5.2689	1.2484	0.2358	0.0255
Total	9.2525	2.2967	1.9339	3.1401

**Table 2.5.** Objective function values at different pressures using optimal parameters  $K_1 - K_6$  obtained at two pressures for emulsions consisting of 50wt% oil and 1wt% Pluronic F-68

Pressure (bar)	Using parameters at 200 and 400 bar	Using parameters at 400 and 600 bar	Using parameters at 200 and 800 bar
200	0.2084	0.9397	0.3229
400	0.1424	0.5308	0.4078
600	0.7554	0.2570	0.8131
800	1.5209	0.4301	1.4176
Total	2.6271	2.1576	2.9614

### 2.4.3.2 Surfactant Concentration

Homogenization experiments were performed at 50% oil, 800 bar and four surfactant concentrations (0.5, 1, 2 and 5%). Drop volume distributions were measured

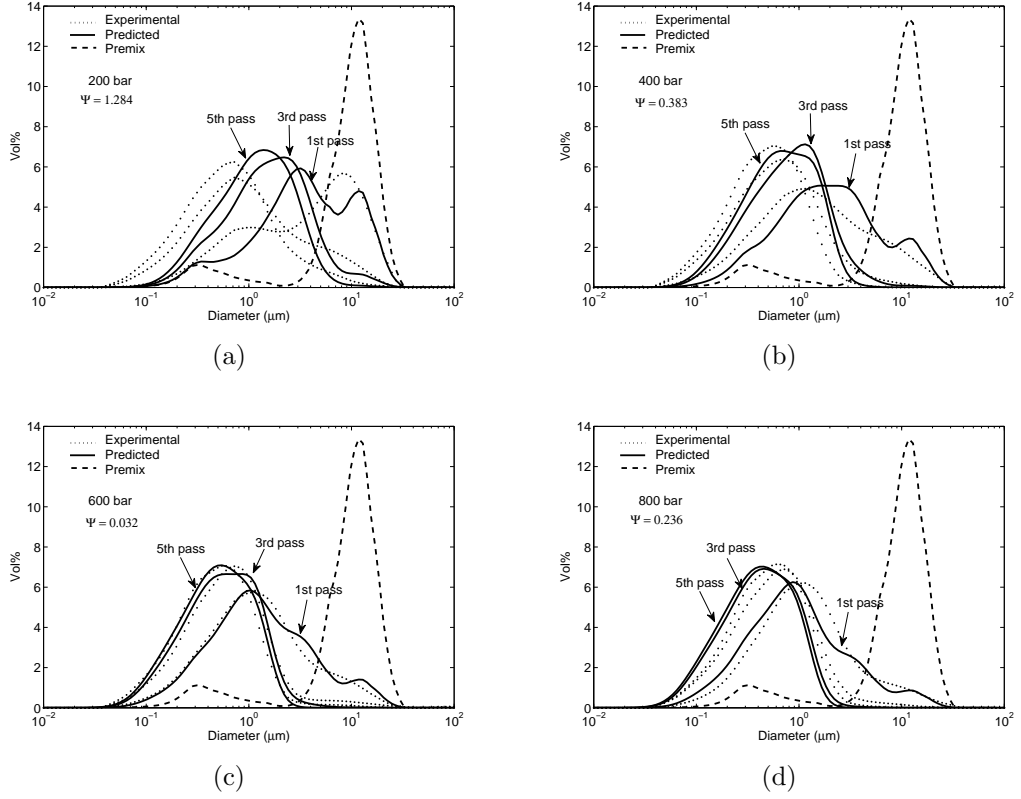


**Figure 2.3.** Experimental and model predicted drop size distributions, obtained using optimized parameters for the case of 50wt% oil, 1wt% Pluronic F-68 homogenized at 600 bar using PBE model with breakage and coalescence functions, at different pressures (a)200 bar ( $\Psi = 1.284$ ), (b)400 bar ( $\Psi = 0.383$ ), (c)600 bar ( $\Psi = 0.032$ ), (d)800 bar ( $\Psi = 0.236$ )

for five passes at each surfactant concentration, and these data were used to estimate a different set of model parameters  $K_1 - K_6$  for each concentration. Then the model parameters found at each concentration were used to predict drop volume distributions at all four concentrations. The results obtained show that parameters estimated at the lowest surfactant concentration (0.5%) generated relatively poor predictions at the other concentrations (Table 2.6), as the breakage-coalescence balance was generally underpredicted. By contrast, parameters estimated at the other three concentrations (1, 2 and 5%) generated acceptable predictions over the surfactant range investigated. The lowest total objective function value was obtained with the

1% concentration parameters, which produced reasonable drop volume distribution predictions for all four surfactant concentrations (Fig. 5.3). Therefore, I concluded that homogenization experiments performed at a single, sufficiently large surfactant concentration provided satisfactory drop distribution data for parameter estimation.

**Table 2.6.** Objective function values at different oil to surfactant ratios using optimal parameters  $K_1 - K_6$  obtained at one oil to surfactant ratio for emulsions homogenized at 800 bar

Oil-surfactant concentrations (wt%-wt%)	Using parameters at			
	50-0.5 wt%-wt%	50-1 wt%-wt%	50-2 wt%-wt%	50-5 wt%-wt%
50-0.5	0.0456	0.4575	1.1376	0.9605
50-1	0.6213	0.0254	0.4193	0.4056
50-2	1.9941	0.4834	0.0376	0.1165
50-5	1.6255	0.2051	0.2268	0.0325
Total	4.2665	1.1714	1.8213	1.5151

### 2.4.3.3 Surfactant Type

As a first step towards emulsion formulation design, I investigated the ability of the PBE model to predict drop volume distributions for two other nonionic surfactants (Pluronic F-127 and Tween 60) at different oil-surfactant ratios. First the model parameters  $K_1 - K_6$  were fixed at the values estimated from Pluronic F-68 base case data, the interfacial tension for each surfactant was calculated from (3.1) according to the surfactant concentration, and the PBE model was simulated with the calculated interfacial tension used in the breakage and coalescence rate functions. Comparisons of interfacial tension data and predictions obtained from (3.1) for Pluronic F-127 and Tween 60 are shown in Figure 5.4. The Pluronic F-127 predictions were generally less accurate than those obtained for Pluronic F-68. As the critical micelle concentration of Tween 60 is very low (0.0026 wt%), the interfacial tension value was assumed to be independent of the surfactant concentration. When the model parameters were fixed at the Pluronic F-68 values, the PBE model generated inaccurate predictions of drop volume distributions for both Pluronic F-127 and Tween 60 as measured by objective

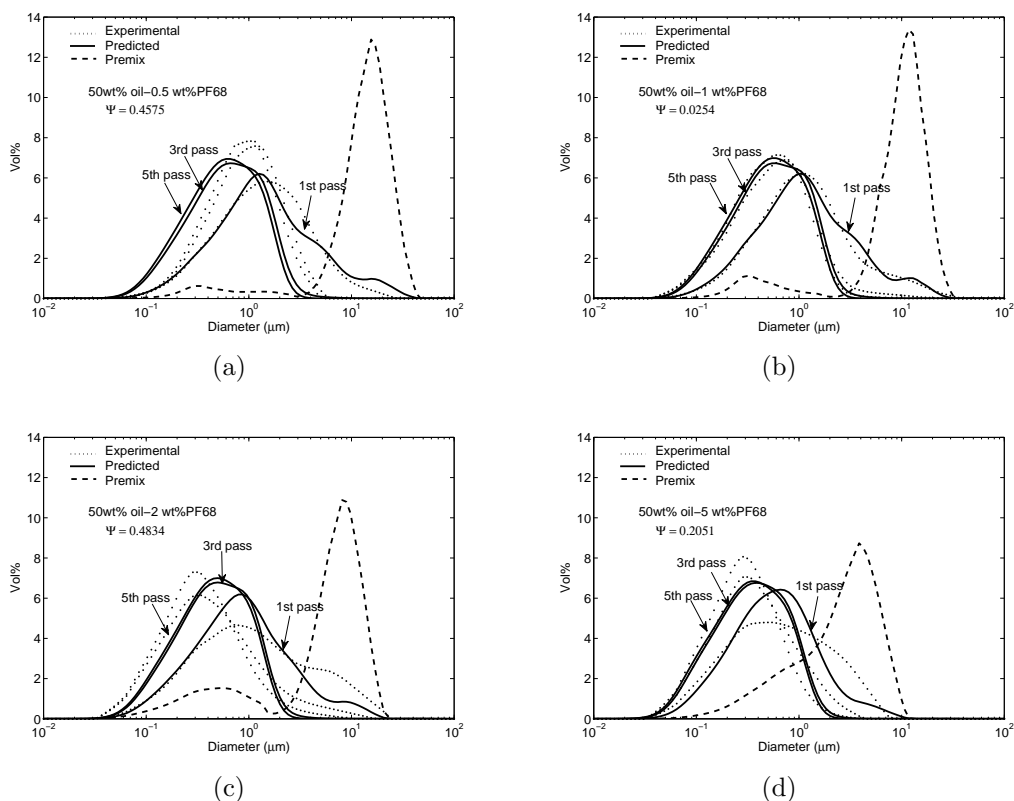


**Figure 2.4.** Experimental and model predicted drop size distributions, obtained using optimized parameters for the base case formulation using PBE model with breakage and coalescence functions, at different oil-surfactant ratios (a)50-0.5 wt% ( $\Psi = 0.4575$ ), (b)50-1wt% ( $\Psi = 0.0254$ ), (c)50-2wt% ( $\Psi = 0.4834$ ), (d)50-5wt% ( $\Psi = 0.2051$ )

function values (Table 2.7). The predictions were particularly poor for Pluronic F-127, demonstrating that one set of model parameters was not sufficient to describe multiple surfactants.

Consequently, I re-estimated the model parameters for each surfactant using bulk emulsion properties, the premix volume distribution and drop volume distributions for 50% oil, 1% surfactant and five homogenization passes following the procedure used for Pluronic F-68. With surfactant specific parameters, the PBE model was able to generate satisfactory predictions over the range of surfactant concentrations investigated (Table 2.7). The Pluronic F-127 PBE model produced reasonable drop

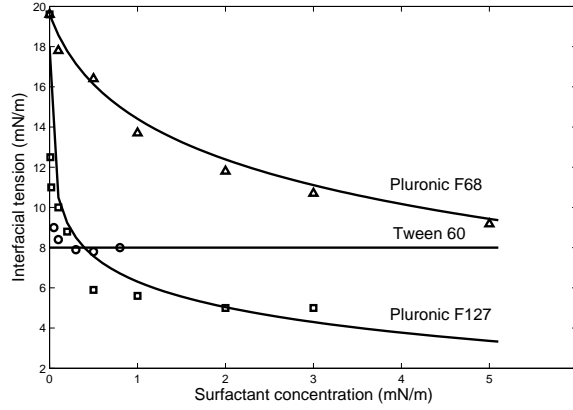


**Figure 2.5.** Interfacial tension values for different surfactants

**Table 2.7.** Objective function values at different oil to surfactant ratios using optimal parameters  $K_1 - K_6$  obtained for one surfactant at 50wt% oil and 1wt% surfactant for emulsions homogenized at 800 bar

Oil-surfactant concentrations (wt%-wt%)	PF-68 with		PF-127 with		Tween60 with	
	PF-68 parameters	PF-68 parameters	PF-127 parameters	PF-127 parameters	PF-68 parameters	Tween 60 parameters
50-0.5	0.4575	2.2807	0.2283	2.7315	0.7497	
50-1	0.0254	2.4369	0.0127	0.8322	0.0308	
50-2	0.4834	3.7747	0.0530	0.2978	0.2539	
50-5	0.2051	7.2886	0.5387	0.1479	0.2550	
Total	1.1714	15.7809	0.8327	4.0094	1.2894	

volume distribution predictions for all four surfactant concentrations, with the largest errors observed at 0.5% and 5% surfactant where the breakage-coalescence balance was overestimated and the model generated smaller drops than observed experimentally (Fig. 5.5). Similar results were obtained with the Tween 60 PBE model except that the breakage-coalescence balance was underestimated at higher surfactant concentrations and the model generated larger drops than observed experimentally (Fig. 5.6) . Therefore, I concluded that the PBE model was extensible to other surfactants if the adjustable model parameters were estimated for each surfactant using suitably chosen base case data.

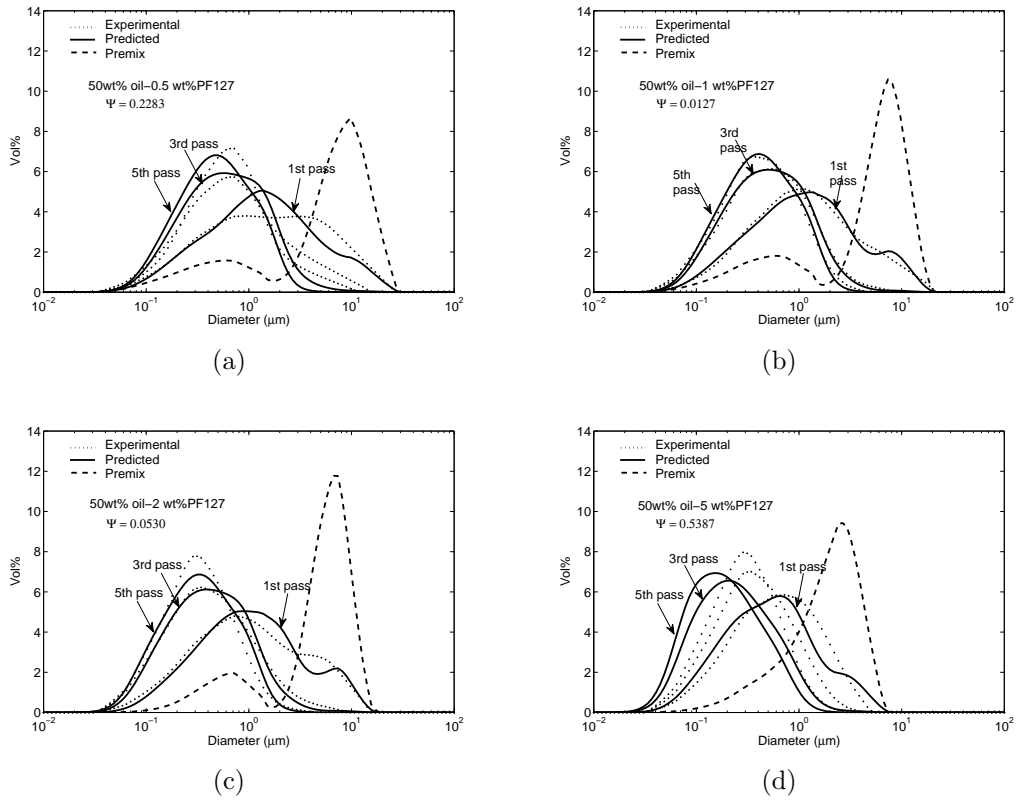


**Figure 2.6.** Experimental and model predicted drop size distributions, obtained using optimized parameters for the case of 50wt% oil, 1wt% Pluronic F127 homogenized at 800 bar using PBE model with breakage and coalescence functions, at different oil-surfactant ratios (a) 50-0.5 wt% ( $\Psi = 0.2283$ ), (b) 50-1wt% ( $\Psi = 0.0127$ ), (c) 50-2wt% ( $\Psi = 0.0530$ ), (d) 50-5wt% ( $\Psi = 0.5387$ )

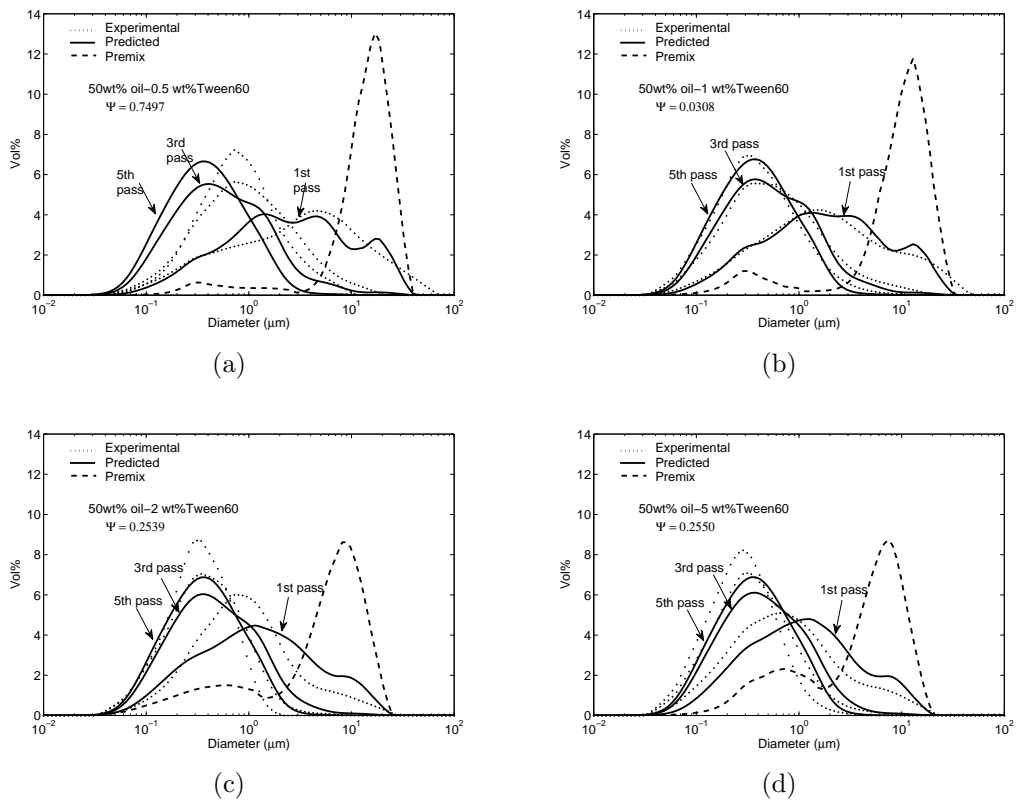


**Figure 2.7.** Experimental and model predicted drop size distributions, obtained using optimized parameters for the case of 50wt% oil, 1wt% Tween 60 homogenized at 800 bar using PBE model with breakage and coalescence functions, at different oil-surfactant ratios (a) 50-0.5 wt% ( $\Psi = 0.7497$ ), (b) 50-1wt% ( $\Psi = 0.0308$ ), (c) 50-2wt% ( $\Psi = 0.2539$ ), (d) 50-5wt% ( $\Psi = 0.2550$ )

## 2.5 Conclusions

I developed a population balance equation (PBE) model of high pressure homogenization that accounts for emulsion drop breakage and coalescence under high oil-to-surfactant ratios commonly encountered in industry. Drop coalescence was incorporated into the previously developed breakage-only PBE model through the addition of two functions for the drop collision rate and the coalescence efficiency of collisions. Mechanistic breakage and coalescence functions were used to allow the PBE model to have predictive capability over a range of emulsion compositions and homogenization conditions. The model contained six adjustable parameters that were estimated by nonlinear optimization from drop volume distribution measurements obtained at a specified base case condition. The PBE model with coalescence was shown to produce vastly superior distribution predictions over a range of homogenization pressures and surfactant concentrations compared to the breakage-only PBE model. The base case condition chosen for parameter estimation was shown to have a substantial impact on predictive capability, with conditions at the low and high extremes of the prediction range being generally unfavorable. While satisfactory predictions were obtained with a single set of model parameters for Pluronic F-68 surfactant, the parameters had to be re-estimated for the other two non-ionic surfactants (Pluronic F-127 and Tween 60) investigated to generate acceptable drop volume distribution predictions. These results suggested that limited homogenization data must be collected for each surfactant of interest for the PBE model to generate sufficiently accurate predictions to be used for emulsified product design.

## CHAPTER 3

# PREDICTING THE EFFECTS OF SURFACTANT COVERAGE ON DROP SIZE DISTRIBUTIONS OF HOMOGENIZED EMULSIONS

### 3.1 Introduction

In this chapter, I present a new PBE model for predicting drop size distributions of homogenized emulsions that is extensible to different surfactant types. This capability was achieved by extending my previous PBE model to include surfactant specific parameters associated with adsorption equilibria under the assumption of fast adsorption kinetics. More specifically, the extended model was developed by adding a surfactant mass balance, including the effects of the free surfactant concentration on the interfacial tension and the surface coverage of drops, and by modeling the coalescence frequency to be a function of the surface coverage. These modifications allowed the amount of drop coalescence to be automatically adjusted for each surfactant without the need for additional homogenization experiments and parameter re-estimation. To evaluate the new model, I performed homogenization experiments with the Pluronic family of non-ionic surfactants. Values of the adjustable model parameters were obtained by nonlinear optimization using measured drop size distributions collected at 50 wt% oil and 1 wt% Pluronic F68 surfactant. Then these parameter values were used to predict drop size distributions at 50 wt% oil and 0.5-2.0 wt% surfactant for Pluronic F68 and three other Pluronic surfactants. The predictive capability of the extended model was assessed by comparing distribution predictions to those generated with my previous model that lacked surfactant specific adsorption equilibria and neglected time-varying surface coverage and interfacial tension.

## **3.2 Experimental Methods**

### **3.2.1 Materials**

Oil-in-water emulsions were prepared using vegetable oil (Fisher Scientific) as the dispersed phase and ultrapure water as the continuous phase. Homogenization experiments were performed using high oil concentration and relatively low surfactant concentrations to promote drop coalescence and mimic typical industrial conditions. The base case emulsion consisted of 50 wt% oil, 1 wt% Pluronic F-68 surfactant (Sigma), and the remainder water. To test predictive capability of the model, additional experiments were performed at two other Pluronic F-68 concentrations (0.5 and 2.0 wt%). To examine model extensibility to other nonionic surfactants, Pluronic F-127 (Sigma), Pluronic F-87 (BASF), and Pluronic F-108 (BASF) were used as the surfactant in place of Pluronic F-68.

### **3.2.2 Emulsion Preparation**

Emulsions were prepared using a two-step procedure. In the first step, approximately 50 ml of coarse pre-emulsion was prepared by mixing the ingredients in a rotor-stator device (Ultra-Turrax Model T25, Rose Scientific Ltd.) at 16000 rpm for 4 minute. The second step was to pass the coarse emulsion through a high-pressure homogenizer (Emulsiflex C-3, Avestin Inc.) to reduce the average drop size. To produce very small drops that were likely to result in surfactant limitation and coalescence, the homogenization pressure was chosen as 800 bar. The emulsion was passed through the homogenizer five times, and after each pass approximately 2 ml was sampled to analyze the drop size distribution.

### **3.2.3 Emulsion Characterization**

Drop size distributions were measured using a standard light scattering device (Mastersizer S, Malvern Instruments). Phase densities and viscosities as well as the interfacial tension were measured prior to each homogenization experiment. Con-

tinuous and dispersed phase densities were measured using a densitometer (Model 36XMX, Bio-Rad). Continuous and dispersed phase viscosities were measured using a Ubbelohde type capillary viscometer (Model CT-1000, Canon Instruments Company) at 25°C. The oil-water interfacial tension  $\sigma_{o/w}$  was measured by drop shape analysis (Model DSA-10 Tensiometer, KRUSS Instruments) at 25°C. The interfacial tension  $\sigma$  at surfactant concentration  $c$  and temperature  $T$  was calculated as,

$$\sigma = \sigma_{o/w} - RT\Gamma_{\infty} \ln \left( 1 + \frac{c}{c_{1/2}} \right) \quad (3.1)$$

where  $\Gamma_{\infty}$  is maximum surface coverage and  $c_{1/2}$  is the surfactant concentration corresponding to half of the maximum surface coverage. The constants  $\Gamma_{\infty}$  and  $c_{1/2}$  were found for each surfactant by fitting Eq. (3.1) to measured interfacial tensions at different surfactant concentrations.

### 3.3 Theory

#### 3.3.1 Population Balance Equation (PBE)

The population balance equation (PBE) is formally derived from a number balance on particles by accounting for their rates of creation and disappearance [63]. Because the light scattering device used in this study most directly measured drop volume distributions, I utilized a volume structured PBE model rather than a model represented in terms of particle number. Although local shear forces can change dramatically near the homogenization valve [28], I assumed the homogenizer to be a well-mixed batch system to avoid complexities associated with modeling spatial variations. The PBE derived from a number balance can be written as follows [16, 49],

$$\begin{aligned} \frac{\partial n(v, t)}{\partial t} = & -g(v)n(v, t) + \int_v^{\infty} \beta(v, v')g(v')n(v', t)dv' \\ & -n(v, t) \int_0^{\infty} C(v, v')n(v', t)dv' + \frac{1}{2} \int_0^v C(v - v', v')n(v - v', t)n(v', t)dv' \end{aligned} \quad (3.2)$$

where  $v$  is the volume of the particle;  $n(v, t)dv$  is the number of drops with volume in the range  $[v, v + dv]$  per unit volume of dispersion at time  $t$ ;  $g(v)$  is the breakage frequency representing the fraction of drops of volume  $v$  breaking per unit time;  $\beta(v, v')$  is the daughter drop distribution function representing the probability of forming a daughter drop of size  $v$  from breakage of a mother drop of size  $v'$ ; and  $C(v, v')$  is coalescence frequency representing the rate at which drops of size  $v$  and size  $v'$  coalesce. The first and third terms on the right hand side of Eq. (6.1) are the rates of disappearance of drops of size  $v$  due to breakage and coalescence, respectively, while the second and fourth terms are the rates of appearance of drops of size  $v$  due to breakage and coalescence, respectively. Assuming that drops are spherical, the number and volume distributions are related as follows,

$$n(v, t) = \frac{V_{tot}n_p(v, t)}{v} \quad (3.3)$$

where  $V_{tot}$  is the conserved total volume of the drops. The PBE (Eq. 6.1) can be written in terms of  $n_p(v, t)$  as follows [49],

$$\begin{aligned} \frac{dn_p(v, t)}{dt} = & -g(v)n_p(v, t) + v \int_v^\infty \frac{\beta(v, v')g(v')n_p(v', t)}{v'} dv' \\ & -n_p(v, t) \int_0^\infty \frac{C(v, v')n_p(v', t)V_{tot}}{v'} dv' \\ & + \frac{v}{2} \int_0^v \frac{C(v - v', v')n_p(v - v', t)n_p(v', t)V_{tot}}{v'(v - v')} dv' \end{aligned} \quad (3.4)$$

I assumed that drop breakage and coalescence only occurred in the valve gap, and that these mechanisms were uniform throughout the gap region. Because the volumetric flow rate through the homogenizer was constant, the emulsion was assumed to have a constant residence time in the gap region and each pass was taken to be one dimensionless time unit. The drop volume distribution of the pre-mix or the previous pass was used as the initial condition for the subsequent pass. The actual homogenizer

had a more complex geometry that would require more complex modeling tools such as computational fluid dynamics (e.g. Raikar et al., 2009) to adequately describe. More sophisticated flow modeling was deemed outside the scope of the present study.

### 3.3.1.1 PBE Functions

The PBE (6.1) requires size-dependent functions for the breakage frequency ( $g(v)$ ), the daughter drop distribution ( $\beta(v, v')$ ), and the coalescence frequency ( $C(v, v')$ ). Following my previous work [49, 60], the breakage function  $g(v)$  was assumed to be sum of two functions representing different breakage mechanisms such that  $g(v) = g_1(v) + g_2(v)$ . The first breakage function  $g_1(v)$  accounts for drop breakage due to collision with turbulent eddies [16],

$$g_1(v) = K_1 v^{-2/9} \epsilon^{1/3} \left[ \exp - \left( \frac{K_2 \sigma (1 + \phi)^2}{\rho_d v^{5/9} \epsilon^{2/3}} \right) \right] \quad (3.5)$$

where  $K_1$  and  $K_2$  are adjustable parameters. The second breakage function  $g_2(v)$  was derived assuming that drop breakage results from turbulent shear [60],

$$g_2(v) = K_3 \left( \frac{2}{\pi} \right)^{1/2} \left( \frac{\epsilon \rho_d}{\eta_d} \right)^{1/2} \left[ \exp \left( - \frac{K_4 \sigma^2 \lambda}{v^{2/3} \epsilon \eta_c} \right) \right] \quad (3.6)$$

where  $K_3$  and  $K_4$  are adjustable parameters. The two breakage functions depend on the homogenizer pressure  $P$  through the energy dissipation rate  $\epsilon$  (see below) and bulk emulsion properties including the dispersed phase volume fraction  $\phi$ , the interfacial tension  $\sigma$ , the dispersed phase density  $\rho_d$ , and the continuous phase viscosity  $\eta_c$  and dispersed phase viscosity  $\eta_d$  through the ratio  $\lambda = \frac{\eta_d}{\eta_c}$ . The daughter drop distribution function  $\beta(v, v')$  was chosen such that multiple daughter drops were formed from a single breakage event. More specifically, a mother drop was assumed to break into a fixed number of daughter drops of potentially different size. In this study, breakage was assumed to produce 80 daughter drops because this number provided the best fit to distribution data in my previous work [49]. However, I found that prediction quality

was not very sensitive to this number as long as it was sufficiently large ( $> 20$ ). Clearly the use of this fixed parameter is a simplification that could potentially be improved if turbulent drop breakage in dense suspensions could be experimentally studied. To my knowledge, the necessary experiments are not currently feasible and the proposed simplification is reasonable given knowledge about turbulent drop breakage.

The coalescence frequency  $C(v, v')$  was calculated as the product of the drop collision frequency  $h(v, v')$  and the coalescence efficiency  $\Lambda(v, v')$  such that  $C(v, v') = h(v, v')\Lambda(v, v')$ . The collision frequency function was derived from the kinetic theory of gases assuming that drops in turbulent conditions behave like gas molecules [16],

$$h(v, v') = \frac{K_5 \epsilon^{1/3}}{(1 + \phi)} (v^{2/3} + v'^{2/3})(v^{2/9} + v'^{2/9})^{1/2} \quad (3.7)$$

where  $K_5$  is an adjustable parameter. The coalescence efficiency function was derived by assuming that drop coalescence occurs if the contact time between two drops is greater than the time required for the liquid film between the drops to drain [16],

$$\Lambda(v, v') = \exp \left[ \frac{-K_6 \eta_c \rho_c \epsilon}{\sigma^2 (1 + \phi)^3} \left( \frac{v^{1/3} v'^{1/3}}{v^{1/3} + v'^{1/3}} \right)^4 \right] \quad (3.8)$$

where  $K_6$  is an adjustable parameter. Similar to the breakage frequency, the coalescence frequency depends on the homogenizer pressure  $P$  through the energy dissipation rate  $\epsilon$  and the bulk emulsion properties  $\rho_c$ ,  $\eta_c$ ,  $\phi$ , and  $\sigma$ . The breakage and coalescence frequency functions both depend on the energy dissipation rate, which was modeled with the following relation [84, 83],

$$\epsilon = \frac{\Delta P Q}{V_{diss}} \quad (3.9)$$

where  $\Delta P$  is the applied pressure,  $Q$  is the volumetric flow rate, and  $V_{diss}$  is the valve gap volume which depends on valve gap distance  $h_{gap}$ . Equations for  $V_{diss}$  and  $h_{gap}$  can be found in the previous work [60].

### 3.3.2 Extended PBE Model

My previous model of combined drop breakage and coalescence consisted of the PBE (Eq. 6.1) with the breakage and coalescence functions described in the previous section [49]. I will refer to this model as the “basic PBE model” in the remainder of the chapter. While the basic model has proved capable of generating satisfactory predictions of the drop size distribution over a range of surfactant concentrations [49], the model lacked a fundamental description of surfactant behavior. Instead, a constant value of the interfacial tension was calculated according to the surfactant concentration used in each experiment. I hypothesized that this simplification was largely responsible for the observed inability of the basic model to describe different surfactants without re-estimation of the adjustable parameters using drop size distribution measurements collected for the new surfactants [49]. I now present a new PBE model that includes a description of time-varying surfactant adsorption and its associated effects on drop surface coverage, interfacial tension, and drop coalescence. I will refer to this model as the “extended PBE model” in the remainder of the chapter. The extended model is based on the assumption of fast adsorption kinetics because kinetic parameters are difficult to obtain experimentally [82, 78]. Moreover, the Pluronic surfactants considered in this study were expected to have fast adsorption kinetics.

The free surfactant concentration decreases as large drops break to form smaller drops and more surfactant molecules are adsorbed on the oil-water interface. The time-dependent free surfactant concentration ( $C_s$ ) was calculated by a surfactant mass balance as follows:

$$\frac{dC_s}{dt} = -\frac{6\phi}{(1-\phi)} \frac{d\left(\frac{\Gamma}{d_{32}}\right)}{dt} \quad (3.10)$$

where  $d_{32}$  is the Sauter mean diameter of the emulsion and  $\Gamma$  is the surface coverage of surfactant. The initial value of the free surfactant concentration  $C_{si}$  was calculated by solving the following mass balance equation:

$$C_{si} = C_{s_{input}} - \frac{6\phi}{1-\phi} \frac{\Gamma_{\infty} C_{si}}{C_{si} + C_{1/2}} \frac{1}{d_{32pre}} \quad (3.11)$$

where  $d_{32pre}$  is Sauter mean diameter of the premix emulsion,  $C_{s_{input}}$  is the surfactant concentration used to prepare the emulsion,  $\Gamma_{\infty}$  is maximum surface coverage, and  $C_{1/2}$  is the surfactant concentration corresponding to half of the maximum surface coverage. The interfacial tension ( $\sigma$ ) was modeled to increase as free surfactant was depleted to stabilize newly formed drop surfaces [10, 8]:

$$\sigma = \sigma_{o/w} - RT\Gamma_{\infty} \ln \left( 1 + \frac{C_s}{C_{1/2}} \right) \quad (3.12)$$

The equilibrium surfactant coverage on the drop surface was assumed to follow the Langmuir isotherm:

$$\Gamma = \Gamma_{\infty} \left( \frac{C_s}{C_s + C_{1/2}} \right) \quad (3.13)$$

The coalescence frequency was modified to depend on the drop surface coverage  $\Gamma$  because the coalescence efficiency should increase as the surface coverage decreases and drops are less stable. This effect was modeled as follows:

$$C^*(v, v', \Gamma) = \left( 1 - \frac{\Gamma}{\Gamma_{\infty}} \right)^2 C(v, v') \equiv \eta^2 C(v, v') \quad (3.14)$$

where  $C^*(v, v', \Gamma)$  is the modified coalescence frequency function and  $C(v, v')$  is the coalescence frequency function used in the basic PBE model. The multiplicative term  $\eta^2 = \left( 1 - \frac{\Gamma}{\Gamma_{\infty}} \right)^2$  captures the increased tendency of two drops to coalesce when the surface coverage is below the maximum coverage. Equations (4.9)–(3.14) represent the new equations added to the basic model to generate the extended model.

### 3.3.3 Dynamic Simulation and Parameter Estimation

The integral expression in the PBE (6.1) was approximated numerically using the fixed pivot technique [40] with 100 equally spaced node points. A larger number

of node points increased the computational cost of simulation but had a negligible effect on solution accuracy. Discretization produced 100 nonlinear ordinary differential equations in time with the dependent variables representing the volume percent distribution at each node point. The extended PBE model included an additional ordinary differential equation (Eq. 4.9) and two algebraic equations (Eqs. 3.12 and 4.26). The ODE system was solved with the Matlab integration code `ode15s` by embedding of the algebraic equations. The premix distribution  $n_p(v, 0)$  was used as the initial condition for the PBE, while Eq. 4.10 was used to calculate the initial condition for the free surfactant concentration. One dimensionless time unit was defined as the time of one homogenization pass such that the distribution after the  $i$ -th pass  $n_P(v, i) = n_P(v, t = i)$ .

The adjustable model parameters  $K_1 - K_6$  in the breakage and coalescence functions were estimated by nonlinear optimization using experimental data from base case homogenization experiments at 50 wt% oil and 1 wt% Pluronic F-68 surfactant. The data used were surfactant properties ( $\Gamma_\infty$ ,  $C_{1/2}$ ), bulk emulsion properties ( $\phi$ ,  $\sigma$ ,  $\rho_c$ ,  $\rho_d$ ,  $\eta_c$ ,  $\eta_d$ ), the premix volume distribution  $n_p(v, 0)$ , and measured drop volume distributions  $n_p(v, t)$  for five homogenization passes. The bulk emulsion properties are listed in the Table 3.1<sup>1</sup>. The ODE system obtained as a result of spatial discretization was temporally discretized using orthogonal collocation with 15 finite elements and 2 internal collocation points per element to obtain a set of nonlinear algebraic equations. Each pass corresponded to 3 finite elements. I found that additional finite elements and/or collocation points had little effect on the parameter estimates but increased computational effort significantly. Nonlinear optimization was performed

---

<sup>1</sup>The continuous phase viscosity  $\eta_c$  was assumed to be constant for all values of the surfactant concentration. For example, the viscosity of 1 wt% PF68 in water was found to be 1.07 mPa.s and the viscosity of pure water was 0.88 mPa.s at 25°C. Since most surfactant molecules were expected to adsorb at the oil-water interface due to the high oil/surfactant ratios used, the amount of free surfactant in the continuous phase was much lower than the added amount and the assumption of constant continuous phase viscosity was deemed reasonable.

to minimize a least square objective function  $\Psi$  with the algebraic equations posed as equality constraints. Also continuity conditions were imposed across the finite elements. The objective function  $\Psi$  used was,

$$\Psi = \sum_{i=1}^N \frac{\sum_{j=1}^n [\hat{n}_p(v_j, i) - n_p(v_j, i)]^2}{\sum_{j=1}^n [n_p(v_j, i)]^2} \quad (3.15)$$

where  $n_p(v_j, i)$  is the measured value of the drop volume distribution at drop volume  $v_j$  and homogenizer pass  $i$ ,  $\hat{n}_p(v_j, i)$  is the corresponding predicted value obtained from the discretized model,  $n$  is the total number of spatial node points, and  $N$  is the number of passes. This objective function ensured that the denominator would remain non-zero even if the number of drops in a particular volume class became identically zero. The optimization problem for the base PBE model was formulated in AMPL [25] and solved using the nonlinear program solver CONOPT. For the extended PBE model, the optimization problem was solved with the Matlab function `lsqnonlin` after obtaining good initial estimates of the parameters  $K_1 - K_6$  using Newton's method. In both cases, objective function  $\Psi$  values were used to quantify model accuracy. Optimized model parameters of base model are listed in appendix A. It is important check the effect of these parameters on the final objective function to make sure that there are no redundancies and to find out degree of linear independence of these parameters (Please see appendix A).

**Table 3.1.** Bulk properties of the emulsion system.

Density of continuous phase ( $\rho_c$ )	997.05 <i>kg/m<sup>3</sup></i>
Density of dispersed phase ( $\rho_d$ )	917.36 <i>kg/m<sup>3</sup></i>
Viscosity of continuous phase ( $\eta_c$ )	0.88 <i>mPa.s</i>
Viscosity of dispersed phase ( $\eta_d$ )	47.8 <i>mPa.s</i>
Interfacial tension of oil in water at 25°C	19.6 <i>mN/m</i>

## 3.4 Results and Discussion

### 3.4.1 Extensibility for the Surfactant Concentration

Both the base PBE model (6.1) and the extended PBE model (6.1,4.9,4.26,3.12) included six adjustable parameters ( $K_1 - K_6$ ) in the breakage and coalescence functions that were estimated from experimental data collected for a particular emulsion formulation. The data used for parameter estimation consisted of bulk emulsion properties ( $\phi, \sigma, \rho_c, \rho_d, \eta_c, \eta_d$ ), the premix drop volume distribution  $n_p(v, 0)$ , and drop volume distributions  $n_p(v, t)$  for five homogenization passes. Additional surfactant specific data were required for the extended model. In this case,  $\Gamma_\infty$  and  $C_{1/2}$  for a particular surfactant were found by fitting Eq.3.12 to data for the equilibrium interfacial tension ( $\sigma$ ) versus the free surfactant concentration ( $C_s$ ) using nonlinear least-squares optimization. The parameter estimates obtained for the four Pluronic surfactants (Table 3.2) produced satisfactory fits of the interfacial tension data (Fig 3.1a). The surfactants PF87, PF108 and PF 127 produced similar interfacial tension trends characterized by small  $C_{1/2}$  values and comparable  $\Gamma_\infty$  values. By contrast, PF68 was characterized by a substantially larger  $C_{1/2}$  value and a smaller  $\Gamma_\infty$  value than the other three surfactants. To demonstrate that the homogenization experiments were performed under surfactant limited conditions, fifth pass  $d_{32}$  values obtained for each surfactant with 50% oil and 0.5-2.0 wt% surfactant were analyzed. The results (Fig. 3.1b) showed that the mean drop size was limited by the amount of surfactant rather than the mechanical energy of the homogenizer.

**Table 3.2.** Surfactant adsorption parameters.

Surfactant	Molecular weight	$\Gamma_\infty$ ( $mol/m^2$ )	$C_{1/2}$ ( $mol/m^3$ )
Pluronic F68	8400	$1.4286 \cdot 10^{-6}$	0.7933
Pluronic F127	12600	$7.5397 \cdot 10^{-7}$	$1.7628 \cdot 10^{-4}$
Pluronic F108	14400	$4.5000 \cdot 10^{-7}$	$7.6065 \cdot 10^{-5}$
Pluronic F87	7700	$3.963 \cdot 10^{-7}$	$9.0792 \cdot 10^{-5}$

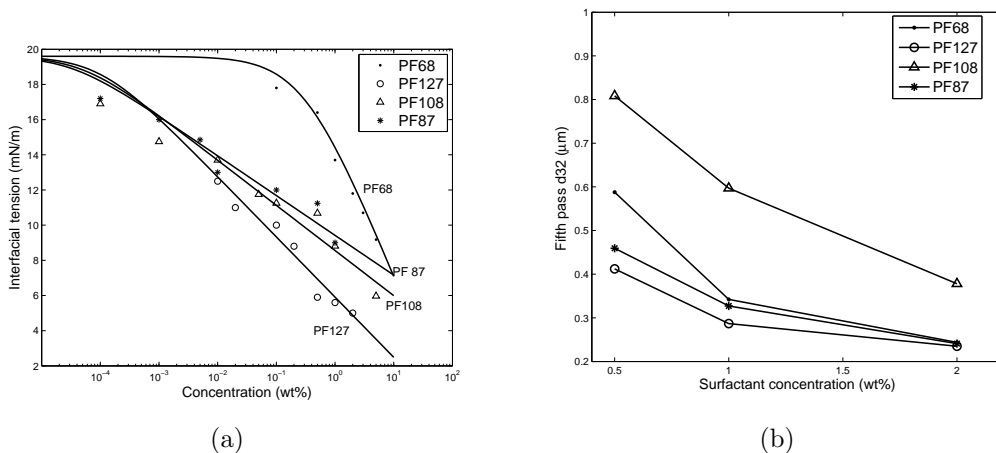


**Figure 3.1.** (a) Interfacial tension values (symbols) and model fits (solid lines) for four Pluronic surfactants; and (b) experimental Sauter mean diameters of fifth pass homogenized emulsions obtained with the four surfactants.

Given the necessary model parameters and distribution data, the six adjustable parameters ( $K_1 - K_6$ ) were estimated for both PBE models at three separate conditions: 50% oil, 0.5 wt% PF68; 50% oil, 1.0 wt% PF68; and 50% oil, 2.0 wt% PF68. The predictions obtained from the base model (Fig. 5.1, first column of Table 3.3) showed that very accurate predictions of the homogenized drop volume distributions could be produced without any surfactant specific information. Similar results were obtained for the extended model (second column of Table 3.3), demonstrating that modeling of surfactant adsorption was not necessary if parameters were estimated separately for each formulation. To investigate model extensibility to different surfactant concentrations, the next tests involved prediction of homogenized distributions at 50wt% oil, 0.5 wt% PF68 and 50% oil, 2.0 wt% PF68 using  $K_1 - K_6$  values estimated at 50 wt% oil, 1.0 wt% PF68. Results for the base model (Fig. 5.2, third column of Table 3.3) showed that distribution predictions were clearly degraded as compared to the case where separate parameter values were generated for each formulation. Although the amount of coalescence appeared to be under predicted at the lower surfactant concentration (0.5wt%) and over predicted at the higher concentration (2wt%), the

model remained capable of generating satisfactory predictions over this surfactant concentration range. Similar results were obtained for the extended model (Fig. 5.3, fifth column of Table 3.3), suggesting that modeling of surfactant adsorption was not necessary to generate acceptable distribution predictions for a single surfactant.

**Table 3.3.** Summary of model results at different oil-PF68 ratios.

Oil-PF68 concentration (wt%-wt%)	Objective function values			
	Optimized results		Extensibility results (using parameters of 50-1 wt% case)	
	Base model	Extended model	Base model	Extended model
50-0.5	0.0454	0.0540	0.4575	0.5434
50-1	0.0254	0.0286	0.0254	0.0286
50-2	0.0376	0.0390	0.4834	0.4946
Total	0.1084	0.1216	0.9663	1.066

#### 3.4.1.1 Extensibility for the Surfactant Type

Homogenization experiments and parameter estimation studies were conducted for three other surfactants (PF127, PF87 and PF108) from the Pluronic family. Like PF68, these surfactants are block co-polymers consisting of polyoxypropylene and polyoxyethylene units. The four Pluronic surfactants have different molecular weights and adsorption behavior (Table 3.2) because the number and arrangement of polyoxypropylene and polyoxyethylene units varies. Using both the basic and extended PBE models, the same set of tests were performed for the PF127, PF87 and PF108 surfactants. First, drop volume distributions collected at 50 wt% oil and 1.0 wt% surfactant were used to estimate the six adjustable parameters ( $K_1 - K_6$ ), and these parameter values were used to predict drop distributions at 50 wt% oil, 0.5 wt% surfactant and 50 wt% oil, 2.0 wt% surfactant. Then the parameter estimates obtained at 50 wt% oil and 1.0 wt% PF68 were used to predict drop volume distributions for the new surfactant without parameter re-estimation using distribution data for

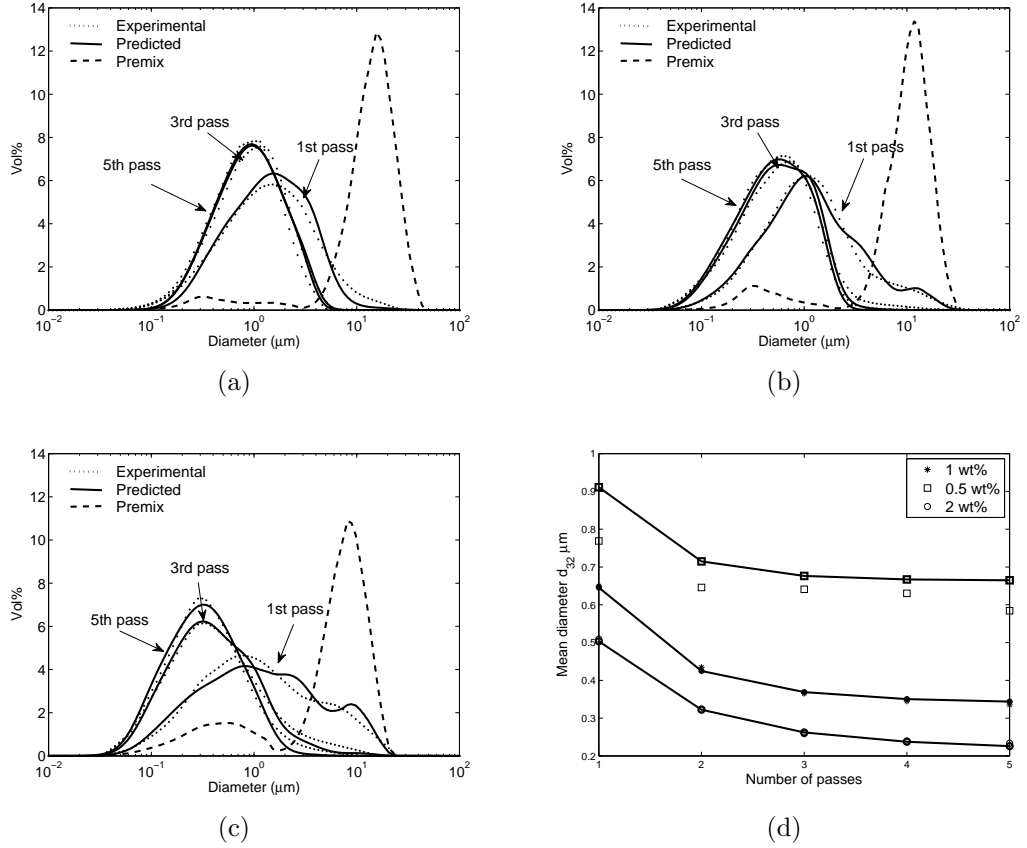


**Figure 3.2.** Experimental and model predicted drop size distributions obtained using optimized parameters found at different oil-PF68 ratios with the base model: (a) 50 wt% oil, 0.5 wt% PF68 ( $\Psi = 0.0454$ ), (b) 50 wt% oil, 1.0 wt% PF68 ( $\Psi = 0.0254$ ), (c) 50 wt% oil, 2.0 wt% PF68 ( $\Psi = 0.0376$ ), e(d) Experimental  $d_{32}$  values (symbols) and model predicted  $d_{32}$  values (solid lines).

that surfactant. In the extended model, the change in surfactant type was taken into account by using the associated surfactant properties  $\Gamma_{\infty}$  and  $C_{1/2}$ . The basic model lacked surfactant adsorption information and was used as a basis for comparison. The change in surfactant type was incorporated into the basic model by calculating an interfacial tension value from the total amount of surfactant added (0.5, 1.0 or 2.0 wt%) and using this constant value in the breakage and coalescence functions. These studies were intended to examine extensibility of the new PBE model to different surfactants using only adsorption parameters for those surfactants.

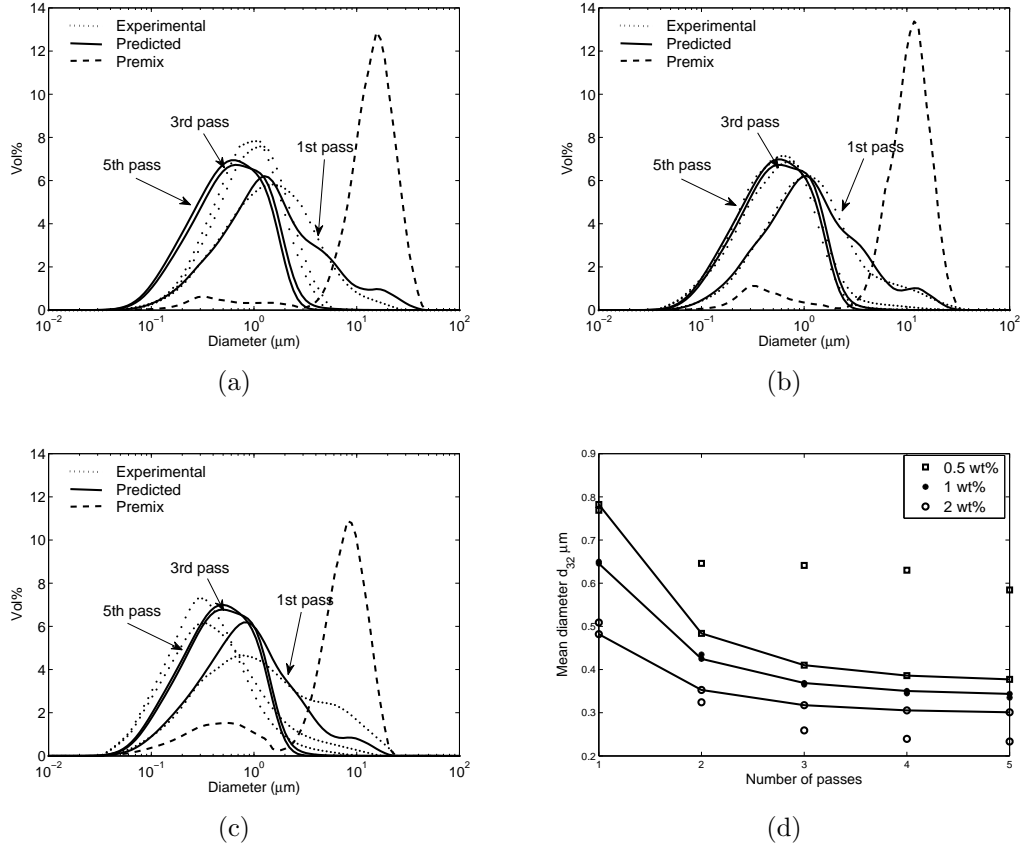


**Figure 3.3.** Experimental and model predicted drop size distributions obtained using optimized parameters found at 50 wt% oil, 1 wt% PF68 with the base model: (a) 50 wt% oil, 0.5 wt% PF68 ( $\Psi = 0.4575$ ), (b) 50 wt% oil, 1.0 wt% PF68 ( $\Psi = 0.0254$ ), (c) 50 wt% oil, 2.0 wt% PF68 ( $\Psi = 0.4834$ ), (d) Experimental  $d_{32}$  values (symbols) and model predicted  $d_{32}$  values (solid lines).

First tests were performed with the Pluronic surfactant F127. Using  $K_1 - K_6$  values estimated for 1.0 wt% PF127, the extended model produced satisfactory predictions of the homogenized distributions obtained for 0.5 and 2.0 wt% PF127 (Fig. 5.4, third column of Table 3.4). Similar results were obtained with the basic model, again suggesting that surfactant adsorption modeling was unnecessary to generate acceptable predictions for a particular surfactant (second column of Table 3.4). However, the basic model proved unacceptable when the parameters estimated for 1.0 wt% PF68 were used to predict distributions obtained with the different surfactant PF127 (Fig. 5.5, fourth column of Table 3.4). As compared to the case where the

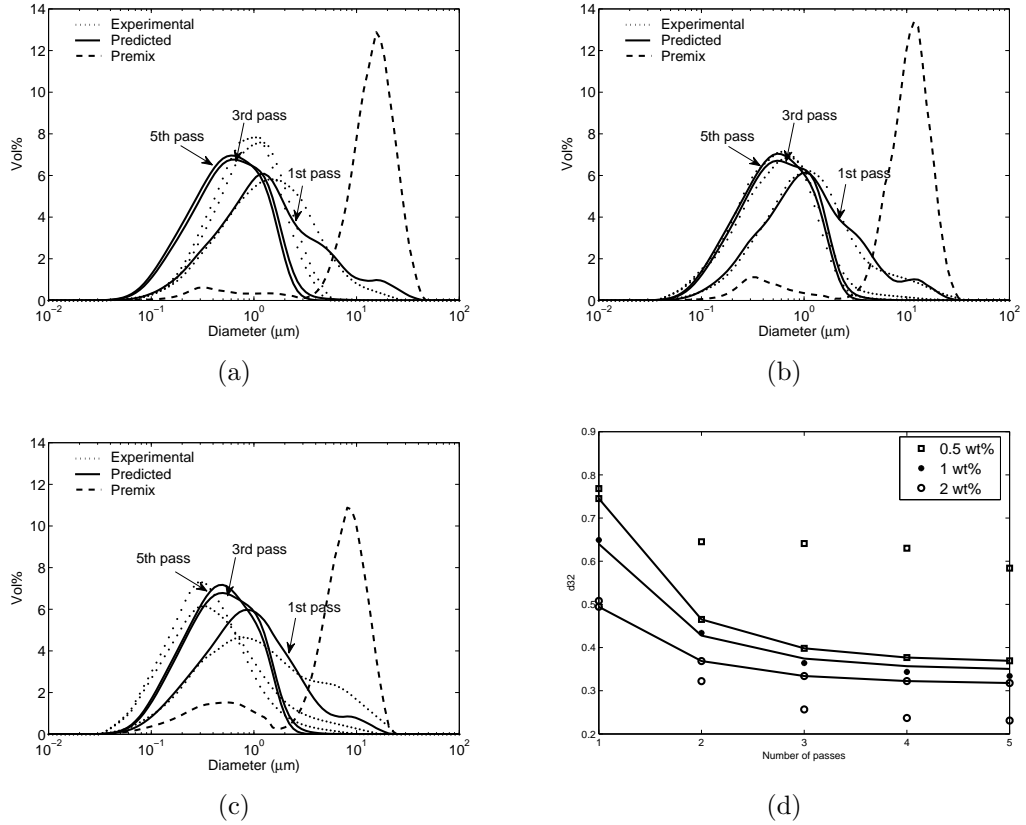


**Figure 3.4.** Experimental and model predicted drop size distributions obtained using optimized parameters found at 50 wt% oil, 1 wt% PF68 with the extended model: (a) 50 wt% oil, 0.5 wt% PF68 ( $\Psi = 0.5434$ ), (b) 50 wt% oil, 1.0 wt% PF68 ( $\Psi = 0.0286$ ), (c) 50 wt% oil, 2.0 wt% PF68 ( $\Psi = 0.4946$ ), (d) Experimental  $d_{32}$  values (symbols) and model predicted  $d_{32}$  values (solid lines).

parameters were estimated for 1.0 wt% PF127, the basic model produced approximately 30 times greater error with the PF68 parameters as measured by the total value of the objective function  $\Psi$ . By contrast, the extended model was far superior when the parameters estimated for 1.0 wt% PF68 were used to predict distributions obtained with PF127 (Fig. 5.6, fifth column of Table 3.4). Although predictions were clearly degraded as compared to the case where the parameters were estimated from PF127 distributions, the extended model remained capable of generating reasonable predictions despite using only adsorption information for PF127. When PF68 parameter values were used, the total objective function value for the extended model

was only 11% of the value obtained with the basic model. While the extended model produced a time-varying value of the interfacial tension, I found that this increase was very small and unlikely to account for the improved performance (Fig. 5.7). By contrast, the decreasing free surfactant concentration produced a large decrease in the drop coverage ( $\frac{\Gamma}{\Gamma_\infty}$ ) and corresponding increase in the coalescence efficiency factor  $\eta$  (Eq. 3.14). I believe that the improved performance of the extended model is mostly attributable to this factor, which varies between surfactants according to their adsorption behavior.

**Table 3.4.** Summary of model results at different oil-P127 ratios.

Oil-PF127 concentration (wt%-wt%)	Objective function values			
	Using base case parameters of PF127 (50wt% oil-1wt% PF127)		Using base case parameters of PF68 (50wt% oil-1wt% PF68)	
	Base Model	Extended Model	Base Model	Extended Model
50-0.5	0.2283	0.2749	2.6046	0.5567
50-1	0.0127	0.0145	2.6126	0.1484
50-2	0.0530	0.0768	3.4692	0.2824
Total	0.2940	0.3662	8.6864	0.9877

Next homogenization experiments and model extensibility studies were performed with PF108. Using  $K_1 - K_6$  values estimated for 1.0 wt% PF108, the basic and extended models produced similar predictions of homogenized distributions obtained for 0.5 and 2.0 wt% PF108 (second and third columns of Table 3.5). However, the basic model performed poorly when the parameters estimated for 1.0 wt% PF68 were used to predict PF108 distributions (fourth column of Table 3.5). The extended model performed much better when the parameters estimated for 1.0 wt% PF68 were used to predict PF108 distributions (Fig. 5.8, fifth column of Table 3.5). However, the improvement obtained with the extended model was not as large as that observed for PF127, with the total objective function value for the extended model being 39% of the value obtained with the basic model when PF68 parameters were used.

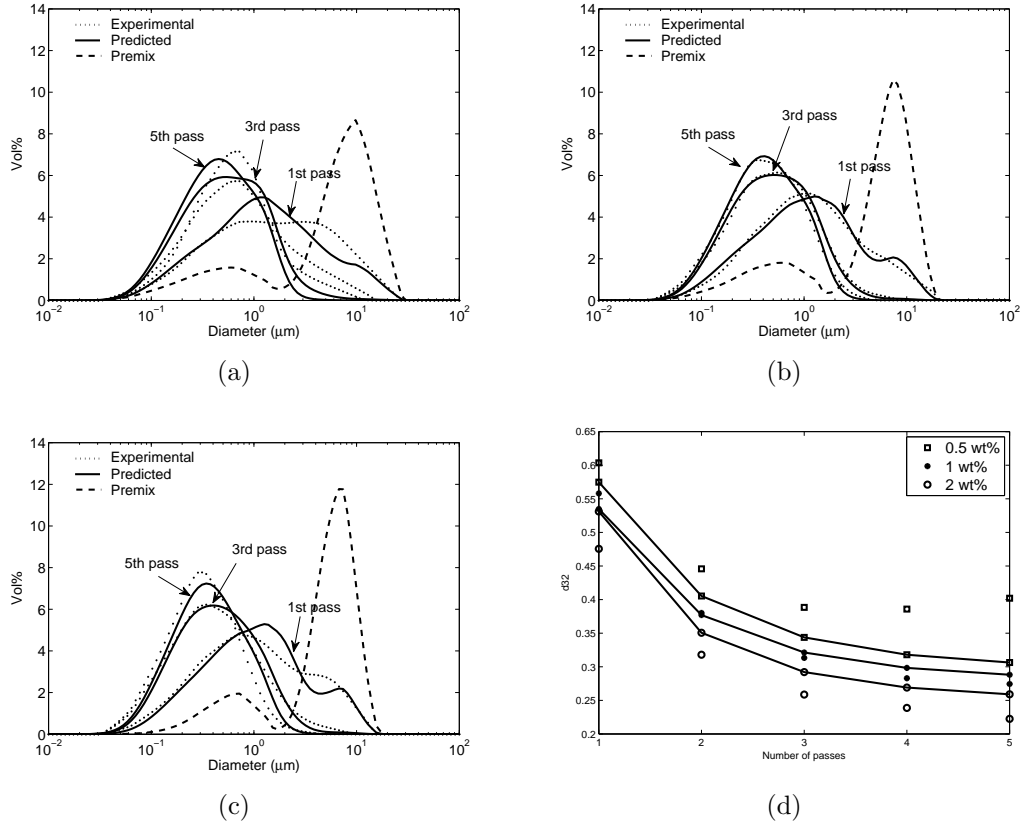


**Figure 3.5.** Experimental and model predicted drop size distributions obtained using optimized parameters found at 50 wt% oil, 1 wt% PF127 with the extended model: (a) 50 wt% oil, 0.5 wt% PF127 ( $\Psi = 0.2749$ ), (b) 50 wt% oil, 1.0 wt% PF127 ( $\Psi = 0.0145$ ), (c) 50 wt% oil, 2.0 wt% PF127 ( $\Psi = 0.0768$ ), (d) Experimental  $d_{32}$  values (symbols) and model predicted  $d_{32}$  values (solid lines).

I believe that this result was partially attributable to inability to more accurately predict PF108 distributions with PF108 parameters (third column of Table 3.5), as similar increases in total objective function values were observed when PF127/PF108 parameters were replaced with PF68 parameters (270% increase for PF127, 264% increase for PF108). Still the extended model produced much improved distribution predictions compared to the basic model due to the inclusion of surfactant adsorption behavior.

Finally tests were performed with PF87. The extended model produced slightly better predictions of homogenized distributions than the basic model using  $K_1 - K_6$

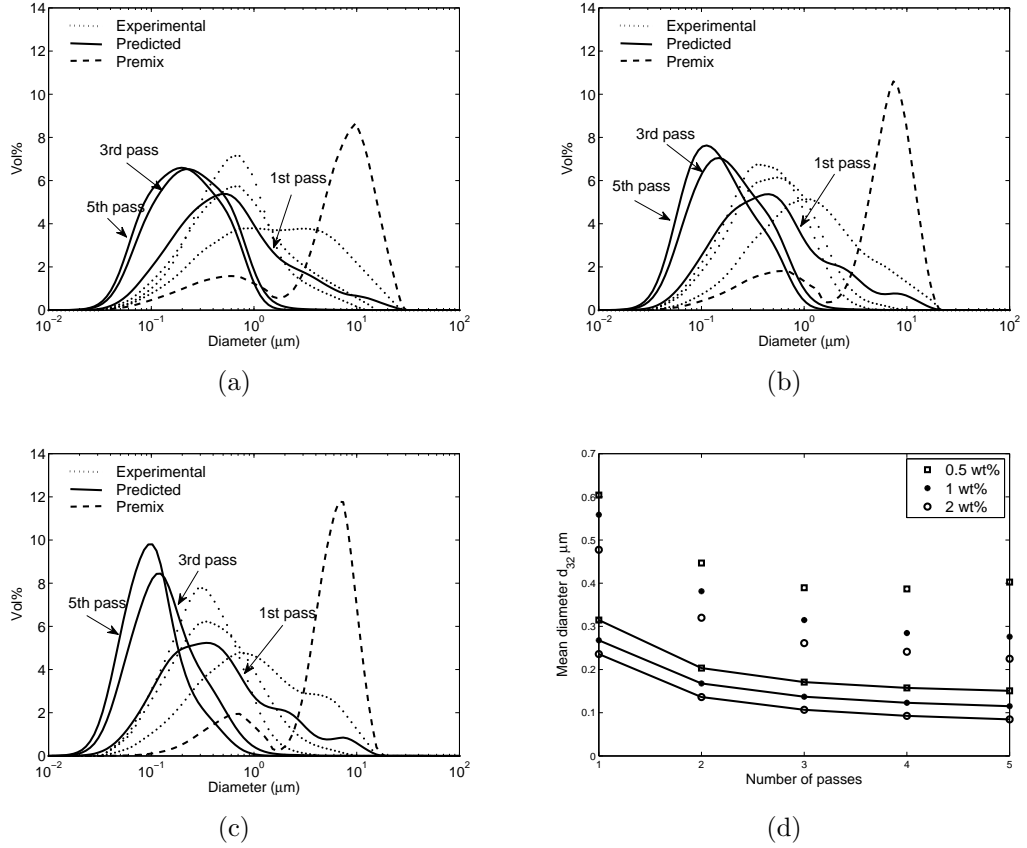


**Figure 3.6.** Experimental and model predicted drop size distributions obtained using optimized parameters found at 50 wt% oil, 1 wt% PF68 with the base model: (a) 50 wt% oil, 0.5 wt% PF127 ( $\Psi = 2.6046$ ), (b) 50 wt% oil, 1.0 wt% PF127 ( $\Psi = 2.6126$ ), (c) 50 wt% oil, 2.0 wt% PF127 ( $\Psi = 3.4692$ ), (d) Experimental  $d_{32}$  values (symbols) and model predicted  $d_{32}$  values (solid lines).

values estimated for 1.0 wt% PF87 (second and third columns of Table 3.6). Because this trend did not hold for the other three surfactants studied, I concluded that this result was an anomaly and the extended model did not improve predictions for a single surfactant. As observed with the other surfactants, the extended model also outperformed the basic model when the parameters estimated for 1.0 wt% PF68 were used to predict PF87 distributions (Fig. 5.9, fourth and fifth columns of Table 3.6). However, the improvement obtained with the extended model was not as large as that observed with the other surfactants, as total objective function value for the extended model was 54% of the value obtained with the basic model. This limited improvement

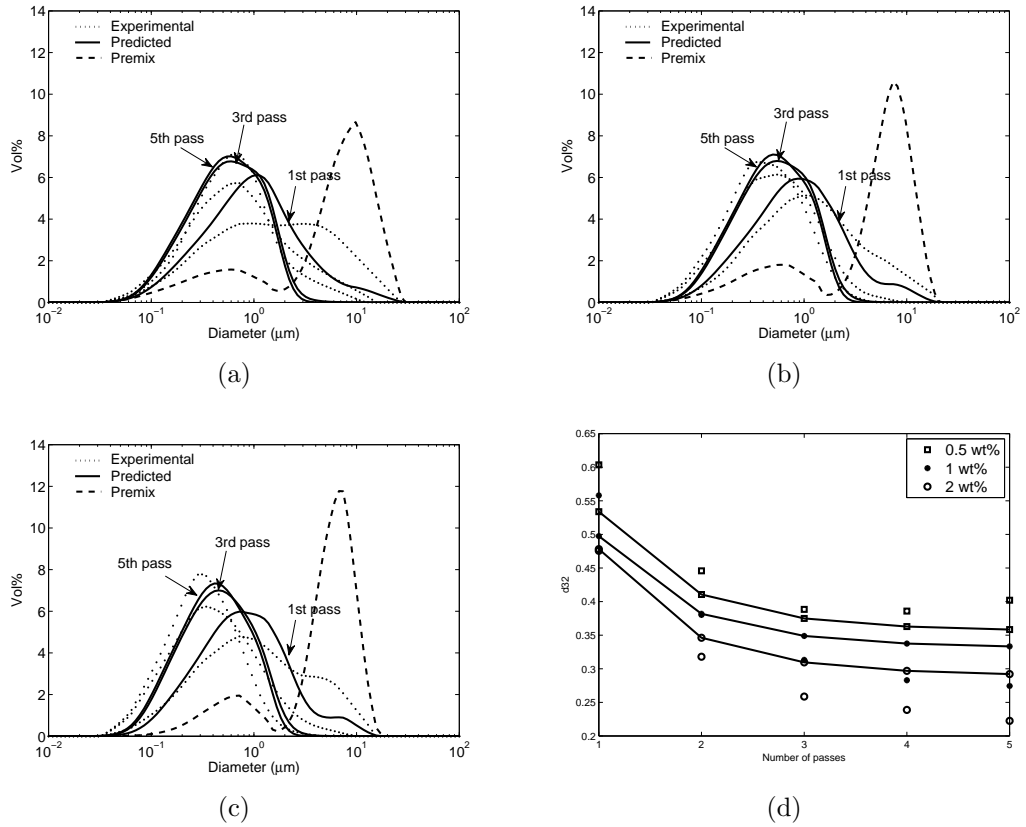


**Figure 3.7.** Experimental and model predicted drop size distributions obtained using optimized parameters found at 50 wt% oil, 1 wt% PF68 with the extended model: (a) 50 wt% oil, 0.5 wt% PF127 ( $\Psi = 0.5567$ ), (b) 50 wt% oil, 1.0 wt% PF127 ( $\Psi = 0.1486$ ), (c) 50 wt% oil, 2.0 wt% PF127 ( $\Psi = 0.2824$ ), (d) Experimental  $d_{32}$  values (symbols) and model predicted  $d_{32}$  values (solid lines).

could be attributable to the relatively slow adsorption kinetics of PF108 because of its bulkier structure and higher molecular weight. The results for PF87 did parallel the other results in the sense that a similar increase in the total objective function value was observed when PF87 parameters were replaced with PF68 parameters (389%). Therefore, I concluded that the addition of surfactant adsorption into the PBE model improved extensibility to new surfactants and that the amount of improvement for a particular surfactant was dependent on the accuracy of extended model predictions when distribution data for that surfactant was used for parameter estimation.

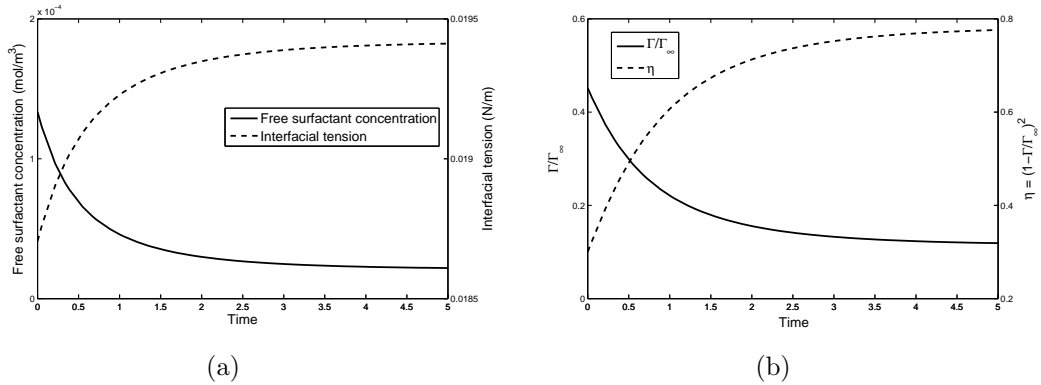


**Figure 3.8.** Extended model variables as a function of dimensionless time for a dynamic simulation of five homogenizer passes with 50 wt% oil, 1 wt% PF127 using optimized parameters found at 50 wt% oil, 1 wt% PF68: (a) free surfactant concentration and interfacial tension, (b) dimensionless surface coverage  $\frac{\Gamma}{\Gamma_\infty}$  and coalescence efficiency factor ( $\eta$ ).

**Table 3.5.** Summary of model results at different oil-PF108 ratios.

Oil-PF108 concentration (wt%-wt%)	Objective function values			
	Using base case parameters of PF108 (50wt% oil-1wt% PF108)		Using base case parameters of PF68 (50wt% oil-1wt% PF68)	
	Base Model	Extended Model	Base Model	Extended Model
50-0.5	0.5057	0.6607	3.3856	1.5758
50-1	0.1179	0.1682	2.0410	0.6452
50-2	0.2415	0.2196	1.6838	0.5477
Total	0.8651	1.0485	7.1104	2.7687

### 3.5 Conclusions

I developed and evaluated a new population balance equation (PBE) model for predicting drop size distributions of oil-in-water emulsions prepared with high pressure homogenization. The goal of the modeling effort was to extend my previous PBE model of combined drop breakage and coalescence to predict distributions obtained with different surfactant types given adjustable model parameters estimated from drop volume distribution data collected for a single surfactant. This capability was deemed essential for emulsified product design, where limited experimental data

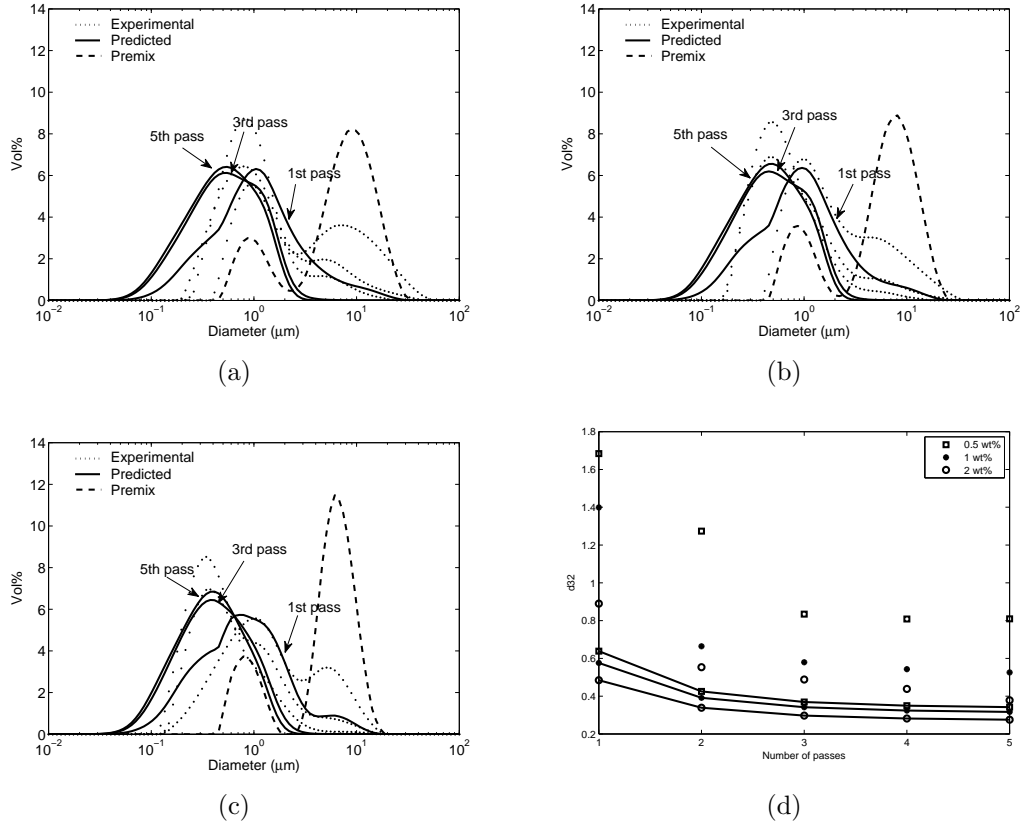


**Figure 3.9.** Experimental and model predicted drop size distributions obtained using optimized parameters found at 50 wt% oil, 1 wt% PF68 with the extended model: (a) 50 wt% oil, 0.5 wt% PF108 ( $\Psi = 1.5758$ ), (b) 50 wt% oil, 1.0 wt% PF108 ( $\Psi = 0.6452$ ), (c) 50 wt% oil, 2.0 wt% PF108 ( $\Psi = 0.5477$ ), (d) Experimental  $d_{32}$  values (symbols) and model predicted  $d_{32}$  values (solid lines).

will be available to parameterize models for prediction of process performance. The extended PBE model was developed from my previous model by adding a surfactant mass balance, including the effects of the free surfactant concentration on the interfacial tension and the surface coverage of drops, and by modeling the coalescence frequency to be a function of the surfactant coverage. Both models contained six adjustable parameters that were estimated by nonlinear optimization to minimize a least-squares objective function for the error between predicted and measured drop volume distributions. To demonstrate model extensibility to different surfactant types and concentrations, these adjustable parameters were estimated using measured drop

**Table 3.6.** Summary of model results at different oil-PF87 ratios.

Oil-PF87 concentration (wt%-wt%)	Objective function values			
	Using base case) parameters of PF87 (50wt% oil-1wt% PF87		Using base case parameters of PF68 (50wt% oil-1wt% PF68)	
	Base Model	Extended Model	Base Model	Extended Model
50-0.5	0.4289	0.3917	2.2194	1.2477
50-1	0.0346	0.0303	1.0902	0.4425
50-2	0.4887	0.1010	0.4264	0.3424
Total	0.9522	0.5230	3.7358	2.0326

volume distributions collected at 50 wt% oil and 1 wt% Pluronic F68 surfactant. These parameter values were used to predict distributions at 50 wt% oil and 0.5-2.0 wt% surfactant with PF68 and three other surfactants from the Pluronic family (PF127, PF108, PF87). I showed that the extended PBE model generated substantially improved distribution predictions for the three other surfactants compared to my previous model. Objective function values were only 11–54% of the values obtained without modeling of surfactant adsorption. The amount of improvement was surfactant dependent and appeared to be correlated with the ability of the extended model to predict distributions for a particular surfactant when those distributions were used directly for parameter estimation.

Despite these promising results, the extended PBE model has limitations that restrict its predictive capability and necessitate further improvements before computational product design can be pursued. The model only accounts for the effect of surfactant adsorption equilibria on the oil-water interfacial tension, the surface coverage of drops, and the coalescence efficiency. Other potentially important effects such as surfactant adsorption kinetics and molecular structure that may effect attractive and repulsive forces between drops have been neglected. These simplifications can be expected to degrade model predictive capability, especially for surfactant types and concentrations that differ strongly from those used to generate distribution data

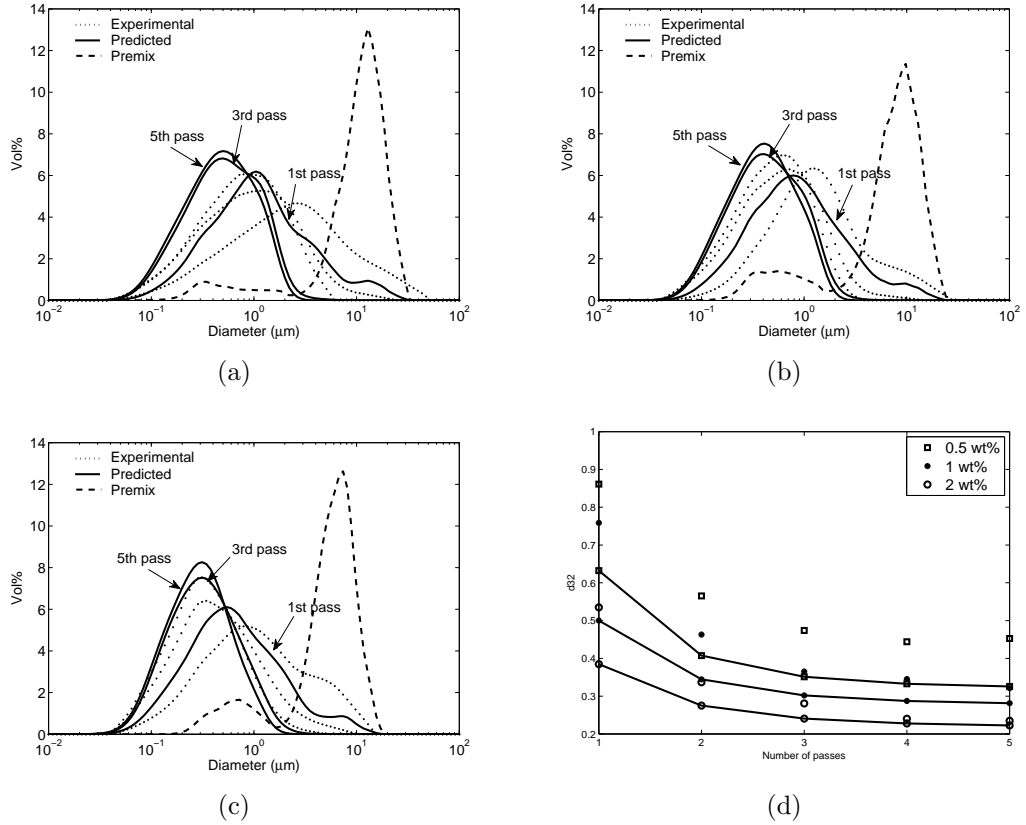


**Figure 3.10.** Experimental and model predicted drop size distributions obtained using optimized parameters found at 50 wt% oil, 1 wt% PF68 with the extended model: (a) 50 wt% oil, 0.5 wt% PF87 ( $\Psi = 1.2477$ ), (b) 50 wt% oil, 1.0 wt% PF87 ( $\Psi = 0.4425$ ), (c) 50 wt% oil, 2.0 wt% PF87 ( $\Psi = 0.3424$ ), (d) Experimental  $d_{32}$  values (symbols) and model predicted  $d_{32}$  values (solid lines).

for parameter estimation. For example, I found that the model was not extensible to 5 wt% surfactant with parameters estimated at 1 wt% PF68. In this case, there was an excess of free surfactant such that the surface coverage of drops became equal to maximum surface coverage ( $\Gamma_{\infty}$ ) and the coalescence frequency was set to zero throughout the simulated homogenization. As a result, the extended model was reduced to a breakage-only model and drop size reduction was overpredicted. The inclusion of surfactant adsorption kinetics may be necessary to improve these predictions, as slower adsorbing surfactants will be unable to achieve complete coverage

and drop coalescence will be present. Such enhancements of the PBE model are the subject of my research described in the next chapter.

## CHAPTER 4

# PREDICTING THE COMBINED EFFECTS OF OIL AND SURFACTANT CONCENTRATIONS ON THE DROP SIZE DISTRIBUTIONS OF HOMOGENIZED EMULSIONS

### 4.1 Introduction

The goal of this chapter was to develop a new PBE model that produced accurate DSD predictions in both the surfactant limited and surfactant rich regimes explored through large variations in the oil concentration (10 to 50 wt%) and surfactant concentration (0.1 to 2 wt%). The key modifications of my previous model required to generate a predictive model were: (1) formulation of a new breakage frequency function that accounts for the breakage of drops smaller than eddy sizes due to turbulent shear; (2) incorporation of a calculated emulsion viscosity instead of the continuous phase viscosity into the drop breakage and coalescence functions; and (3) development of a dynamic surface coverage model rather than assuming fast adsorption kinetics. Drop breakage parameters were estimated by nonlinear optimization using measured DSDs collected at 30 wt% oil and 2 wt% surfactant (surfactant rich regime), and the remaining drop coalescence parameters were estimated using measured DSDs collected at 30 wt% oil and 0.1 wt% surfactant (surfactant limited regime). I show that the parameterized PBE model was capable of generating satisfactory DSD predictions for 10–50 wt% oil and 0.1–2 wt% surfactant without parameter re-estimation.

## **4.2 Experimental Methods**

### **4.2.1 Materials**

Oil-in-water emulsions were prepared using sunflower oil (Sigma) as the dispersed phase and Pluronic F68 (PF68, Sigma) surfactant in nanopure water as the continuous phase. High oil concentrations and relatively low surfactant concentrations were selected to promote drop coalescence and mimic typical industrial conditions. To study the effect of emulsion formulation, experiments were performed at different concentrations of sunflower oil (10, 30 and 50 wt%) and PF68 surfactant (0.1, 0.25, 0.5, 1 and 2 wt%).

### **4.2.2 Emulsion Preparation and Characterization**

Emulsions were prepared following a two step procedure. In the first step, approximately 100 ml of coarse pre-emulsion was prepared by mixing the ingredients in a rotor-stator device (Ultra-Turrax Model T25, Rose Scientific Ltd.) at 13000 rpm for 20 minutes. The coarse emulsion was then passed through a high-pressure homogenizer (Emulsiflex C-3, Avestin Inc.) to reduce the drop size. All experiments were performed at a constant homogenization pressure of 400 bar. Each emulsion was passed through the homogenizer five times, and after each pass approximately 2 ml of emulsion was sampled for analysis. Drop size distributions were measured using static light scattering (Mastersizer 2000, Malvern Instruments).

## **4.3 Theory**

### **4.3.1 Population Balance Equation (PBE)**

The population balance equation (PBE) is formally derived from a number balance on particles by accounting for their rates of creation and disappearance [16, 63]. As the light scattering device used in this study most directly measured drop volume

distributions, I formulated the PBE in terms of drop volume fraction rather than drop number [49, 50].

$$\begin{aligned} \frac{\partial N(v, t)}{\partial t} = & -g(v)N(v, t) + v \int_v^\infty \frac{\beta(v, v')g(v')N(v', t)}{v'} dv' \\ & - N(v, t) \int_0^\infty \frac{C(v, v')N(v', t)V_t}{v'} dv' + \frac{v}{2} \int_0^v \frac{C(v - v', v')N(v - v', t)N(v', t)V_t}{v'(v - v')} dv' \end{aligned} \quad (4.1)$$

where  $v$  is the volume of the drop;  $N(v, t)dv$  is the volume fraction of drops with volume in the range  $[v, v + dv]$  per unit volume of dispersion at time  $t$ ;  $V_t$  is the conserved total volume of the drops per unit volume of dispersion;  $g(v)$  is the breakage frequency representing the fraction of drops of volume  $v$  breaking per unit time;  $\beta(v, v')$  is the daughter drop distribution function representing the probability of forming a daughter drop of size  $v$  from breakage of a mother drop of size  $v'$ ; and  $C(v, v')$  is coalescence frequency representing the rate at which drops of size  $v$  and size  $v'$  coalesce. The first and third terms on the right hand side of Eq. (6.1) represent the rates of disappearance of drops of size  $v$  due to breakage and coalescence, respectively, while the second and fourth terms represent the rates of appearance of drops of size  $v$  due to breakage and coalescence, respectively. I assumed that drop breakage and coalescence only occurred in the homogenizer valve gap, and that these mechanisms were uniform throughout the gap region. The measured drop volume distribution of the coarse premix emulsion  $N(v, 0)$  was used as the initial condition to solve the PBE.

Below I present three PBE models that differ with respect to the drop breakage and coalescence functions, the surfactant adsorption model and the emulsion viscosity model to determine the critical features required for quantitative DSD prediction over wide ranges of surfactant and oil concentrations. Model 1 represents the PBE model presented in my most recent publication [50] and is summarized here for completeness. Model 2 is a new PBE model that includes several modifications of Model 1 including

the incorporation of size-independent surfactant adsorption dynamics. Model 3 is a modified version of Model 2 that included size-dependent surfactant adsorption dynamics.

### 4.3.2 Model 1

The breakage frequency function  $g(v)$  was assumed to be the sum of two functions representing different breakage mechanisms such that  $g(v) = g_1(v) + g_2(v)$ . The first function  $g_1(v)$  accounts for breakage due to drop collisions with turbulent eddies [16],

$$g_1(v) = K_1 \frac{v^{-2/9} \epsilon^{1/3}}{1 + \phi} \exp\left(-K_2 \frac{\sigma(1 + \phi)^2}{\rho_d v^{5/9} \epsilon^{2/3}}\right) \quad (4.2)$$

where  $K_1$  and  $K_2$  are adjustable parameters. The second breakage function  $g_2(v)$  accounts for drop breakage resulting from turbulent shear [60],

$$g_2(v) = K_3 \left(\frac{2}{\pi}\right)^{1/2} \left(\frac{\epsilon \rho_d}{\eta_d}\right)^{1/2} \exp\left(-K_4 \frac{\sigma^2 \lambda}{v^{2/3} \epsilon \eta_c}\right) \quad (4.3)$$

where  $K_3$  and  $K_4$  are adjustable parameters. The coalescence frequency  $C(v, v')$  was calculated as the product of the drop collision frequency  $h(v, v')$  and the coalescence efficiency  $\Lambda(v, v')$  such that  $C(v, v') = h(v, v')\Lambda(v, v')$ . The collision function was derived from the kinetic theory of gases assuming that drops in turbulent flow behave like gas molecules [16],

$$h(v, v') = \frac{K_5 \epsilon^{1/3}}{(1 + \phi)} (v^{2/3} + v'^{2/3})(v^{2/9} + v'^{2/9})^{1/2} \quad (4.4)$$

where  $K_5$  is an adjustable parameter. The efficiency function was derived by assuming that drop coalescence occurs when the contact time between two drops is greater than the time required for the liquid film between the drops to drain [16],

$$\Lambda(v, v') = \exp\left[\frac{-K_6 \eta_c \rho_c \epsilon}{\sigma^2 (1 + \phi)^3} \left(\frac{v^{1/3} v'^{1/3}}{v^{1/3} + v'^{1/3}}\right)^4\right] \quad (4.5)$$

where  $K_6$  is adjustable parameter.

The breakage and coalescence functions depend on the homogenizer pressure  $P$  through the energy dissipation rate  $\epsilon$  (see below) and formulation variables through bulk emulsion properties including the dispersed phase volume fraction  $\phi$ , the interfacial tension  $\sigma$ , the dispersed phase density  $\rho_d$ , and the continuous phase viscosity  $\eta_c$  and dispersed phase viscosity  $\eta_d$  through the ratio  $\lambda = \frac{\eta_d}{\eta_c}$ . The daughter drop distribution function  $\beta(v, v')$  was chosen such that 80 daughter drops were formed from a single breakage event. The breakage and coalescence frequency functions both depend on the energy dissipation rate, which was modeled as follows [84, 83],

$$\epsilon = \frac{\Delta P Q}{V_{diss}} \quad (4.6)$$

where  $\Delta P$  is the operating pressure,  $Q$  is the volumetric flow rate and  $V_{diss}$  is the valve gap volume which depends on valve gap distance  $h_{gap}$ . Equations for  $V_{diss}$  and  $h_{gap}$  can be found in the previous work [60].

The coalescence frequency function was modified to depend on the equilibrium surface coverage  $\Gamma_{eq}$  as follows:

$$C_1(v, v', \Gamma_{eq}) = \left(1 - \frac{\Gamma_{eq}}{\Gamma_{\infty}}\right)^2 C(v, v') \quad (4.7)$$

where  $C_1(v, v', \Gamma_{eq})$  is the modified function and  $\Gamma_{\infty}$  is the maximum surface coverage. The multiplicative term  $\left(1 - \frac{\Gamma_{eq}}{\Gamma_{\infty}}\right)^2$  captures the increased tendency of two drops to coalesce when the surface coverage is below the maximum coverage. Under the assumption of fast adsorption kinetics, the Langmuir isotherm was used to calculate the equilibrium surfactant coverage  $\Gamma_{eq}$  on the drop surface,

$$\Gamma_{eq} = \Gamma_{\infty} \left( \frac{C_s}{C_s + C_{1/2}} \right), \quad C_{1/2} = \frac{1}{K_{eq}} = \frac{K_d}{K_a} \quad (4.8)$$

where  $C_{1/2}$  is the free surfactant concentration corresponding to half of the maximum surface coverage,  $K_{eq}$  is equilibrium rate constant,  $K_a$  is adsorption rate constant,  $K_d$  is desorption rate constant, and  $C_s$  is the free surfactant concentration in the

continuous phase. Note that the equilibrium surfactant coverage  $\Gamma_{eq}$  is assumed to be independent of drop size. The depletion of free surfactant from solution was determined from a surfactant mass balance:

$$\frac{dC_s}{dt} = -\frac{6\phi}{1-\phi} \frac{d}{dt} \left( \frac{\Gamma}{d_{32}} \right) \quad (4.9)$$

where  $d_{32}$  is the Sauter mean diameter of the emulsion droplets. The initial value of the free surfactant concentration  $C_{s_{init}}$  was calculated by solving the following mass balance equation:

$$C_{s_{init}} = C_{s_{input}} - \frac{6\phi}{1-\phi} \frac{\frac{\Gamma_{\infty} C_{s_{init}}}{C_{s_{init}} + C_{1/2}}}{d_{32,pre}} \quad (4.10)$$

where  $d_{32,pre}$  is Sauter mean diameter of the coarse premix emulsion and  $C_{s_{input}}$  is the total surfactant concentration used to prepare the emulsion.

### 4.3.3 Model 2

Model 2 was formulated to rectify shortcomings of Model 1 recognized through theoretical analysis and simulation studies. The first modification of Model 1 involved the incorporation of a calculated emulsion viscosity in the drop breakage and coalescence functions. In Model 1, the continuous phase viscosity  $\eta_c$  was assumed to be equal to the viscosity of water under the assumption that the oil and free surfactant concentration were small. For high oil fractions, droplets are expected to interact and the influence of surrounding drops must be considered by replacing the continuous phase viscosity with the apparent emulsion viscosity. In my recent work on colloid mill modeling [48], I fit viscosity versus shear rate data collected for my emulsion system to a commonly used rheology model [33]. I found that the emulsion viscosity can increase by two orders of magnitude as the oil fraction is increased from 10wt% to 50wt%. The viscosity model provided a satisfactory fit of experimental data over the range of measured shear rates (1–1000 s<sup>-1</sup>) and allowed extrapolation to very

low and very high shear rates. As the shear rate increases, oil drops start to align in streamlines until the drops cannot align any further and the viscosity reaches a low plateau value indicative of a Newtonian fluid. The emulsion viscosity  $\eta_{em}$  at very high shear rates can be calculated as follows [33],

$$\eta_{em} = \eta_c \exp\left(\frac{2.5\lambda+1}{\lambda+1}\phi\right); \quad \lambda = \frac{\eta_d}{\eta_c} \quad (4.11)$$

where the continuous phase viscosity  $\eta_c$  was calculated from the following empirical equation obtained by fitting viscosity data of PF68 solutions [26].

$$\eta_c = 7.501 \times 10^{-6} C_s^2 + 0.000104 C_s + 0.00088 \quad (4.12)$$

The second modification of Model 1 involved the breakage frequency function due to turbulent inertia,  $g_1(v)$ . This function exhibits a maximum due to the form of the pre-exponential term. Because drop breakage is expected to increase monotonically with respect to droplet size, the characteristic breakage time was assumed to be constant [14] and the function was modified as:

$$g_3(v) = K_1^* \frac{1}{1+\phi} \exp\left(-K_2^* \frac{\sigma(1+\phi)^2}{\rho_d v^{5/9} \epsilon^{2/3}}\right) \quad (4.13)$$

where  $K_1^*$  and  $K_2^*$  are adjustable parameters. The third modification involved the breakage frequency function due to turbulent viscous shear,  $g_2(v)$ . I observed that this function incorrectly operated in a size range larger than the Kolmogorov length scale. To remedy this problem, the breakage frequency function was reformulated as follows:

$$g_4(v) = K_3^* \dot{\gamma} \exp\left(-K_4^* \frac{\Pi}{\tau_{vs}}\right) \exp\left(-\frac{\left(\frac{6}{\pi}v\right)^{1/3}}{\lambda_K}\right) \quad (4.14)$$

where  $\dot{\gamma}$  is turbulent shear rate,  $\tau_{vs}$  is turbulent viscous shear stress,  $\Pi$  is Laplace pressure,  $\lambda_K$  is length scale of the smallest size eddies (Kolmogorov length scale), and

$K_3^*$  and  $K_4^*$  are adjustable parameters. This expression accounts for the breakage of drops smaller than the Kolmogorov length scale with Laplace pressure smaller than the viscous shear stress. Kolmogorov derived the following expressions for the time scale, length scale and velocity scale for the smallest size eddies,

$$\text{time scale} = \left( \frac{\eta_c}{\epsilon \rho_c} \right)^{1/2} \quad (4.15)$$

$$\text{length scale} = \lambda_K = \left( \frac{\eta_c^3}{\epsilon \rho_c^3} \right)^{1/4} \quad (4.16)$$

$$\text{velocity scale} = \left( \frac{\eta_c \epsilon}{\rho_c} \right)^{1/4} \quad (4.17)$$

These expressions were substituted in Equation 4.14 to yield the new breakage frequency function,

$$\dot{\gamma} = \frac{1}{\text{time scale}} = \left( \frac{\epsilon \rho_c}{\eta_c} \right)^{1/2} \quad (4.18)$$

$$\tau_{vs} = \eta_c \dot{\gamma} = (\epsilon \rho_c \eta_c)^{1/2} \quad (4.19)$$

$$g_4(v) = K_3^* \left( \frac{\epsilon \rho_c}{\eta_c} \right)^{1/2} \exp \left( -K_4^* \frac{\sigma}{(\epsilon \rho_c \eta_c)^{1/2} v^{1/3}} \right) \exp \left( -\frac{(\frac{6}{\pi} v)^{1/3}}{\lambda_K} \right) \quad (4.20)$$

The fourth modification of Model 1 involved a different approach of accounting for the oil fraction in the drop breakage and coalescence functions. The turbulent velocity has been proposed to dampen with increasing dispersed phase volume fraction due to the larger number of drops interfering with the turbulent eddies, yielding the following expression for the apparent mean turbulent velocity [16],

$$\overline{u_\phi^2} = \frac{\overline{u_{\phi=0}^2}}{(1 + \phi)^2} \quad (4.21)$$

The shear rate ( $\dot{\gamma}$ ) and shear stress ( $\tau_{vs}$ ) can be expressed on a velocity scale such that the dampening effect due to the dispersed phase can be included in the breakage frequency function as follows,

$$g_4(v) = K_3^* \frac{(\epsilon \rho_c / \eta_c)^{1/2}}{(1 + \phi)^2} \exp \left( -K_4^* \frac{\sigma (1 + \phi)^2}{(\epsilon \rho_c \eta_c)^{1/2} v^{1/3}} \right) \exp \left( -\frac{(\frac{6}{\pi} v)^{1/3}}{\lambda_K} \right) \quad (4.22)$$

The breakage frequency function due to turbulent inertia in Equation (4.13) remained unchanged because the dampening effect was considered [16]. Additionally, I observed that the term  $1 + \phi$  in the denominator of  $h(v, v')$  in Equation (4.4) reduces the collision frequency with increasing oil fraction. However, the collision frequency should increase with increasing oil fraction because more drops reduce the free space for drop movement and increase collisions [45, 86, 89]. Therefore, the term  $1 + \phi$  in the denominator of the collision frequency function  $h(v, v')$  was replaced with  $1 - \phi$ . The coalescence efficiency function in Equation (4.5) remained unchanged except that the adjustable parameter  $K_6$  was fixed to be unity since it had a negligible effect on model predictions. Therefore, the coalescence functions assumed the form,

$$C_2(v, v', \Gamma, \Gamma') = \left(1 - \frac{\Gamma}{\Gamma_\infty}\right) \left(1 - \frac{\Gamma'}{\Gamma_\infty}\right) h(v, v') \Lambda(v, v') \quad (4.23)$$

$$h(v, v') = K_5^* \frac{\epsilon^{1/3}}{(1 - \phi)} (v^{2/3} + v'^{2/3}) (v^{2/9} + v'^{2/9})^{1/2} \quad (4.24)$$

$$\Lambda(v, v') = \exp \left[ \frac{-\eta_c \rho_c \epsilon}{\sigma^2 (1 + \phi)^3} \left( \frac{v^{1/3} v'^{1/3}}{v^{1/3} + v'^{1/3}} \right)^4 \right] \quad (4.25)$$

where  $\Gamma$  and  $\Gamma'$  are the surface coverages of the two drops and  $K_5^*$  is an adjustable parameter.

The fifth and final modification of Model 1 involved the incorporation of a dynamic surfactant adsorption model in place of the equilibrium model used previously.

Considering dynamic model is very important in case of large molecule surfactants such as proteins and polymers, as the adsorption kinetics of these surfactants are slow. While in case of small and fast adsorbing surfactants, the equilibrium model is sufficient. To find effect of adsorption kinetics of Pluronic F68, I formulated dynamic model in place of previously used equilibrium model, from rates of surfactant adsorption and desorption. The dynamic model had the form (derivation in Appendix B),

$$\frac{d\Gamma}{dt} = K_a (\Gamma_\infty - \Gamma) C_s - K_d \Gamma - \frac{\Gamma}{\int_0^\infty (N/d) dv} \int_0^\infty \left( \frac{1}{d} \frac{\partial N}{\partial t} \right) dv; \quad d = \left( \frac{6v}{\pi} \right)^{1/3} \quad (4.26)$$

#### 4.3.4 Model 3

Model 3 was developed from Model 2 by incorporating size dependent surfactant adsorption dynamics in place of the size independent dynamics in Equation (4.26). The size dependent surface coverage of emulsion droplets in turbulent flows has been modeled as [55],

$$\frac{\partial \Gamma}{\partial t} \propto \frac{(d_H + d)^3}{d^2}; \quad d < 2\lambda_K \quad (4.27)$$

$$\frac{\partial \Gamma}{\partial t} \propto \frac{(d_H + d)^{7/3}}{d^2}; \quad d \geq 2\lambda_K \quad (4.28)$$

where  $d_H$  is the hydrodynamic diameter of the surfactant molecule. As droplets in my system generally had diameters less than  $2\lambda_K$ , the following expression was derived for size dependent surfactant adsorption assuming that  $d_H \ll d$ ,

$$\begin{aligned}
\frac{\partial M_v}{\partial t} &= A_v (K_a (\Gamma_\infty - \Gamma_v) C_s d - K_d \Gamma_v) \\
\Gamma_v &= \frac{M_v}{A_v} \quad \text{if } N > 0 \\
&= 0 \quad \text{if } N = 0
\end{aligned} \tag{4.29}$$

where  $M_v dv$  is amount of adsorbed surfactant on the interfaces of drops of size between  $v$  and  $v + dv$  and  $A_v dv$  is total surface area of drops of size between  $v$  and  $v + dv$ . For clarity, the equations used for free surfactant, adsorbed surfactant, initial conditions and interfacial tension are summarized in Table 4.3.4 for size independent surfactant adsorption dynamics (Model 2) and size dependent surfactant adsorption dynamics (Model 3). These equations are derived in the Appendix B.

**Table 4.1.** Model equations used for size independent and dependent surfactant adsorption dynamics.

	Size Independent (Model 2)	Size Dependent (Model 3)
Free surfactant	$\frac{dC_s}{dt} = -\frac{6\phi}{1-\phi} \frac{d}{dt} \left( \frac{\Gamma}{d_{32}} \right)$	$\frac{dC_s}{dt} = -\frac{\phi}{1-\phi} \frac{1}{\int_0^\infty NV_t dv} \int_0^\infty \frac{\partial M_v}{\partial t} dv$
Adsorbed surfactant	$\frac{d\Gamma}{dt} = K_a (\Gamma_\infty - \Gamma) C_s - K_d \Gamma$ $-\frac{\Gamma}{\int_0^\infty (N/d) dv} \int_0^\infty \left( \frac{1}{d} \frac{\partial N}{\partial t} \right) dv$	$\frac{\partial M_v}{\partial t} = A_v (K_a (\Gamma_\infty - \Gamma_v) C_s d - K_d \Gamma_v)$ $\Gamma_v = \frac{M_v}{A_v}; \quad A_v = \int_v^{v+dv} \left( \frac{NV_t}{v} \right) \pi d^2 dv$
Initial conditions	$C_{sin} - C_{sinit} - \frac{6\phi}{1-\phi} \frac{\Gamma_\infty}{d_{32pre}}$ $\frac{C_{sinit}}{C_{sinit} + C_{1/2}} = 0$ $\Gamma_{init} = \Gamma_\infty \frac{C_{sinit}}{C_{sinit} + C_{1/2}}$	$C_{sin} - C_{sinit} - \frac{6\phi}{1-\phi} \frac{\Gamma_\infty C_{sinit}}{\int_0^\infty N dv}$ $\int_0^\infty \frac{N}{d} \frac{1}{C_{sinit} + C_{1/2}/d} dv = 0$ $M_{vinit} = \Gamma_\infty \frac{C_{sinit}}{C_{sinit} + C_{1/2}/d} A_{vinit}$
Interfacial tension	$\sigma = \sigma_{o/w} + RT\Gamma_\infty \log \left( 1 - \frac{\Gamma}{\Gamma_\infty} \right)$	$\sigma_v = \sigma_{o/w} + RT\Gamma_\infty \log \left( 1 - \frac{\Gamma_v}{\Gamma_\infty} \right)$

### 4.3.5 Dynamic Simulation and Parameter Estimation

To generate predictions for each model, the PBE and associated equations must be integrated in time. The integral expressions in the PBE (Eq. 6.1) were numerically approximated using the fixed pivot technique [40] with 100 node points equally spaced in a logarithmic scale. A larger number of node points increased the computational cost of simulation but did not affect solution accuracy. Spatial discretization produced 100 nonlinear ordinary differential equations (ODEs) in time with the the volume percent distribution at each node point as the dependent variables. Models 1, 2, and 3 included an additional ODE for the free surfactant concentration and an algebraic equation for the interfacial tension (see Table 4.3.4). For surface coverage, Model 1 included an additional algebraic equation (Eq. 4.8), Model 2 included an additional ODE (Eq. 4.26) and Model 3 included 100 additional ODEs due to discretization. For each discretized model, the ODE system was solved with the Matlab integration code `ode15s` by embedding the algebraic equations. The premix distribution  $N(v, 0)$  was used as the initial condition for the PBE, while the equations in Table 4.3.4 were used to generate initial conditions for the free surfactant concentration and the surface coverage or adsorbed surfactant. A homogenization pass was defined to be one dimensionless time unit.

Model 1 had six adjustable parameters  $K_1 - K_6$  in the breakage and coalescence functions, while Models 2 and 3 had five adjustable parameters  $K_1^* - K_5^*$ . These parameters were estimated by nonlinear optimization using experimental data from homogenization experiments performed at 30 wt% oil. First the breakage parameters ( $K_1 - K_4$  and  $K_1^* - K_4^*$ ) were estimated from data collected at 30 wt% oil and 2 wt% surfactant under the assumption that coalescence was negligible due to high surface coverage. With these breakage parameters fixed, the coalescence parameters ( $K_5 - K_6$  and  $K_5^*$ ) were estimated from data collected at 30 wt% oil and 0.1 wt% surfactant. The input data used for parameter estimation were surfactant properties ( $\Gamma_\infty$ ,  $C_{1/2}$ ,

$K_a$ , and  $K_d$ ), bulk emulsion properties ( $\phi, \sigma, \rho_c, \rho_d, \eta_{em}$ ), operating condition ( $\epsilon$ ), the premix volume distribution  $N(v, 0)$  and measured drop volume distributions  $N_e(v, t)$  for five homogenization passes. The bulk emulsion properties are listed in the Table 4.2.

**Table 4.2.** Bulk properties of the emulsion system.

Density of water ( $\rho_c$ )	997.05 kg/m <sup>3</sup>
Density of sunflower oil ( $\rho_d$ )	917.36 kg/m <sup>3</sup>
Viscosity of water ( $\eta_w$ )	0.88 mPa.s
Viscosity of sunflower oil ( $\eta_d$ )	47.8 mPa.s
Interfacial tension of sunflower oil in water at 25°C	27 mN/m

To perform parameter estimation, the ODE system obtained from spatial discretization was temporally discretized using orthogonal collocation with 15 finite elements and 2 internal collocation points per element to obtain a set of nonlinear algebraic equations. I found that additional finite elements and/or collocation points had no significant effect on the parameter estimates but increased computational effort significantly. The algebraic equations were posed as equality constraints and continuity conditions were imposed across the finite elements. The objective function  $\Psi$  to be minimized was,

$$\Psi = \sum_{i=1}^{N_p} \frac{\sum_{j=1}^{100} [N(v_j, i) - N_e(v_j, i)]^2}{\sum_{j=1}^{100} [N_e(v_j, i)]^2} \quad (4.30)$$

where  $N_e(v_j, i)$  is the measured value of the drop volume distribution at drop volume  $v_j$  and homogenizer pass  $i$ ,  $N(v_j, i)$  is the corresponding predicted value obtained from the discretized model and  $N_p$  is the number of passes. This objective function ensured that the denominator would remain non-zero even if the number of drops in a particular volume class became identically zero. The optimization problem for each model was formulated in AMPL [25] and solved using the nonlinear program solver

CONOPT. Objective function values  $\Psi$  were used to quantify the quality of model fit.

## 4.4 Results and Discussion

### 4.4.1 Experimental Results

Homogenization experiments were performed at three different oil fractions (10, 30, and 50 wt%) and five different surfactant concentrations (0.1, 0.25, 0.5, 1, and 2 wt%) to investigate both the surfactant limited and surfactant rich regimes. A representative set of DSDs for five homogenization passes at 30 wt% oil and 2 wt% surfactant is shown in Fig. 4.1(a). The drop size decreased dramatically for the first pass and less substantially for the subsequent passes due to limited energy dissipation. As the surfactant concentration was increased at 30 wt% oil, the fifth pass DSD moved to smaller drop sizes due to the availability of more free surfactant for drop stabilization (Fig. 4.1(b)). The impact was most substantial at low surfactant concentrations (e.g. the surfactant limited regime) and was diminished at high surfactant concentrations (e.g. the surfactant rich regime) because energy dissipation was the limiting factor. As the oil fraction was increased, the total interfacial area to be stabilized increased and the average drop size decreased substantially with increasing surfactant concentration in the surfactant limited regime (Figs. 4.1(c) and 4.1(d)). Conversely, the surfactant concentration had little effect in the surfactant rich regime.

### 4.4.2 Estimating Surfactant Properties

Model 1 involves two surfactant specific parameters,  $\Gamma_\infty$  and  $C_{1/2}$ , while models 2 and 3 involve three surfactant specific parameters,  $\Gamma_\infty$ ,  $K_a$  and  $K_d$ . Experimental methods to measure surface coverage include stagnation point flow reflectometry [82], Fourier transform infrared spectroscopy [78] and interfacial tension data [8, 35]. Equilibrium interfacial tension data can be used to estimate  $\Gamma_\infty$  and  $C_{1/2}$ , while

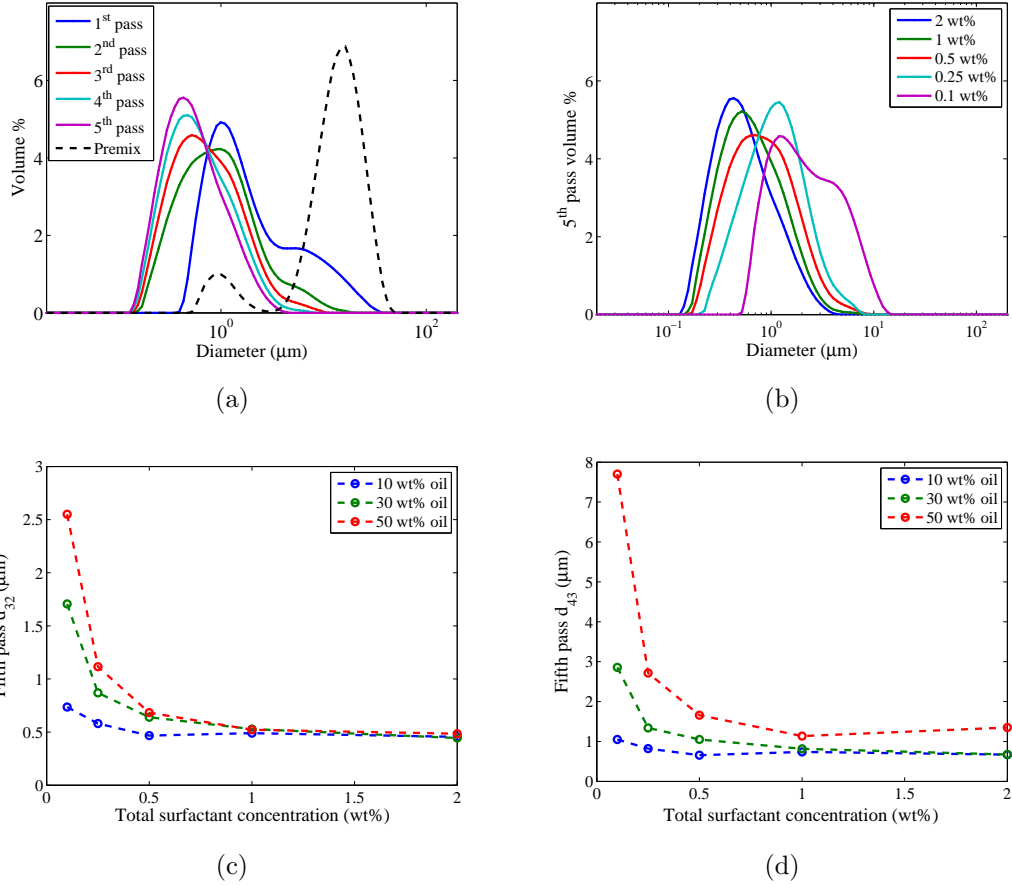


**Figure 4.1.** Experimental results: (a) DSDs for 30 wt% oil and 2 wt% PF68 for five homogenization passes; (b) fifth pass DSDs for 30 wt% oil and different surfactant concentrations; (c) fifth pass  $d_{32}$  for different oil and surfactant concentrations; and (d) fifth pass  $d_{43}$  for different oil and surfactant concentrations.

dynamic interfacial tension data can be used to estimate the rate constants  $K_a$ ,  $K_d$  [35]. In my previous work [50],  $\Gamma_\infty$  and  $C_{1/2}$  for PF68 adsorption on the vegetable oil-water interface were estimated by fitting an interfacial tension equation to equilibrium interfacial tension data. While similar experiments could have been performed to determine these parameters for the PF68/sunflower oil/water system used in this study, I pursued a different approach designed to more clearly delineate the surfactant limited and rich regimes. I estimated the maximum surface coverage  $\Gamma_\infty$  from my DSD data as follows. The DSDs obtained with 10 wt% oil were very similar for different PF68 concentrations except at 0.1 wt% PF68, in which case the measured

drop sizes were slightly larger (Fig. 4.2(a)). I assumed that all emulsions with 10 wt% oil were in surfactant rich regime except at 0.1 wt% PF68, which was assumed to be in the surfactant limited regime. Assuming the actual surface coverage to be equal to the maximum surface coverage, the free surfactant concentration  $C_s$  for each case was calculated from the following equation,

$$C_s = C_{s_{in}} - \frac{6\phi}{1-\phi} \frac{\Gamma}{d_{32}}; \quad \Gamma = \Gamma_{\infty} \quad (4.31)$$

I expected this calculation to yield positive  $C_s$  values only in the surfactant rich regime where the assumption that drops were fully covered held. At  $\Gamma_{\infty} = 2 \times 10^{-7}$  mol/m<sup>2</sup>, calculated  $C_s$  values were positive for all surfactant concentrations except 0.1 wt% PF68. This value of  $\Gamma_{\infty}$  was used in Model 1 because it properly delineated the surfactant rich and limited regimes. Furthermore, I used  $C_{1/2} = 0.3$  mol/m<sup>3</sup> based on my previous work [50].

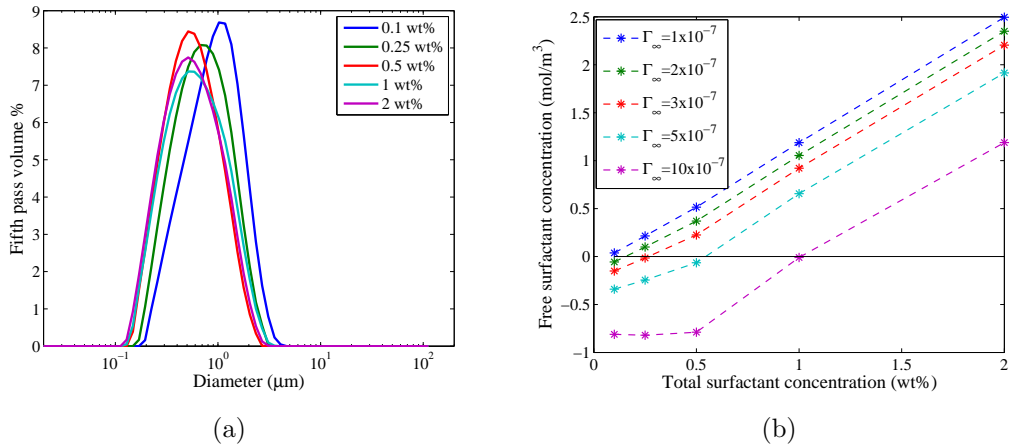


**Figure 4.2.** (a) Fifth pass DSDs with 10 wt% oil and different surfactant concentrations; and (b) free surfactant concentrations calculated with different maximum surface coverage values assuming all drops were fully covered.

Models 2 and 3 further required the specification of the surfactant adsorption rate constants  $K_a$  and  $K_d$ . These constants are known to vary significantly with the adsorbing compound (see Table 3 in [10]). For instance,  $K_a \approx 2$  m<sup>3</sup>/mol/s

and  $K_d \approx 0.02$  1/s for different poly(ethylene oxide) alkylethers [82], while  $K_a = 64$   $\text{m}^3/\text{mol}/\text{s}$  and  $K_d = 80$  1/s for 1,9-nonanediol [35]. Based on published rate constants, I selected  $K_a = 10$   $\text{m}^3/\text{mol}/\text{s}$  and  $K_d = 0.1$  1/s to establish reasonable order-of-magnitude values in model 2. Due to the size dependence of surfactant adsorption in model 3, I selected  $K_a = 10^6$   $\text{m}^2/(\text{mol}\cdot\text{s})$  and  $K_d = 0.1$  1/s for this model.

#### 4.4.3 Model Predictions

Model 1 contained six adjustable model parameters  $K_1 - K_6$  that were estimated from DSD data collected at 30 wt% oil, 2 wt% surfactant and 30 wt% oil, 0.1 wt% surfactant as described in Section 3.5. With the exception of 2wt% surfactant, fifth pass DSD predictions were generally poor for all three oil concentrations (Figs. 5.3(a) and 5.3(b)). The poor DSD prediction accuracy of model 1 was reflected in relatively large values of the objective function across the studied range of oil and surfactant concentrations (columns 2–4 in Table 4.3).

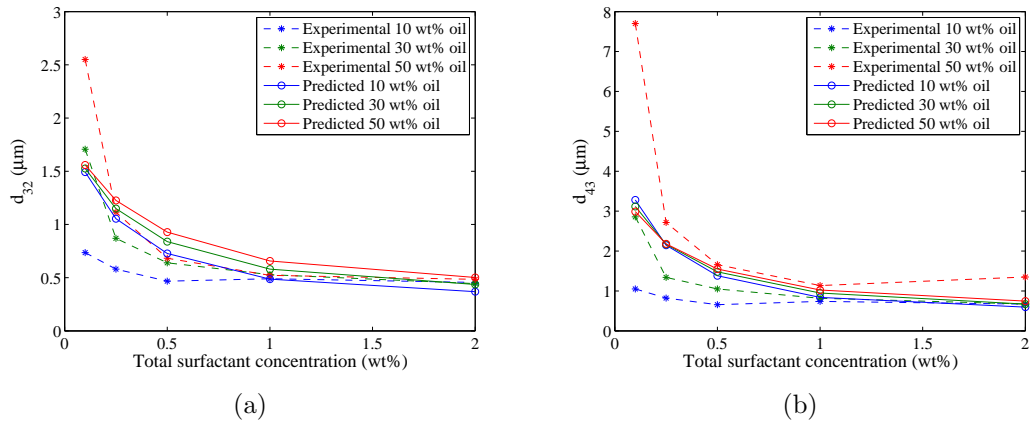


**Figure 4.3.** Model 1: Comparison of experimental and predicted (a)  $d_{32}$  and (b)  $d_{43}$  values calculated from fifth pass DSDs.

I attributed the unsatisfactory performance of model 1 to several shortcomings of the model formulation, most notably: (1) the continuous phase viscosity was assumed to be equal to the viscosity of water; (2) the breakage frequency function due

**Table 4.3.** Objective function values obtained with the three different PBE models

PF68 concentration (wt%)	Model 1			Model 2			Model 3		
	Oil fraction (wt%)			Oil fraction (wt%)			Oil fraction (wt%)		
	10	30	50	10	30	50	10	30	50
0.1	0.465	0.142	0.708	0.053	0.173	0.425	0.112	0.428	1.019
0.25	0.367	0.154	0.354	0.028	0.081	0.271	0.057	0.077	0.401
0.5	0.231	0.093	0.238	0.058	0.049	0.134	0.049	0.063	0.161
1	0.026	0.042	0.148	0.036	0.040	0.055	0.071	0.041	0.070
2	0.047	0.038	0.184	0.023	0.050	0.085	0.037	0.046	0.095
<b>Total</b>	<b>1.136</b>	<b>0.469</b>	<b>1.632</b>	<b>0.198</b>	<b>0.393</b>	<b>0.756</b>	<b>0.326</b>	<b>0.655</b>	<b>1.746</b>

to turbulent inertia,  $g_1(v)$ , exhibited an undesirable maximum with respect to drop size; (3) the breakage frequency function due to turbulent viscous shear,  $g_2(v)$ , incorrectly operated in a size range larger than the Kolmogorov length scale; (4) the drop breakage and coalescence functions exhibited incorrect trends with respect to the oil fraction; and (5) surfactant adsorption was assumed to be sufficiently fast to warrant an equilibrium description. As discussed in detail in Section 3.3, model 2 was explicitly formulated to address these five shortcomings. For example, the emulsion viscosity model predicted that the apparent viscosity at high shear rates would increase by an order of magnitude over the range of oil concentrations studied (Fig. 5.4).

Model 2 contained five adjustable parameters  $K_1^*-K_5^*$  that were estimated from DSD data collected at 30 wt% oil, 2 wt% surfactant and 30 wt% oil, 0.1 wt% surfactant as described in Section 3.5. Model 2 generated satisfactory predictions of fifth pass  $d_{32}$  and  $d_{43}$  values for all formulations investigated with the exception of 50 wt% oil and 0.1 wt% surfactant, the most strongly surfactant limited formulation (Figs. 5.5(a) and 5.5(b)). The prediction accuracy of model 2 was superior to that of model 1 as measured by the relatively small objective function values obtained across the range of oil and surfactant concentrations (columns 5–7 in Table 4.3). I partially

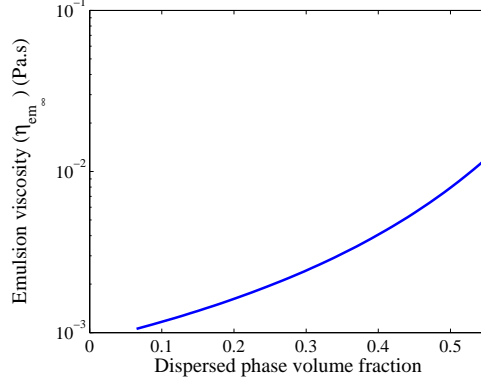


**Figure 4.4.** Predicted emulsion viscosity at high shear rates. The dashed line represents the viscosity of water.

attributed the improved prediction accuracy of model 2 to its ability to dramatically increase the coalescence rate in the surfactant limited regime due to decreased surface coverage owing to the inclusion of surfactant adsorption dynamics. In the surfactant rich regime, the model predicted nearly constant  $d_{32}$  and  $d_{43}$  values with increasing surfactant due to the inclusion of the term  $(1 - \Gamma/\Gamma_\infty)^2$  in the coalescence rate function (Eq. 4.23).

Model 3 was formulated from model 2 by allowing the surfactant adsorption dynamics to be size dependent. To examine the impact of this modification, the five adjustable parameters  $K_1^*$ - $K_5^*$  in model 3 were estimated from DSD data and predictions were generated across a range of oil and surfactant concentrations. Model 3 generally produced more accurate predictions than model 1 and similar predictions as model 2 in the surfactant rich regime (Figs. 5.5(c) and 4.5(d)). However, model 3 predictions were comparatively poor in the surfactant limited regime as measured by objective function values (columns 8–10 in Table 4.3). I attributed this behavior to the size dependent surfactant adsorption model which favored coalescence of smaller drops over larger drops and therefore undepredicted coalescence at high oil/surfactant ratios that produce larger drops. Given the increased complexity and inferior predic-

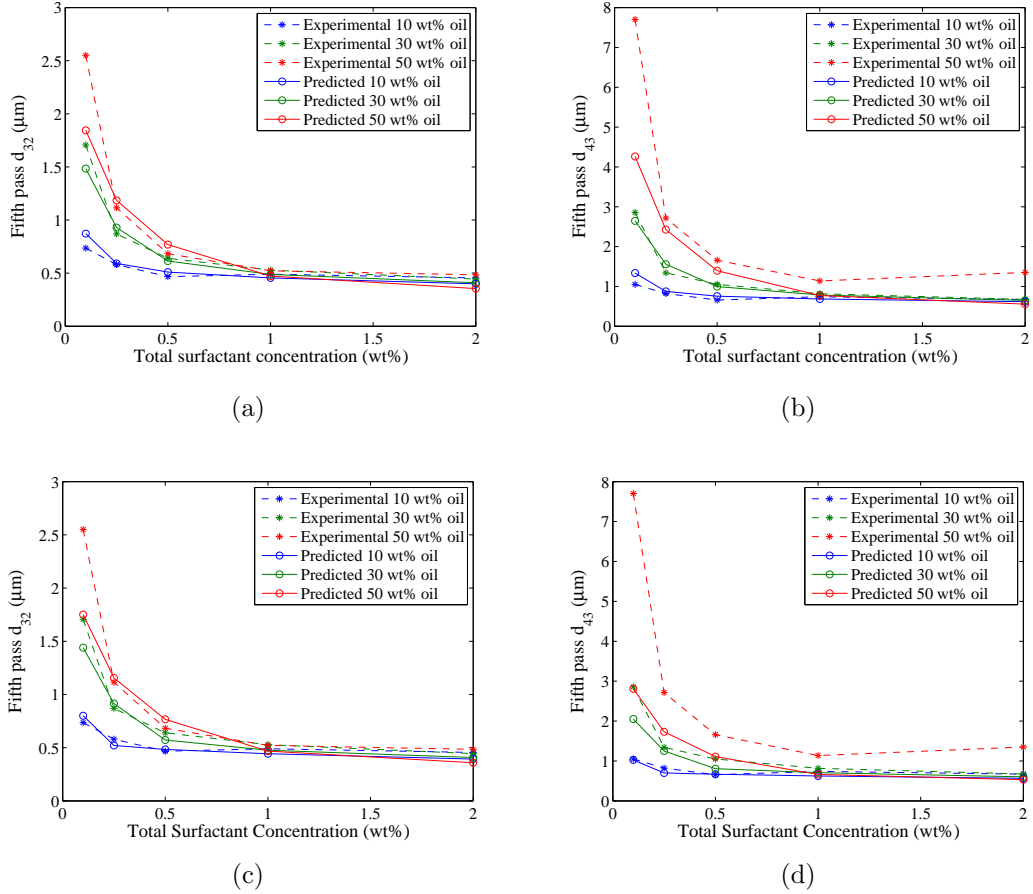


**Figure 4.5.** Models 2 and 3: Comparison of experimental and predicted mean drop sizes calculated from fifth pass DSDs. (a)  $d_{32}$  and (b)  $d_{43}$  values obtained using Model 2; and (c)  $d_{32}$  and (d)  $d_{43}$  values obtained using Model 3.

tion accuracy of model 3, the remainder of the chapter focuses exclusively on model 2.

#### 4.4.4 Effect of Oil Concentration

To study the effect of oil concentration on DSD predictions, model parameters were estimated from DSD data collected at 30 wt% oil and predictions were generated at 10 and 50 wt% oil as described previously. Given the same surfactant concentration, increasing the oil content resulted in the formation of larger drops (Figs. 4.1(c) and 4.1(d)). This effect, which was most pronounced in the surfactant limited regime, was well captured by model 2 except at the most extreme case of 50 wt% oil and 0.1

wt% surfactant (Figs. 5.5(a) and 5.5(b)). A more detailed analysis of this behavior is depicted in Figure 5.6, which shows results for 2 wt% surfactant. The breakage frequency functions due to turbulent viscous shear ( $g_3$ ) and turbulent inertia ( $g_4$ ) varied such that primarily larger drops were broken at high oil fractions (Fig. 5.6(a)). I found that this trend was largely attributable to the increased emulsion viscosity at high oil fractions, which caused the turbulent shear stress and Kolmogorov eddy size to increase in  $g_3$  and the dissipated energy per drop to decrease in  $g_4$ . At low oil fractions the contribution of  $g_3$  to the overall breakage frequency was negligible, while both  $g_3$  and  $g_4$  were important at higher oil fractions. The model produced satisfactory DSD predictions for all passes with the fifth pass predictions being particularly accurate (Figs. 5.6(b)–5.6(d)).

#### 4.4.5 Effect of Surfactant Concentration

The effect of the surfactant concentration on DSD predictions was evaluated by estimating model parameters from DSD data collected at 2.0 wt% and 0.1 wt% surfactant and generating predictions at 0.25–1.0 wt% surfactant as described previously. For a given oil content, the mean drop size was observed to decrease with increasing surfactant concentration in the surfactant limited regime and to remain essentially constant in the surfactant rich regime. The model was able to capture these trends for the fifth pass data (Fig. 5.5(a) and 5.5(b)) as well as for the individual passes except at the lowest concentration of 0.1 wt% surfactant where the mean drop size was generally underestimated (Figs. 5.7(a) and 5.7(b)).

I attributed this predictive capability to the dynamic surfactant adsorption model. Due to the relatively small interfacial area, the premix emulsion droplets were assumed to be completely covered ( $\Gamma \approx \Gamma_\infty$ ) regardless of the formulation. The first pass through the homogenizer caused a large increase in interfacial area due to substantial drop breakage. The model predicted a corresponding decrease in drop coverage

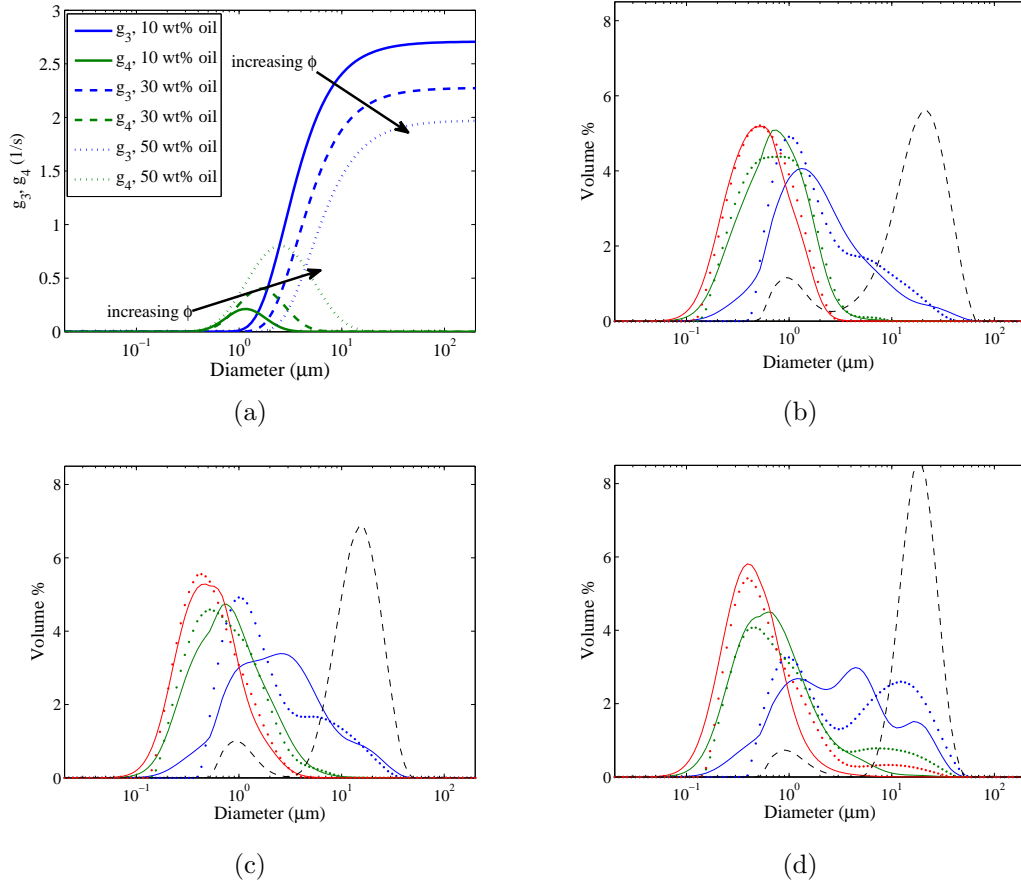


**Figure 4.6.** Effect of the oil fraction on model 2 predictions at 2 wt% PF682 wt% surfactant. (a) Breakage frequency functions; (b) premix (black), first (blue), third (green) and fifth (red) pass DSD predictions for 10 wt% oil; (c) premix (black), first (blue), third (green) and fifth (red) pass DSD predictions for 30 wt% oil; and (d) premix (black), first (blue), third (green) and fifth (red) pass DSD predictions for 50 wt% oil.

( $\Gamma/\Gamma_\infty$ ) due to adsorption dynamics (Fig. 4.7(c)). This effect was most prominent in the surfactant limited regime because limited free surfactant was available for adsorption (Fig. 4.7(d)). The relatively small drop coverage values substantially increased the coalescence rate (Eq. 4.7) and resulted in larger mean drop sizes in the surfactant limited regime (Figs. 5.7(a) and 5.7(b)). At subsequent passes, drop breakage was less dramatic and drop coverage slowly increased with time in the surfactant

rich regime due an abundance of free surfactant. By contrast, drop coverage slowly decreased with time in the surfactant limited regime.

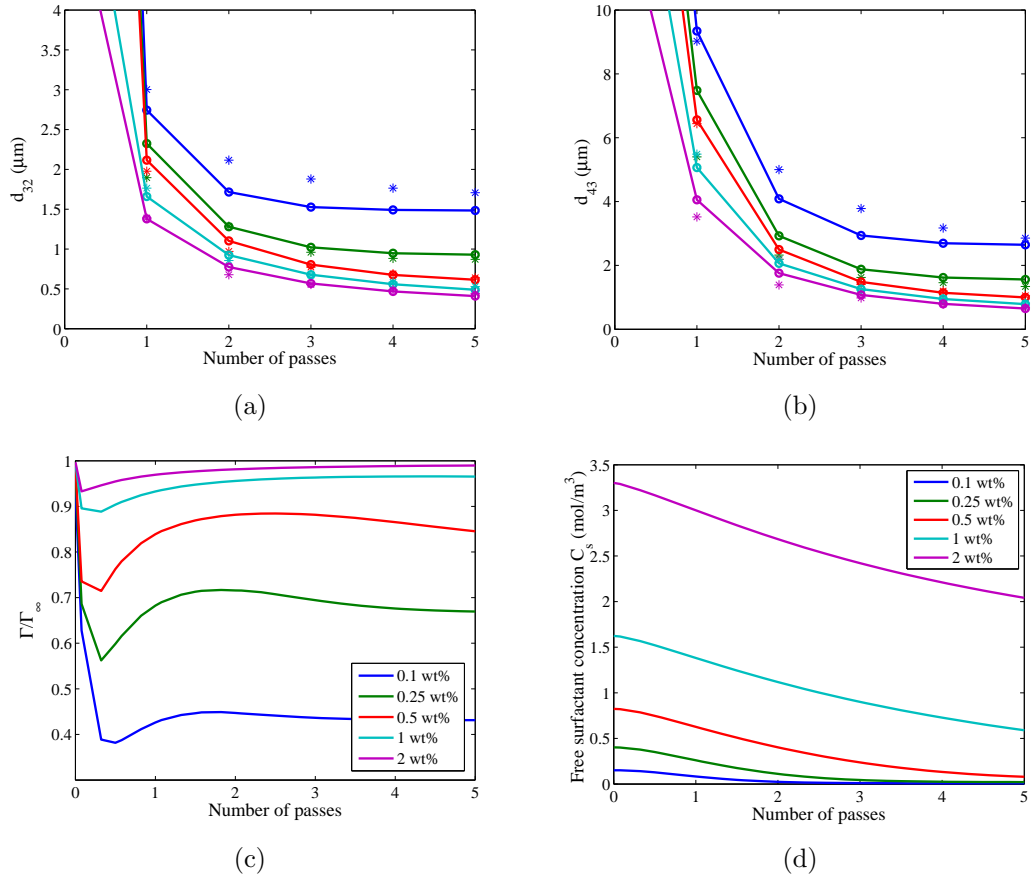


**Figure 4.7.** Effect of the oil fraction on model 2 predictions for all five passes at 30 wt% oil. (a)  $d_{32}$ , (b)  $d_{43}$ , (c) free surfactant concentration and (d) relative drop coverage for 0.1–2.0 wt% surfactant.

## 4.5 Conclusions

I developed a new population balance equation (PBE) model to predict drop size distributions (DSDs) of homogenized emulsions over a wide range of oil and surfactant concentrations representing “surfactant limited” and “surfactant rich” regimes. The model was formulated to address several shortcomings observed in my most recent model [50]. The key modifications involved: (1) reformulating the two break-

age frequency functions to behave properly with respect to drop size; (2) replacing the constant continuous phase viscosity with a calculated emulsion viscosity that increased strongly with oil content; (3) reformulating the drop breakage and coalescence functions to behave properly with respect to oil content; and (4) replacing the equilibrium model of surfactant adsorption with a size independent dynamic model. Using a single set of adjustable parameters, the new PBE model was able to satisfactorily predict pass-by-pass DSDs for emulsion formulations with 10–50 wt% oil and 0.1—2.0 wt% surfactant with the exception of the most surfactant limited formulation with 50 wt% oil/0.1 wt% surfactant. As compared to my most recent model [50], the new PBE model generated substantially improved predictions with objective function values reduced by 15-90% depending on the particular formulation. Furthermore, I found that the inclusion of a size dependent dynamic adsorption model degraded predictive performance due to enhanced coalescence of smaller drops that lead to the underprediction of mean drop sizes in the surfactant limited regime.

## CHAPTER 5

# PREDICTION OF EMULSION DROP SIZE DISTRIBUTIONS IN COLLOID MILLS

### 5.1 Introduction

In this chapter, the first PBE model of a colloid mill is developed that includes both drop breakage and coalescence. Drop breakage was assumed to follow the usual capillary instability mechanism with the number of daughter drops formed by a breakage event studied in detail. A new daughter drop distribution function consistent with previous experimental studies was formulated to improve PBE model predictions. The drop breakage and coalescence functions depend on the emulsion viscosity. The PBE model was integrated with a viscosity model that allowed the emulsion viscosity to be predicted as a function of the oil content and extrapolated to high shear rates. Adjustable model parameters were determined by nonlinear least-squares estimation using drop size distributions measured for multiple emulsification passes. The model was used to evaluate model extensibility with respect to the oil fraction, emulsion flow rate and rotor speed.

### 5.2 Experimental Methods

#### 5.2.1 Materials

Oil-in-water emulsions were prepared using commercial sunflower oil as the dispersed phase and ultrapure water as the continuous phase. A high oil-to-surfactant ratio (10:1) was used to mimic typical industrial conditions that promote drop coalescence. The base case emulsion (Table 5.1) consisted of 30wt% oil, 3wt% Pluronic

F-68 surfactant (Sigma) and the remainder water. Other formulations with a 10:1 oil-to-surfactant ratio were used to cover a wide range of oil contents (10wt% oil, 1wt% Pluronic F-68; 50wt% oil, 5wt% Pluronic F-68; 70wt% oil, 7wt% Pluronic F-68).

**Table 5.1.** Base case emulsion formulation and homogenization conditions

Sunflower oil	30 wt%
Pluronic F-68 surfactant	3 wt%
Continuous phase density ( $\phi_c$ )	997 g/L
Dispersed phase density ( $\phi_d$ )	917 g/L
Interfacial tension ( $\sigma$ )	27 mN/m
Premixing speed and time	16000 RPM, 15 minutes
Colloid mill rotor speed ( $\omega$ )	5000 RPM
Flow rate ( $Q$ )	16 kg/hr
Gap between rotor and stator	2 mm
Number of passes	4
Emulsion viscosity at shear rate of $10^5$ 1/s ( $\eta_{em}$ )	2.6 mPa.s

### 5.2.2 Emulsion Preparation

Coarse emulsions were prepared by mixing the ingredients using a high shear mixer (LT5, Silverson). The coarse emulsion was passed through the colloid mill (Presto Mill PM30, Oskar-Krieger Ltd.) to achieve drop size reduction. Multiple emulsification passes were performed by repassing the emulsion through the colloid mill to further reduce the drop size. After each pass, approximately 2 ml of the emulsion was sampled to analyze the drop size distribution. Emulsions were prepared at two different rotor speeds (5000, 10000 RPM), three different flow rates (16, 35, 70 kg/hr) and two different gap sizes (2, 8 mm) to test their impact on the drop size distribution.

### 5.2.3 Emulsion Characterization

Drop size distributions were measured using a static light scattering device (Mastersizer 2000, Malvern Instruments). Viscosities and the interfacial tension were mea-

sured prior to each homogenization experiment. Emulsion and dispersed phase viscosities were measured using a rheometer (2000EX, TA instruments) at 25°C. The oilwater interfacial tension was measured by drop shape analysis (DSA-10 Tensiometer, KRUSS Instruments) at 25°C.

## 5.3 Theory

### 5.3.1 Population Balance Equation (PBE)

The population balance equation (PBE) is particle number balance that accounts for rates of particle creation and disappearance [63]. Although the gap region where breakage occurs is non-homogeneous (see Fig. 2.1(c)), I model the colloid mill as a well mixed system to avoid the complexities associated with modeling spatially dependent flow fields through computational fluid dynamics [24, 92]. The resulting PBE is [16, 49],

$$\begin{aligned} \frac{\partial n(v, t)}{\partial t} = & -g(v)n(v, t) + \int_v^\infty \beta(v, v')g(v')n(v', t)dv' \\ & -n(v, t) \int_0^\infty C(v, v')n(v', t)dv' + \frac{1}{2} \int_0^v C(v - v', v')n(v - v', t)n(v', t)dv' \end{aligned} \quad (5.1)$$

where  $v$  is the volume of the droplet;  $n(v, t)dv$  is the number of drops with volume in the range  $[v, v + dv]$  at time  $t$ ;  $\beta(v, v')$  is the daughter drop distribution function which represents the probability of forming a daughter drop of size  $v$  from breakage of a mother drop of size  $v'$ ;  $g(v)$  is the breakage frequency which represents the fraction of drops of volume  $v$  breaking per unit time; and  $C(v, v')$  is the coalescence frequency which represents the rate at which drops of size  $v$  and size  $v'$  coalesce. The first and third terms on the right hand side of Eq. (6.1) account for disappearance of drops of size  $v$  due to breakage and coalescence, respectively, while the second and fourth terms account for the appearance of drops of size  $v$ . The functions that describe the

breakage and coalescence processes, namely  $g(v)$ ,  $\beta(v, v')$  and  $C(v, v')$ , are described below.

The PBE (6.1) describes the evolution of the number of drops of different sizes  $n(v, t)dv$ , while standard particle size analyzers provide measurements of the volume percent distribution. Under the reasonable assumption that drops are spherical, the volume percent distribution of drops can be represented as follows,

$$n(v, t) = \frac{V_{tot}n_p(v, t)}{v} \quad (5.2)$$

where  $n_p(v, t)dv$  is the volume fraction of drops in the range  $[v, v + dv]$  at time  $t$  and  $V_{tot}$  is the conserved total volume of the drops. The PBE (6.1) can be reformulated in terms of  $n_p(v, t)$  to yield,

$$\begin{aligned} \frac{\partial n_p(v, t)}{\partial t} = & -g(v)n_p(v, t) + v \int_v^\infty \frac{\beta(v, v')g(v')n_p(v', t)}{v'} dv' \\ & - n_p(v, t) \int_0^\infty \frac{C(v, v')n_p(v', t)V_{tot}}{v'} dv' \\ & + \frac{v}{2} \int_0^v \frac{C(v - v', v')n_p(v - v', t)n_p(v', t)V_{tot}}{v'(v - v')} dv' \end{aligned} \quad (5.3)$$

### 5.3.2 PBE Functions

The PBE (6.1) contains three functions ( $g(v)$ ,  $\beta(v, v')$ ,  $C(v, v')$ ) that must be specified to compute the drop size distribution. The coalescence frequency  $C(v, v')$  of drops of size  $v$  and  $v'$  can be modeled as the product of the drop collision frequency  $F(v, v')$  and the coalescence efficiency  $E(v, v')$  [16]. For the case of simple shear flows, the coalescence frequency can be calculated as function of the shear rate  $\dot{\gamma}$  and the oil volume fraction  $\phi$  as follows [38],

$$F(v, v') = K_1 \frac{\dot{\gamma}}{(1 - \phi)} (v^{1/3} + v'^{1/3})^3 \quad (5.4)$$

where  $K_1$  is an adjustable model parameter. The average shear rate in Couette flow is calculated from rotor speed ( $\omega$ ) by,

$$\dot{\gamma} = \frac{2\pi\omega R_1}{R_2 - R_1} \quad (5.5)$$

where  $R_1$  is the radius of the rotor and  $R_2$  is inner radius of the stator. The coalescence efficiency depends on the contact time between two drops and the time required for drainage of the liquid film between the two drops. If the contact time exceeds the film drainage time, the drops will coalesce. I used the following expression originally derived for the coalescence efficiency of partially mobile, deformable drops [15],

$$E(v, v') = \exp \left[ -K_2 \frac{\eta_d}{\eta_{em}} Ca(v_{eq})^{3/2} \left( \frac{\sigma v_{eq}^2}{A} \right)^{1/3} \right] ; \quad v_{eq} = \frac{12}{\pi} \frac{v^{1/3} v'^{1/3}}{v^{1/3} + v'^{1/3}} \quad (5.6)$$

where  $v_{eq}$  is the equivalent diameter of colliding drops of volume  $v$  and  $v'$ ,  $\eta_{em}$  is the apparent emulsion viscosity,  $A$  is Hamaker constant,  $K_2$  is an adjustable model parameter, and  $Ca$  is the capillary number of drop of diameter  $d$ . The capillary number is calculated as follows,

$$Ca = \eta_{em} \dot{\gamma} d / 2\sigma \quad (5.7)$$

I assumed that the drop breakage frequency  $g(v)$  is determined by the capillary number  $Ca$  of the drop. If  $Ca$  is more than the critical capillary number  $Ca_{cr}$ , the drop will stretch under shear flow and break into smaller daughter drops. The following expression was derived under the assumption that the breakage frequency is proportional to the shear rate  $\dot{\gamma}$ ,

$$g(v) = K_3 \dot{\gamma} \exp \left( -K_4 \frac{Ca_{cr}}{Ca(v)} \right) = K_3 \dot{\gamma} \exp \left( -K_4 \frac{Ca_{cr} \sigma}{\dot{\gamma} \eta_{em} v^{1/3}} \right) \quad (5.8)$$

where  $K_3$  and  $K_4$  are adjustable model parameters. The critical capillary number was calculated by solving the following empirical equation developed for simple shear flow [18],

$$0.94 \log(\lambda)^2 + 1.11 \log(\lambda) \log(10Ca_{cr}) - 2.15 \times 10^{-5} \log(10Ca_{cr})^2 - 0.0038 \log(\lambda) - 1.5 \log(10Ca_{cr}) + 1 = 0 \quad (5.9)$$

Due to high Reynolds numbers (Table 5.2), drop breakage in the emulsions prepared at 10 and 30 wt% oil is expected to be caused by Taylor vortices [1] and not by simple shear flow (Fig. 3.1(b)). Unlike drop breakage in simple Couette flow, the breakage of drops in Taylor vortices is not well studied. Drops smaller than the Taylor vortices break due to viscous shear when the shear stress ( $\eta_{em} \dot{\gamma}_{TV}$ ) becomes more than the Laplace pressure ( $4\sigma/d$ ). Thus the breakage frequency would be expected to depend on the ratio of local viscous shear stress to the surface tension force. Because no method is available to calculate the local shear rate in Taylor vortices, I assumed the average local shear rate to be proportional to the rotor speed for simplicity. The breakage frequency function (5.8) was derived assuming the frequency depends on the ratio of the viscous stress to the surface tension force as represented by the capillary number. Therefore I used the breakage frequency function (5.8) with  $Ca_{cr} = 1$  and a distinct set of adjustable constants ( $K_3, K_4$ ) to describe drop breakage due to Taylor vortices.

**Table 5.2.** Reynolds numbers for emulsions prepared with different oil weight fractions

Emulsion oil fraction (wt%)	Emulsion density ( $kg/m^3$ )	Emulsion viscosity ( $Pa \cdot s$ )	Reynolds number ( $Re = \rho_{em} \omega R_i h / \eta_{em}$ )
10	989	0.0013	2536
30	972	0.0032	1013
50	955	0.0147	216
70	940	0.5652	5.5

Based on my previous work on PBE modeling of high pressure homogenizers [49, 50], I considered the beta function as the daughter drop distribution function  $\beta(v, v')$  (see Table 5.3). The beta function describes the breakage of a mother drop of size  $v'$  into  $p$  daughter drops with the equal probability of daughter drops of any

size ( $v < v'$ ) being formed. The number of daughter drops  $p = 15$ . I have found that PBE model predictions are not highly sensitive to this parameter as long as  $p$  is sufficiently larger. I also investigated the other commonly used drop distribution functions listed in Table 5.3.

**Table 5.3.** Daughter drop distribution functions

$\beta(v, v')$	Reference	
$\beta(v, v') = \frac{p}{v'}(p-1)\left(1 - \frac{v}{v'}\right)^{p-2}$	Hill-Ng [31]	Beta function: $p$ daughter drops form with equal probability of daughter drops of any size ( $v < v'$ ) being formed due to breakage of a mother drop of size $v'$
$\beta(v, v') = 4.8 \exp \left[ -4.5 \left( 4 \frac{v^2}{v'} - \frac{v}{v'} + 1 \right) \right]$	Liao [44]	Bell-shaped distribution function: mother drop breaks into two nearly equal sized daughter drops
$\beta(v, v') = 37.75 \left( \frac{1}{\frac{v}{v'} + 1} + \frac{1}{2 - \frac{v}{v'}} - 1.33 \right)$	Liao [44]	U-shaped distribution function: mother drop breaks into two unequal sized daughter drops

I also formulated a new daughter drop distribution function that better captured drop breakage under laminar shear flow conditions commonly encountered in colloid mills. When the viscous shear force overcomes the surface tension force, drops elongate and break to form two or more smaller drops and a large number of very small satellite drops [93]. Hence, the following bimodal daughter distribution function (Fig. 5.1) was formulated,

$$\beta_N(v, v') = M_1 \exp \left[ \frac{-1}{\left(\frac{8v}{v'}\right)^2 + \left(\frac{v'}{M_2 v}\right)^2} \right] \exp \left[ - \left( \frac{M_3 v}{v'} \right)^2 \right] \exp \left[ - \left( \frac{v'}{M_3 v} \right)^2 \right] \quad (5.10)$$

where  $M_2$  is a parameter that determines the size of satellite drops and  $M_3$  is a parameter that determines the relative probability of forming smaller drops and satellite drops. The parameter  $M_1$  is chosen to ensure that the following volume conservation equation is satisfied,

$$\int_0^{v'} \beta_N(v, v') v dv = v' \quad (5.11)$$

The choice of the parameters  $M_2$  and  $M_3$  are discussed below.

The bimodal distribution function is valid for emulsions with viscosity ratios greater than one. For emulsions with viscosity ratios less than one, a mother drop breaks into nearly uniform daughter drops due to stretching in the shear flow [93]. For this situation, a new uni-modal function was developed,

$$\beta(v, v') = M_4 \exp \left[ - \left( \frac{v'}{M_5 v} \right)^2 \right] \exp \left[ - \left( \frac{M_5 v}{v'} \right)^2 \right] \quad (5.12)$$

where  $M_5$  is a parameter that determines the size of daughter drops and  $M_4$  is a parameter that ensures volume conservation by satisfying equation 5.11. The choice of the parameter  $M_5$  is discussed below. All the daughter drop distribution functions used in this study are plotted in Fig. 5.1 for comparison. The parameters  $M_2$  and  $M_3$  in the new bimodal function (Eq. 5.10)) were chosen to yield a small peak at larger drop sizes to capture the formation of a small number of large drops and a large peak at small drop sizes to capture the formation of very large number of small satellite drops. I found that model predictions were relatively insensitive to the value of  $M_5$  in the new unimodal function (Eq. 5.12) which was chosen to yield 15 equally sized daughter drops from breakage of a mother drop by satisfying following equation for average number of daughter drops ( $p$ ) [40].

$$p = \int_0^{v'} \beta(v, v') dv \quad (5.13)$$

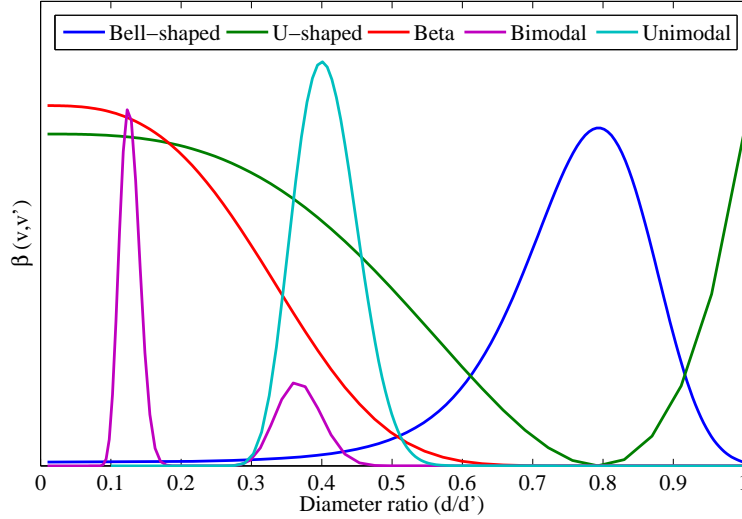


**Figure 5.1.** Daughter drop distribution functions: (1) bell-shaped function; (2) U-shaped function; (3) beta function ( $p = 15$ ); (4) new bimodal function ( $M_1 = 1, M_2 = 27; M_3 = 512$ ); (5) new unimodal function ( $M_4 = 2162, M_5 = 17.5$ ).

### 5.3.3 Emulsion Viscosity Model

Typically the continuous (water) phase viscosity is used to calculate the capillary number [34]. To capture the apparent viscosity of the fluid surrounding the drops, the continuous phase viscosity should be replaced with the emulsion viscosity for non-dilute oil mixtures. To generate a predictive model, the emulsion viscosity  $\eta_{em}$  must be calculated from known variables including the shear rate  $\dot{\gamma}$ , the oil volume fraction  $\phi$ , density  $\rho_d$  and viscosity  $\eta_d$ , the continuous phase density  $\rho_c$  and viscosity  $\eta_c$ , the surfactant concentration and the temperature  $T$ . Several models have been developed predicting the emulsion viscosity from these variables [19, 56, 33, 5]. At very low shear rates, the oil drops exist in a three-dimensional isotropic and random distribution resulting in a constant viscosity. As the shear rate increases, the drops start to align along the stream lines and the viscosity decreases due to reduced resistance to the fluid flow. At very high shear rate, drops cannot align any further and the emulsion behaves as a Newtonian fluid with a constant viscosity. Assuming no temperature

change during emulsification, the emulsion viscosity was predicted as a function of the shear rate using the following model [33],

$$\begin{aligned}
\frac{\eta_{em}}{\eta_c} &= \eta_\infty + \frac{\eta_0 - \eta_\infty}{1 + KF^m}; & F &= \frac{4\pi\eta_c\dot{\gamma}d_{32}^2d_m}{kT\phi} & (5.14) \\
\eta_0 &= \exp(K_\lambda\phi^{a_1}), & \phi &\leq \phi_c \\
&= \exp(K_\lambda\phi^{a_1})(1 + a_2(\phi - \phi_c)), & \phi &> \phi_c \\
\eta_\infty &= \exp\left(\frac{2.5\lambda+1}{\lambda+1}\phi\right), & \phi &\leq \phi_c \\
&= \exp\left(\frac{2.5\lambda+1}{\lambda+1}\phi\right)\exp(a_3(\lambda+1)(\phi - \phi_c)), & \phi &> \phi_c
\end{aligned}$$

where  $d_{32}$  is the Sauter mean diameter of the emulsion drops;  $d_m$  is hydrodynamic diameter of the surfactant molecule (assumed to be  $30 \text{ \AA}$  based on typical values of  $d_m$ );  $\phi_c$  is the critical oil volume fraction above which drops are in close contact and the interaction mechanism changes (assumed to be 0.6 from [33]);  $k$  is the Boltzmann constant ( $1.38 \times 10^{-23} \text{ J/K}$ );  $K_\lambda$ ,  $K$ ,  $m$ , and  $a_1$  are fitting parameters for  $\phi \leq \phi_c$ ; and  $a_2$  and  $a_3$  are additional fitting parameters for  $\phi > \phi_c$ . As the shear rate  $\dot{\gamma}$  is increased, the ratio  $\eta_{em}/\eta_c$  asymptotically approaches the value  $\eta_\infty$ . Therefore, the model (5.14) can be extrapolated to very high shear rates ( $> 10^4 \text{ 1/s}$ ) to calculate the emulsion viscosity inside a colloid mill. The viscosity model parameters were estimated by minimizing the least square error between measured and predicted viscosity values over a range of shear rates and oil fractions. The minimization problem was solved with the Matlab function `lsqnonlin`.

### 5.3.4 Dynamic Simulation and Parameter Estimation

The PBE (6.1) was solved numerically by approximating the integral expression using the fixed pivot technique [40] with 100 equally spaced node points. While there were small changes in solutions after increasing the number of node points, these

small improvements were accompanied by substantial increases in the computational cost for simulation and optimization (see below). Following volume discretization, 100 nonlinear ordinary differential equations were obtained in which time was the independent variable and the volume percent distribution at each node point were the dependent variables. The ODEs were solved by specifying the measured volume percent distribution of the coarse emulsion as the initial condition  $n_p(v, 0)$  for the first pass through colloid mill. Each pass corresponded to the colloid mill residence time  $t_{res}$ , calculated as the ratio of volume between stator and rotor to the volumetric flow rate through the unit. The initial condition for each subsequent pass was the predicted volume percent distribution from the previous pass. The Matlab integration code `ode15s` was used to solve the ODE system.

Given a prespecified daughter drop distribution function, the constants  $K_1 - K_4$  in the coalescence and breakage functions were estimated from base case emulsification experiments (30 wt% oil, 3 wt% surfactant). The data used for parameter estimation consisted of the bulk emulsion properties ( $\phi$ ,  $\sigma$ ,  $\eta_{em}$ ), operating conditions ( $\dot{\gamma}$ ,  $t_{res}$ ), the measured premix volume distribution ( $n_p(v, 0)$ ), and measured volume distributions  $n_p(v, t)$  for four passes through the colloid mill. The 100 ODEs obtained from volume discretization of the PBE model were temporally discretized using orthogonal collocation with 12 finite elements and 2 internal collocation points per element to produce a large set of nonlinear algebraic equations. Each pass corresponded to 3 finite elements. This set of algebraic equations was posed as a set of equality constraints in the nonlinear optimization problem. I found that additional spatial node points, finite elements, and/or collocation points did not affect the parameter estimates but increased the computational effort significantly. The least-square objective function  $\Psi$  used for parameter estimation was,

$$\Psi = \frac{1}{N} \sum_{i=1}^N \frac{\sum_{j=1}^n [\hat{n}_p(v_j, i) - n_p(v_j, i)]^2}{\sum_{j=1}^n [n_p(v_j, i)]^2} \quad (5.15)$$

<sup>1</sup>where  $n_p(v_j, i)$  is the measured value of the drop volume distribution at drop volume  $v_j$  and emulsification pass  $i$ ;  $\hat{n}_p(v_j, i)$  is the corresponding predicted value from the discretized PBE model;  $n$  is the total number of spatial node points; and  $N = 4$  is the number of passes. The objective function was minimized subject to equality constraints representing the discretized PBE as well as continuity conditions across the finite elements. The optimization problem was formulated in AMPL [25] and solved with the nonlinear program solver CONOPT [23]. Furthermore, values of the objective function  $\Psi$  were used to judge the quality of model predictions for different experiments.

## 5.4 Results and Discussion

### 5.4.1 Prediction of Emulsion Viscosity

The adjustable parameters in the viscosity model (equation 5.14) were estimated from the emulsion viscosity data shown in Figure 5.2 and from  $d_{32}$  values computed from measured drop size distributions. Data were collected over a range of oil fractions (10-70 wt%) and shear rates (1–1000 1/s) determined by the operating limits of the used rheometer. As the oil fraction was increased, the emulsion viscosity was observed to increase several orders of magnitude. Model predictions extrapolated to low and high shear rates are also shown in Figure 5.2. Although not highly accurate, the model predictions captured the large changes in emulsion viscosity observed experimentally as the oil fraction was varied. The emulsion viscosity  $\eta_{em}$  used in the PBE model was computed from the viscosity model as the plateau value at high shear rates.

---

<sup>1</sup>As  $n_p(v_j, i)$  has some values equal to zero, least square errors were normalized by sum of  $n_p(v_j, i)^2$  to avoid the denominator to go to zero.

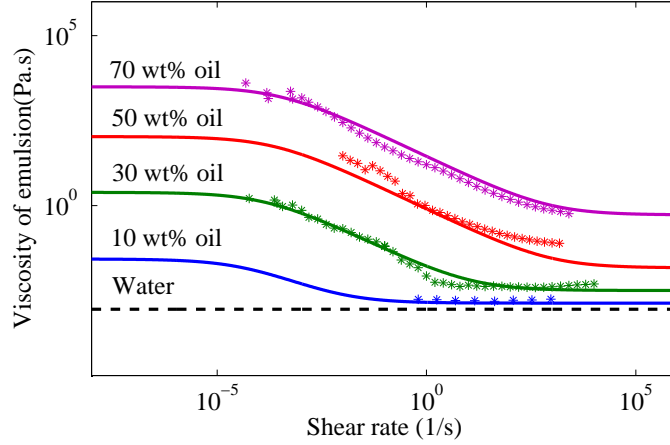


**Figure 5.2.** Emulsion viscosity predictions at different oil volume fractions and shear rates with model parameters  $K_\lambda = 19.5$ ,  $k = 1900$ ,  $m = 0.59$ ,  $a_1 = 0.8$ ,  $a_2 = 0.2$  and  $a_3 = 0.01$ .

#### 5.4.2 Evaluation of Daughter Drop Distribution Functions

The adjustable parameters  $K_1 - K_4$  in the breakage and coalescence frequency functions were estimated from experimental data collected at the base case conditions (Table 5.1) to determine the most appropriate daughter drop distribution function. First parameter estimation was performed for each of the distribution functions shown in Table 5.3. The bell-shaped and u-shaped daughter drop distributions failed to capture the small peak at small drop sizes observed experimentally (Fig. 5.3(a),5.3(b)). The u-shaped function also produced poor predictions at larger drop sizes, suggesting that most breakage events do not produce a single small drop and a single large drop. I also performed parameter optimization using the beta daughter drop distribution function with  $p = 20$  daughter drops (Fig. 5.3(c)) and  $p = 200$  daughter drops (Fig. 5.3(d)). Although the predicted drop size distributions matched well with data in the large drop size range, the models again failed to capture a second peak at small drop sizes. When predicted drop size distributions were converted to number distributions and compared to data, all four daughter distributions were observed to produce large predictions errors (Fig. 5.4).

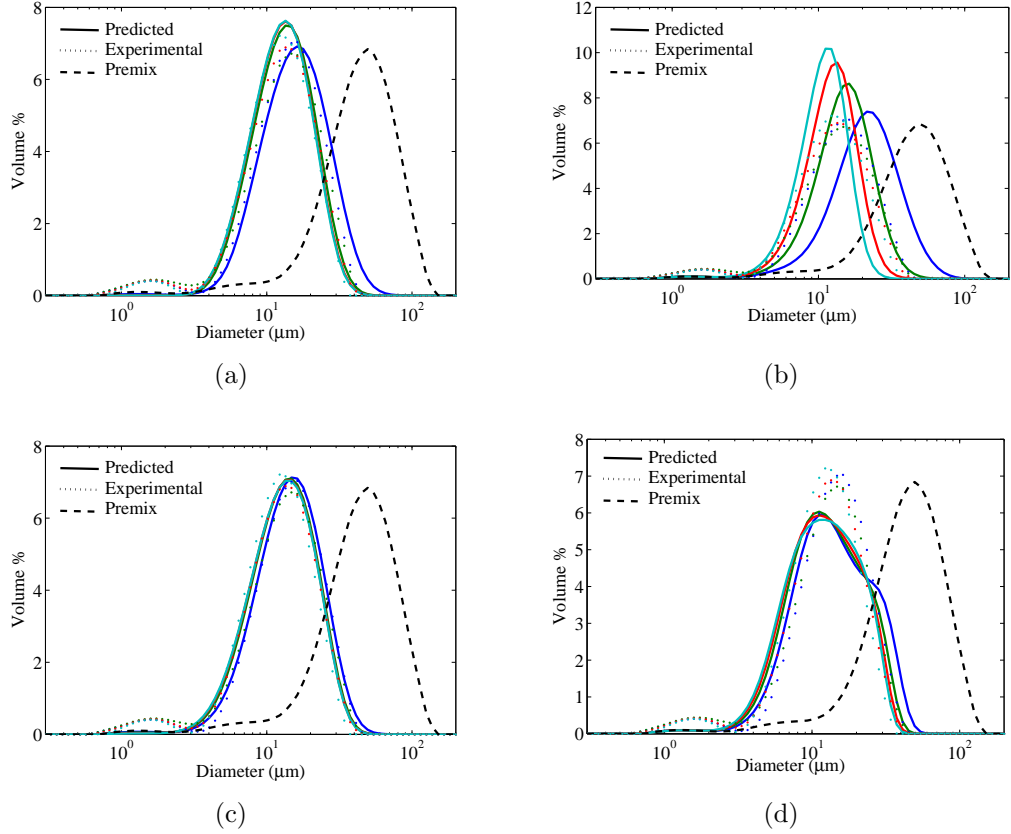


**Figure 5.3.** Drop volume distributions (—: first pass, —: second pass, —: third pass, —: fourth pass) obtained using the (a) bell-shaped daughter distribution function ( $\Psi = 0.01335$ ), (b) u-shaped daughter distribution function ( $\Psi = 0.1475$ ), (c) beta daughter distribution function ( $p = 20$ ,  $\Psi = 0.0071$ ), and (d) beta daughter distribution function ( $p = 200$ ,  $\Psi = 0.0401$ ) for the base case conditions.

Next the proposed bimodal daughter distribution (Eq (5.10)), which captures the breakage of drops into a relatively small number of larger drops and many small satellite drops, was used for parameter estimation. Based on preliminary simulation results (not shown), the parameters  $M_2 - M_3$  in the bimodal distribution that produced the best fit of the base case drop volume distribution data were determined as  $M_2 = 38.3$  and  $M_3 = 5.832 \times 10^3$ . With these parameter values fixed, the adjustable parameters  $K_1 - K_4$  in the breakage and coalescence frequency functions were estimated as before. The bimodal distribution function produced substantially improved predictions of the volume and number drop size distributions as well as very accurate

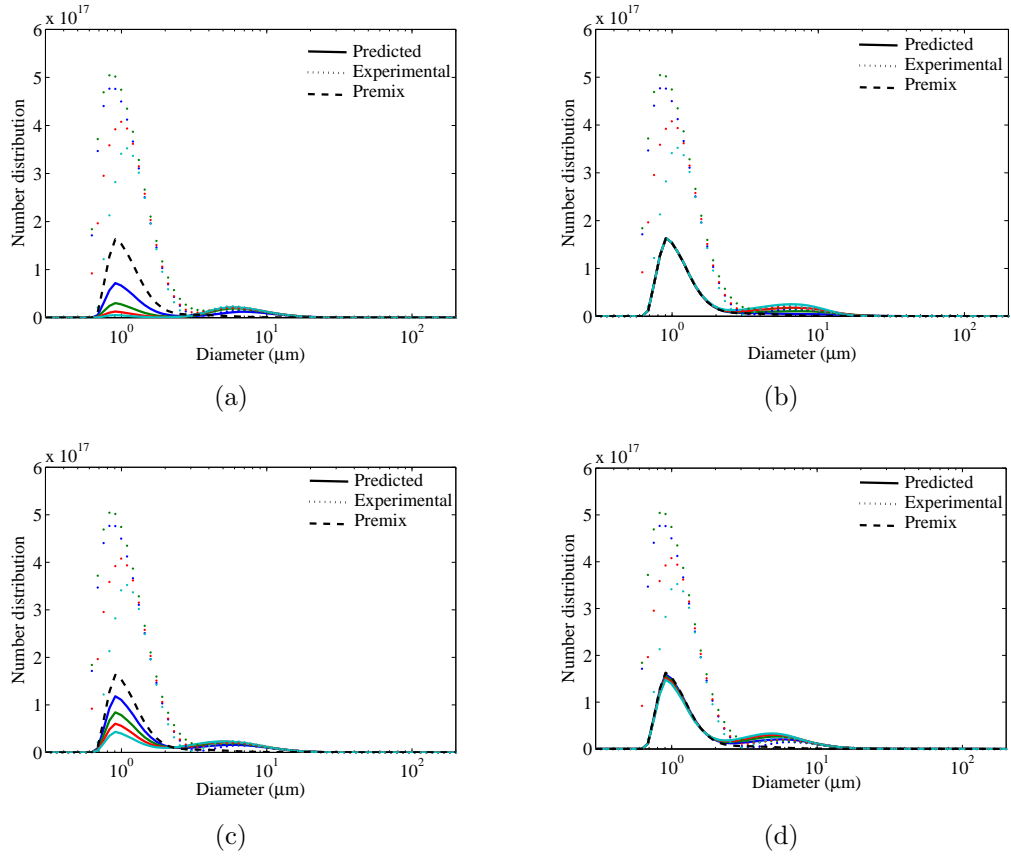


**Figure 5.4.** Number distributions (—: first pass, —: second pass, —: third pass, —: fourth pass) obtained using the (a) bell-shaped daughter distribution function, (b) u-shaped daughter distribution function, (c) beta daughter distribution function ( $p = 20$ ), and (d) beta daughter distribution function ( $p = 200$ ) for the base case conditions.

predictions of the Sauter mean diameter  $d_{32}$  (Fig. 5.5). This bimodal distribution function was used throughout the remainder of the study.

### 5.4.3 Effect of Oil Volume Fraction

The oil fraction was expected to have a strong impact on the drop size distribution, with higher oil fractions producing more drop collisions and smaller drop sizes. To investigate this effect, emulsification experiments were performed using four different oil fractions (10, 30, 50, 70 wt%) while maintaining a constant oil-to-surfactant ratio (10/1). The colloid mill operating variables were held constant at their base base

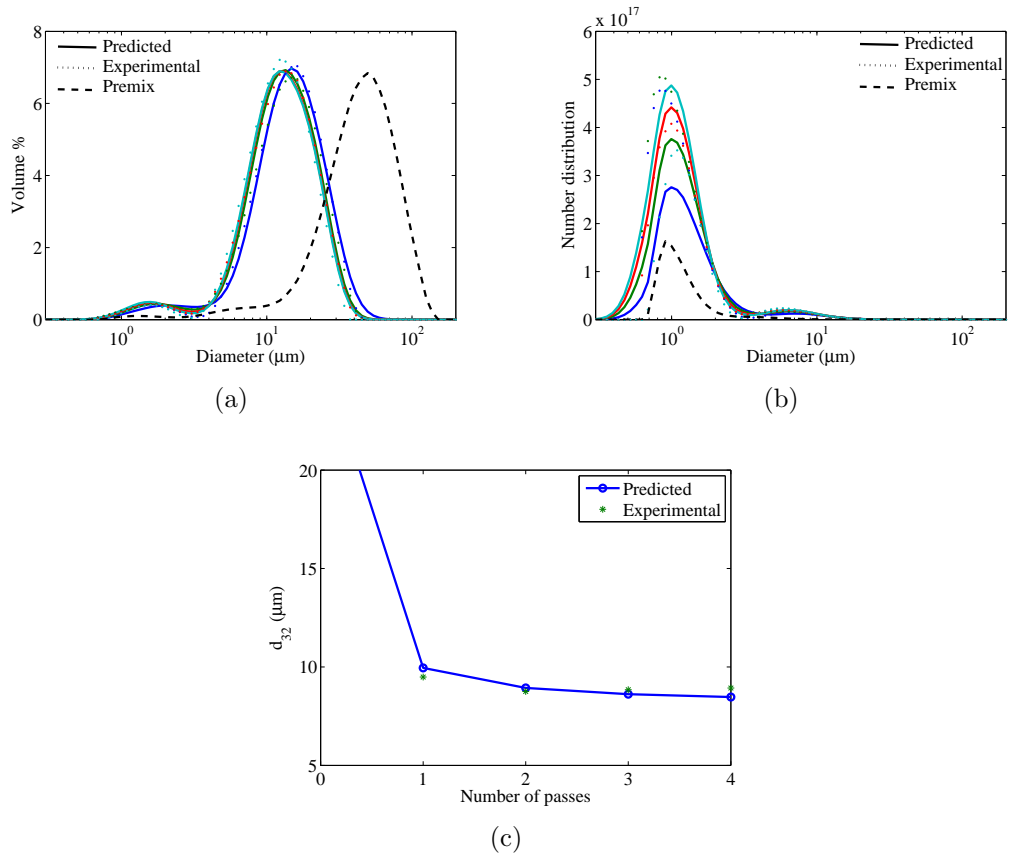


**Figure 5.5.** (a) Drop volume distributions (—: first pass, —: second pass, —: third pass, —: fourth pass) ( $\Psi = 0.0048$ ), (b) number distributions, and (c) Sauter mean diameter obtained using the proposed bimodal daughter drop distribution function for base case conditions

values (5000 RPM rotor speed, 16 kg/hr flow rate, 2 mm gap size). Because emulsions with 70 wt% oil became too viscous to process after several passes through the colloid mill, drop volume distributions were collected only for the first two passes. The Sauter mean diameter was observed to decrease with increasing oil fraction (Fig. 5.6(d)) due to increased viscous shear stress. As has been previously reported [93], bi-modal drop size distributions were produced because large viscosity ratios tend to cause drop stretching with filaments that generate many small satellite drops in addition to larger daughter drops. Larger viscosity ratios were expected to produce a larger number of daughter drops due to increased stretching. While in principle this behavior could have been captured by making the daughter drop distribution function a function of

the viscosity ratio, this approach would be complex and lead to difficult optimization problems.

Instead, the adjustable parameters  $K_1 - K_4$  were estimated for each oil fraction separately such that the breakage frequency would increase with increasing viscosity ratio. The PBE models produced satisfactory predictions of measured drop size distributions at 10, 30, and 50 wt% oil (Fig. 5.6). Moreover, the models were able to properly balance drop breakage and coalescence such that the predicted drop size distributions did not substantially change after the first pass as observed experimentally. For the 70 wt% oil emulsion, the viscosity ratio was less than one and drop breakage was expected to follow the proposed uni-modal daughter distribution function (Eq. (5.12)). Following estimation of the adjustable model parameters  $K_1 - K_4$  with the uni-modal distribution function, the PBE model produced accurate predictions of the measured drop volume distributions (Fig. 5.7).

#### 5.4.4 Effect of Flow Rate

The flow rate through the colloid mill affects the residence time, which in turn influences the degree of drop breakage. Higher flow rates are preferred to increase process throughput, while lower flow rates produce smaller drops. To investigate these trade offs, emulsification experiments were performed at three different flow rates (16, 35, 70 kg/hr) at high rotor speed (10000 RPM) using emulsions with 50 wt% oil. As expected, increasing flow rates resulted in the formation of relatively large drops (Fig. 5.8(d)). The flow rate effect was most dominant at the highest flow rate (70 kg/hr) where the residence time was not sufficiently large to allow complete drop breakage, while the drop sizes obtained at the smaller flow rates (16, 35 kg/hr) were very similar. To examine the ability of the PBE model to predict this trend, the parameters  $K_1 - K_4$  in the drop breakage functions and the parameters  $M_2$  and  $M_3$  in the daughter drop distribution function were estimated from data collected at

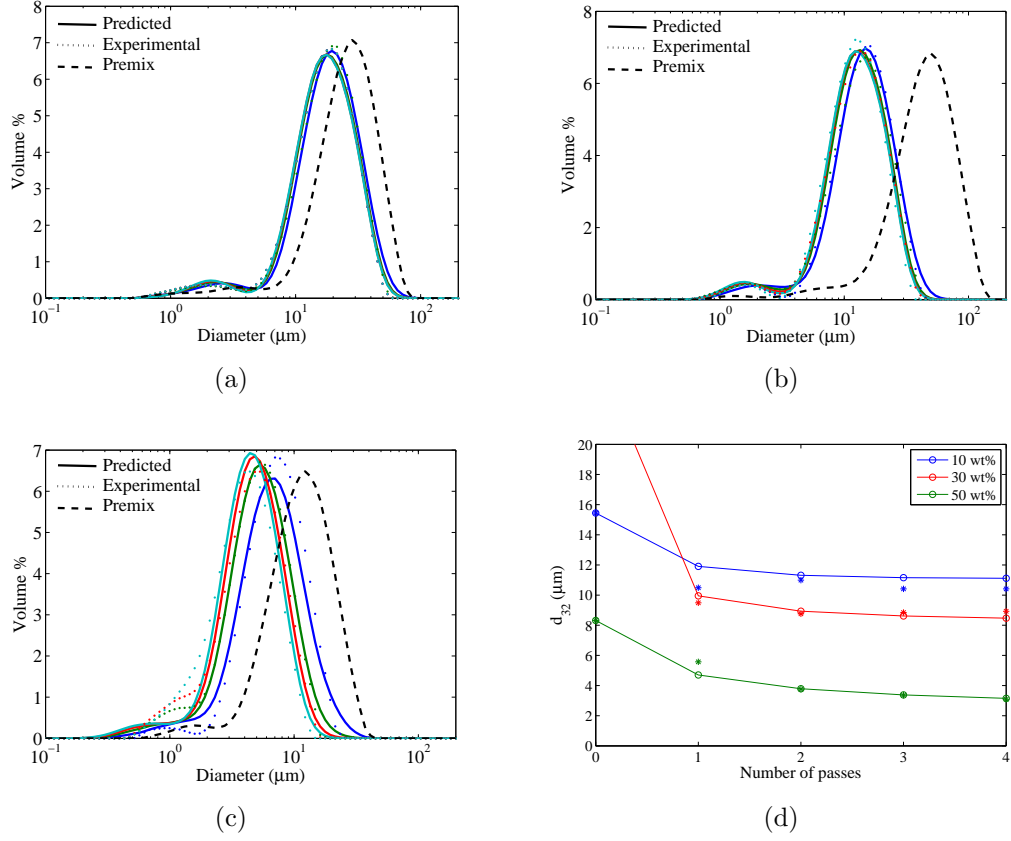


**Figure 5.6.** Drop volume distribution predictions (—: first pass, —: second pass, —: third pass, —: fourth pass) of emulsions with (a) 10 wt% oil ( $\Psi = 0.0050$ ), (b) 30 wt% oil ( $\Psi = 0.0048$ ), (c) 50 wt% oil ( $\Psi = 0.0118$ ), and (d) predicted and measured Sauter mean diameters obtained using the proposed bimodal daughter drop distribution function.

a flow rate of 16 kg/hr and used without re-estimation to predict the drop volume distributions at the two higher flow rates. Only the residence time, calculated as the ratio of the volume between the stator and rotor to the volumetric flow rate, was varied between the three cases. The model produced very good agreement with the measured distributions at 16 kg/hr (Fig. 5.8(a)) and 35 kg/hr (Fig. 5.8(b)). However, the model overpredicted the degree of drop breakage for the first and fourth passes at 70 kg/hr (Fig. 5.8(c)). These results suggest that some further model refinements may be needed to more accurately predict the flow rate effect.

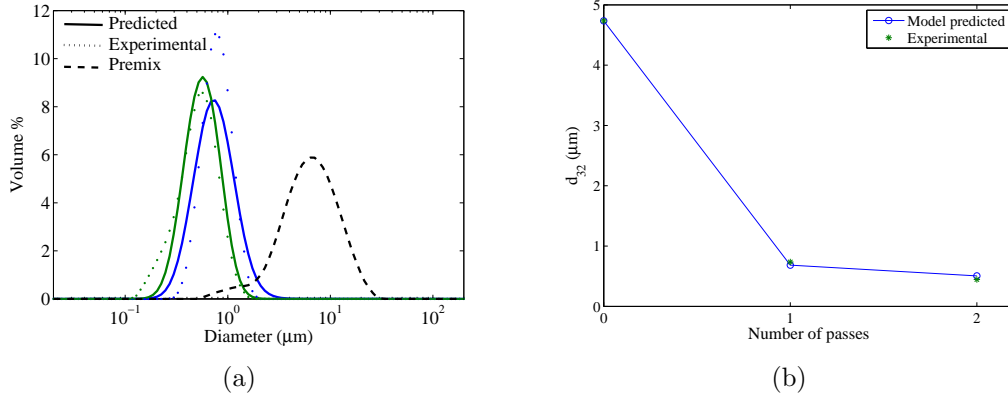


**Figure 5.7.** (a) Drop volume distribution predictions (—: first pass, —: second pass) and (b) predicted and measured Sauter mean diameters of an emulsion with 70 wt% oil ( $\Psi = 0.059$ ) obtained using the proposed uni-modal daughter drop distribution function.

#### 5.4.5 Effect of Rotor Speed

According to Eq. 5.5, the shear rate is directly proportional to the rotor speed. Consequently, the rotor speed was expected to have a strong impact on the drop size distribution with increased drop breakage resulting from increased rotor speeds. To investigate this effect, emulsification experiments were performed at two rotor speeds (5000, 10000 RPM) over a range of oil fractions (10, 30, 50, 70 wt%). For each oil fraction, the PBE model parameters  $K_1 - K_4$ ,  $M_2$  and  $M_3$  were estimated from data collected at 5000 RPM and used to predict drop volume distributions at 10000 RPM. In the case of 70 wt% oil, the emulsion was too viscous to be processed at 10000 RPM and data was collected from a single pass at 8000 RPM. While the model predictions were generally satisfactory at 10 wt% (Fig. 5.9(a)) and 30 wt% (Fig. 5.9(b)) oil, the model overpredicted drop breakage and/or under-predicted drop coalescence at 50 wt% (Fig. 5.9(c)) and 70 wt% oil (5.9(d)). One possibility for improving model predictions at high oil fractions is to allow the shear rate to depend nonlinearly on the rotor speed. This modification along with other attempts to improve model extensibility would require additional research.

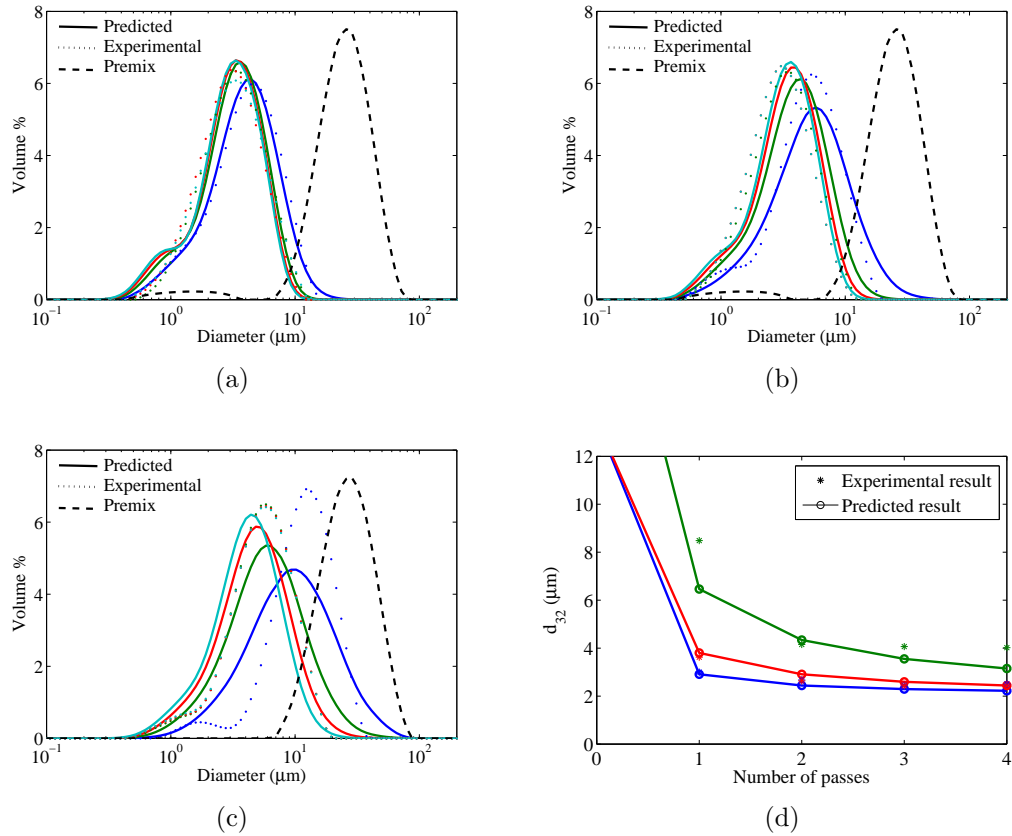


**Figure 5.8.** Drop volume distributions (—: first pass, —: second pass, —: third pass, —: fourth pass) of emulsions with 50 wt% oil passed through the colloid mill at a flow rate of (a) 16 kg/hr ( $\Psi = 0.0207$ ), (b) 35 kg/hr ( $\Psi = 0.0543$ ), (c) 70 kg/hr ( $\Psi = 0.0765$ ); and (d) Sauter mean diameters at the different flow rates ( \* : 16 kg/hr, \* : 35 kg/hr, \* : 70 kg/hr) using model parameters estimated from data collected at 16 kg/hr.

## 5.5 Conclusions

I developed a population balance equation (PBE) model to predict drop size distributions in the colloid mill emulsification process. The model accounts for drop breakage due to capillary instability, drop coalescence due to shear driven drop collisions, and the effects of emulsion viscosity on the breakage and coalescence rates. I used the model to investigate drop breakage mechanisms and to examine predictive capability for changes in operating conditions. A published emulsion viscosity model was fit to viscosity data collected over a range of shear rates and oil fractions and

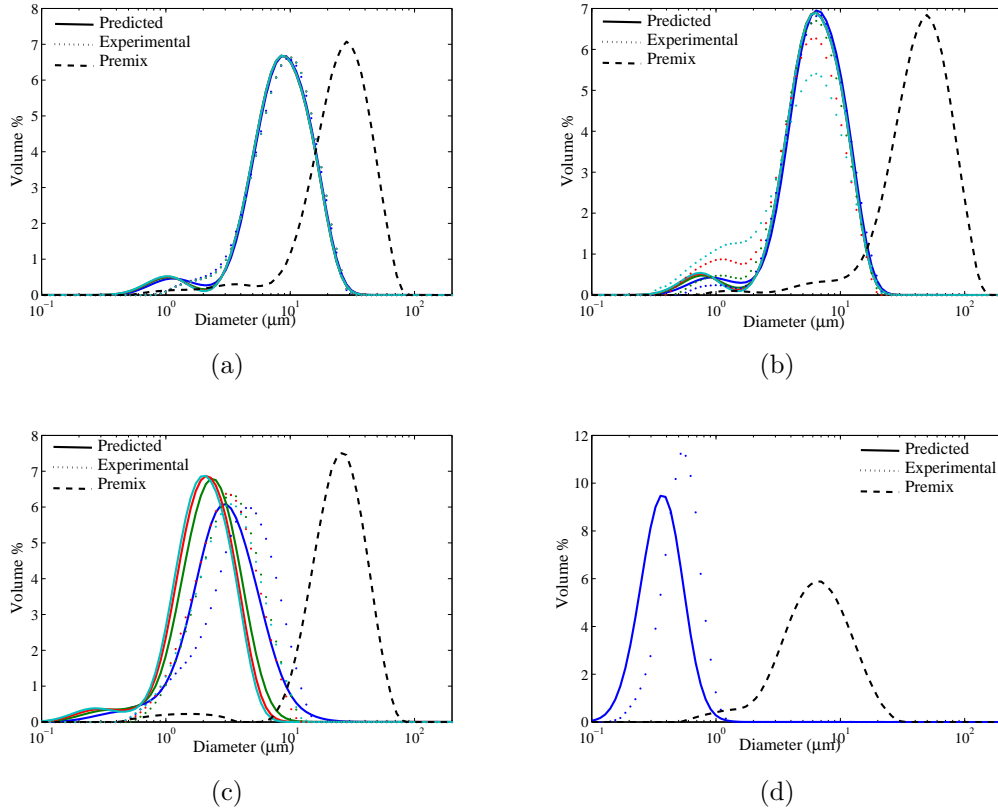


**Figure 5.9.** Drop volume distributions (—: first pass, —: second pass, —: third pass, —: fourth pass) of emulsions with (a) 10 wt% oil processed at 10000 RPM ( $\Psi = 0.007$ ), (b) 30 wt% oil processed at 10000 RPM ( $\Psi = 0.0325$ ), (c) 50 wt% oil processed at 10000 RPM ( $\Psi = 0.325$ ), and (d) 70 wt% oil processed at 8000 RPM ( $\Psi = 0.41$ ),

extrapolated to very high shear rates for use within the PBE model. The used colloid mill produced bimodal drop size distributions that could not be predicted with functions commonly used for the daughter drop distribution, which determines the number and size of the drops that result from a breakage event. I proposed a new bimodal daughter distribution function that captured the formation of many small satellite drops and produced acceptable drop distribution predictions with respect to both volume percent and absolute number. While this bimodal distribution function proved satisfactory for emulsions with 10-50 wt% oil, a unimodal distribution function that captured more uniform drop breakage was used at 70 wt% oil to gen-

erate acceptable predictions. The oil fraction, flow rate and rotor speed were varied to examine model extensibility to new operating conditions with adjustable model parameters estimated from drop volume distribution measurements collected at a different operating condition. The model was reasonably extensible to different flow rates, while prediction accuracy for changes in rotor speed was less satisfactory. I believe my model represents the first attempt to develop a full PBE description of the colloid mill process and will provide a template for future research efforts aimed at predicting emulsion size distributions.

## CHAPTER 6

# ACHIEVING TARGET EMULSION DROP SIZE DISTRIBUTIONS USING POPULATION BALANCE EQUATION MODELS OF HIGH PRESSURE HOMOGENIZATION

### 6.1 Introduction

In chapter 2, I incorporated drop coalescence functions to allow the drop volume distribution to be predicted for a much higher oil-to-surfactant ratio (50% oil, 1% surfactant). Nonlinear optimization was used to estimate six adjustable parameters in the drop breakage and coalescence functions to match measured size distributions. In this chapter, the resulting model is used to develop a methodology for computing the number of homogenizer passes and the operating pressure of each pass such that target emulsion drop size properties are achieved in a least-squares sense.

### 6.2 PBE Model Development

#### 6.2.1 Model Formulation

The PBE is formally derived from a number balance on particles by accounting for the various rate processes such as breakage and coalescence that affect particle size [63]. In this study, a volume structured PBE was used because light scattering most directly measures drop volume. Although homogenizers have distinct zones where local shear forces can change dramatically [28], I treat the homogenizer as a well-mixed batch system to avoid the complexities associated with including spatial variations. In this case, the PBE can be written as [60, 16],

$$\begin{aligned} \frac{\partial n(v, t)}{\partial t} = & -g(v)n(v, t) + \int_v^\infty \beta(v, v')g(v')n(v', t)dv' \\ & - n(v, t) \int_0^\infty C(v, v')n(v', t)dv' + \frac{1}{2} \int_0^v C(v - v', v')n(v - v', t)n(v', t)dv' \end{aligned} \quad (6.1)$$

where  $v$  is the volume of the particle;  $n(v, t)dv$  is the number of drops with volume in the range  $[v, v + dv]$  per unit volume of dispersion at time  $t$ ;  $g(v)$  is the breakage rate representing the fraction of drops of volume  $v$  breaking per unit time;  $\beta(v, v')$  is the daughter drop distribution function representing the probability of forming a daughter drop of size  $v$  from breakage of a mother drop of size  $v'$ ; and  $C(v, v')$  is coalescence frequency representing the rate at which drops of size  $v$  and drops of size  $v'$  coalesce. The model requires specification of the functions that describe the breakage and coalescence processes, namely  $g(v)$ ,  $\beta(v, v')$  and  $C(v, v')$ . The PBE (6.1) describes the evolution of the number density  $n(v, t)$ , while particle size analysis usually provides measurements of the volume percent distribution  $n_p(v, t)$ . Under the standard assumption that drops are spherical, the two distributions are easily related [60]. The measured volume distribution of the coarse pre-emulsion is used as initial condition for the first homogenizer pass. Each pass corresponds to one dimensionless time unit, and the initial condition for each subsequent pass is the predicted volume distribution from the previous pass.

The PBE (6.1) contains three functions that must be specified to compute the drop size distribution. Following the previous work [60], the breakage rate  $g(v)$  is assumed to be determined by turbulent breakage of drops by both inertial and viscous forces such that  $g(v) = g_1(v) + g_2(v)$ . The first breakage function  $g_1(v)$  is derived assuming drops break due to collision with turbulent eddies [16],

$$g_1(v) = K_1 v^{-2/9} \epsilon^{1/3} \left[ \exp \left( -\frac{K_2 \sigma (1 + \phi)^2}{\rho_d v^{5/9} \epsilon^{2/3}} \right) \right] \quad (6.2)$$

where  $K_1$  and  $K_2$  are adjustable constants. The second breakage rate function  $g_2(v)$  is derived assuming that drop breakage results from turbulent shear [60],

$$g_2(v) = K_3 \left( \frac{2}{\pi} \right)^{1/2} \left( \frac{\epsilon \rho_d}{\eta_d} \right)^{1/2} \left[ \exp \left( -\frac{K_4 \sigma^2 \lambda}{v^{2/3} \epsilon \eta_c} \right) \right] \quad (6.3)$$

where  $K_3$  and  $K_4$  are the adjustable constants. The two breakage rates depend on the homogenizer pressure  $P$  through the energy dissipation rate  $\epsilon$  (see below) and emulsion properties including the dispersed phase volume fraction  $\phi$ , the interfacial tension  $\sigma$ , the dispersed phase density  $\rho_d$ , the continuous phase viscosity  $\eta_c$  and the dispersed phase viscosity  $\eta_d$  through the ratio  $\lambda = \frac{\eta_d}{\eta_c}$ . I have shown that these dependencies are necessary for the PBE model to be predictive over a range of formulation and homogenization conditions with a single set of constants  $K_1$ – $K_4$  [60, 59].

The breakage rate function is specialized to high-pressure homogenizers by using the following relation for the energy dissipation rate [84, 83],

$$\epsilon = \frac{\Delta P Q}{V_{diss}} \quad (6.4)$$

where  $\Delta P$  is the applied pressure,  $Q$  is the volumetric flow rate and  $V_{diss}$  is the valve gap volume which depends on valve gap distance  $h_{gap}$ . Equations for  $V_{diss}$  and  $h_{gap}$  can be found in the previous work [60]. As in the previous breakage-only PBE model, I use the power law product form of the generalized Hill-Ng distribution [31, 91] as the daughter drop distribution function  $\beta(v, v')$  to model the breakage of a mother drop into multiple daughter drops. The parameter  $q$  is chosen as unity to represent the uniform probability of daughter drops of any size ( $v < v'$ ) being formed due to breakage of a mother drop of size  $v'$ . In this case, the daughter drop distribution function has the form,

$$\beta(v, v') = (p - 1) \left(1 - \frac{v}{v'}\right)^{p-2} \quad (6.5)$$

where  $p \geq 2$  is the number of daughter drops formed from breakage of a single mother drop. Based on preliminary simulation results (not shown), I determined that the best fit of drop volume distribution data was obtained for  $p = 80$ . While laminar flow experiments have established that a mother drop can break into numerous daughter drops [94], the assumption that turbulent homogenization conditions could produce as many as 80 daughter drops from a single mother drop requires experimental testing beyond the scope of this study.

The coalescence frequency  $C(v, v')$  of drops of size  $v$  and  $v'$  is modeled as the product of the drop collision frequency  $h(v, v')$  and the coalescence efficiency  $\lambda(v, v')$ :  $C(v, v') = h(v, v')\lambda(v, v')$ . While certainly not mechanistically correct, I follow the common practice of modeling the collision frequency assuming that drops in turbulent flow behave like gas molecules [16],

$$h(v, v') = \frac{K_5 \epsilon^{1/3}}{1 + \phi} (v^{2/3} + v'^{2/3})(v^{2/9} + v'^{2/9})^{1/2} \quad (6.6)$$

where  $K_5$  is an adjustable constant. The coalescence efficiency is modeled to depend on the contact time of droplets, with coalescence occurring if the contact time is greater than the time required for the liquid film between two drops to drain [16],

$$\lambda(v, v') = \exp \left[ \frac{-K_6 \eta_c \rho_c \epsilon}{\sigma^2 (1 + \phi)^3} \left( \frac{v^{1/3} v'^{1/3}}{v^{1/3} + v'^{1/3}} \right)^4 \right] \quad (6.7)$$

where  $K_6$  is an adjustable constant. Similar to the breakage rate, the coalescence frequency depends on the homogenizer pressure  $P$  through the energy dissipation rate  $\epsilon$  and emulsion properties including the continuous phase density  $\rho_c$  and  $\phi$ ,  $\sigma$  and  $\eta_c$ .

### 6.2.2 Emulsification Experiments

Oil-in-water emulsions were prepared using vegetable oil (Fisher Scientific) as the dispersed phase and water as the continuous phase. Emulsions consisted of 50 wt% oil and 1 wt% Pluronic F-68 surfactant with the remainder water. Emulsions were prepared using a two-step process. First approximately 400 ml of coarse pre-emulsion was prepared by mixing the ingredients in a stator-rotor device (Ultra-Turrax Model T25, Rose Scientific Ltd.) at 16000 rpm for 15 minute. About 100 ml of pre-emulsion was processed in a high-pressure homogenizer (Emulsiflex C-3, Avestin Inc.) to reduce the average drop size. The base case homogenization pressure was chosen as 800 bar to produce small drops likely to undergo coalescence. Multiple passes were performed by reprocessing the emulsion obtained from the previous homogenizer pass. After each pass approximately 2 ml of emulsion was sampled to analyze the drop size distribution. Extensibility experiments were performed at three lower pressures (200, 400 and 600 bar). Drop size distributions were measured using static light scattering (Mastersizer S, Malvern Instruments). Densities, viscosities and the interfacial tension were measured prior to each homogenization experiment. Continuous and dispersed phase densities were measured using a Bio-Rad 36XMX densitometer. The oil-water interfacial tension  $\sigma_{o/w}$  was measured by drop shape analysis (Model DSA-10 Tensiometer, KRUSS Instruments) at 25°C.

### 6.2.3 Parameter Estimation and Model Extensibility

The PBE model (6.1) was solved numerically by approximating the integral expression using the fixed pivot technique [40] with 100 equally spaced node points. The discretized PBE model consisted of 100 nonlinear ordinary differential equations in which the independent variable was time and the dependent variables represented the volume percent distribution at each node point. The ODE system was solved

with the Matlab integration code `ode45` using the measured premix distribution as the initial condition  $n_p(v, 0)$ .

The constants  $K_1$ – $K_4$  in the breakage rate function and  $K_5$ – $K_6$  in the coalescence frequency function were estimated from base case homogenization experiments. The data used for parameter estimation were emulsion properties  $(\phi, \sigma, \rho_c, \rho_d, \eta_c, \eta_d)$ , the premix volume distribution  $n_p(v, 0)$  and the measured drop volume distribution  $n_p(v, t)$  after each homogenization pass. The 100 ODEs obtained from spatial discretization of the PBE model were temporally discretized using orthogonal collocation with 15 finite elements and 2 internal collocation points per element to produce a large set of nonlinear algebraic equations. Each homogenizer pass corresponded to 3 finite elements. The algebraic equation system was posed as a set of equality constraints in the nonlinear optimization problem. The least-squares objective function  $\Psi$  used for parameter estimation was,

$$\Psi = \sum_{i=1}^N \frac{\sum_{j=1}^n [\hat{n}_p(v_j, i) - n_p(v_j, i)]^2}{\sum_{j=1}^n [n_p(v_j, i)]^2} \quad (6.8)$$

where  $n_p(v_j, i)$  is the measured value of the drop volume distribution at drop volume  $v_j$  and homogenizer pass  $i$ ,  $\hat{n}_p(v_j, i)$  is the corresponding predicted value from the discretized PBE model,  $n$  is the total number of spatial node points, and  $N$  is the number of passes. The objective function was minimized subject to the large number of equality constraints representing the discretized model equations as well as continuity conditions across the finite elements. The optimization problem was formulated in AMPL [25] and solved using the nonlinear program solver CONOPT [23]. Values of the objective function  $\Psi$  were used to judge the quality of model predictions for different experiments.

At the base case conditions where parameter estimation was performed, the PBE model produced very accurate predictions of the volume distribution and mean diameter (Figure 6.1) following each homogenizer pass. Next the model parameters were

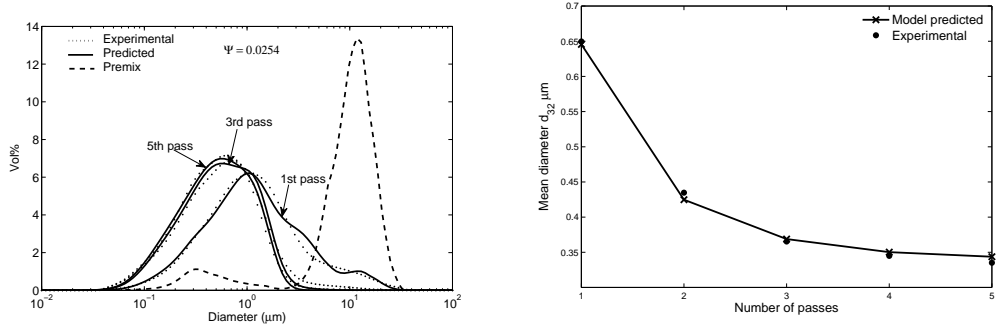


**Figure 6.1.** Experimental and model predicted results for homogenization with 50wt% oil, 1wt% PF-68 homogenized at 800 bar. (a) Drop volume distributions, (b) Sauter mean diameters.

re-estimated at homogenization pressures different than the base case value to further access predictive capability. The homogenization pressure was incorporated into the model through the energy dissipation rate (6.4). For each pressure, drop volume distributions measured following five homogenization passes were used to estimate  $K_1$ – $K_6$ . As shown in the second column of Table 6.1, parameter re-estimation yielded very accurate predictions of drop volume distributions at each pressure. Finally the model parameters estimated at 600 bar were used to predict drop volume distributions at the other three pressure without re-estimation. The results are shown in the third column of Table 6.1 and Figure 6.2. Although the model showed good qualitative agreement with data, I found that the predictions were not sufficiently accurate at other pressures to be used for model-based design. Analysis of the estimation results showed that the model parameters  $K_2$  and  $K_4$  that determine efficiencies of the two breakage mechanisms varied significantly between the four pressures. Therefore, these parameter values were interpolated to generate improved predictions (see below).

**Table 6.1.** Minimized objective function values at different pressures

Pressure (bar)	Estimation at each pressure	Estimation at 600 bar
200	0.077	1.284
400	0.074	0.383
600	0.032	0.032
800	0.025	0.236
Total	0.208	1.934

## 6.3 Model-Based Design of Homogenizer Operating Conditions

### 6.3.1 Optimization Methodology

The PBE model was used to predict homogenization conditions that would achieve the specified emulsion drop size properties. In this study, the product design problem was formulated as a nonlinear least-squares optimization problem with the number of homogenizer passes and the operating pressure at each pass chosen as decision variables. As discussed in the previous section, improved predictions were achieved by interpolating the breakage rate parameters  $K_2$  and  $K_4$  using values estimated at four pressures that covered the range of interest (Figure 6.3).

The optimization formulation requires specification of an objective function for achieving the target emulsion drop size properties. I considered two alternative least-squares objectives for this purpose. The first objective represents the drop size distribution in terms of the Sauter mean diameter ( $d_{32}$ ) and the polydispersity ( $PD$ ),

$$\Psi_1 = \sqrt{\frac{(d_{32tar} - d_{32})^2}{d_{32tar}^2} + \frac{(PD_{tar} - PD)^2}{PD_{tar}^2}} \quad (6.9)$$

where the *tar* subscript represents target values and the other variables represent model predicted values. While these target values are relatively simple to specify for a particular problem, their attainment does not ensure that a satisfactory drop

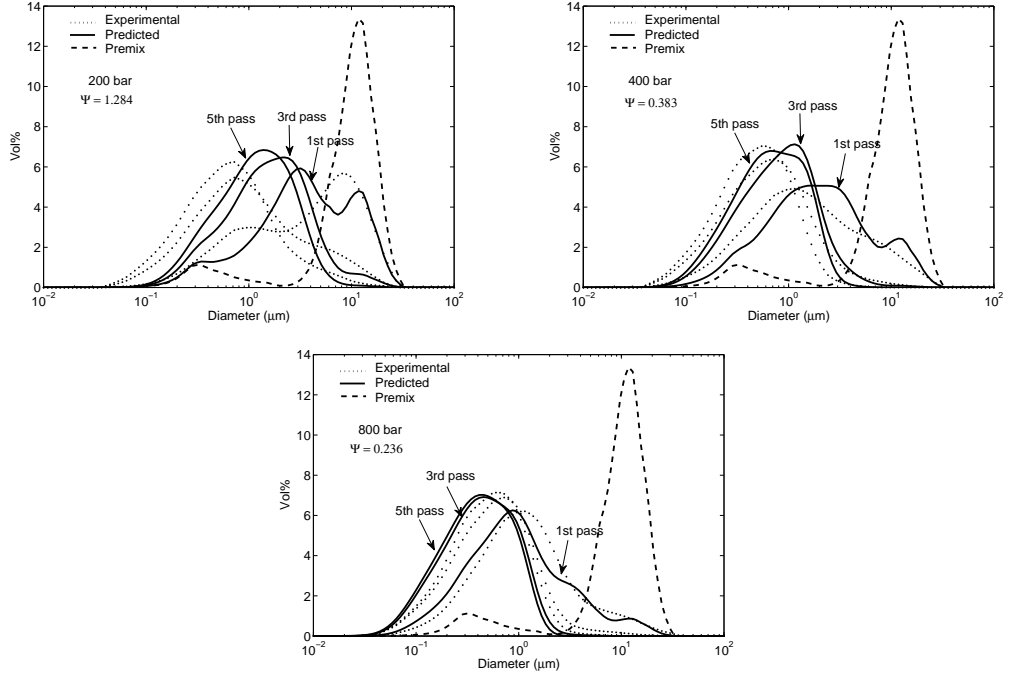


**Figure 6.2.** Experimental and model predicted drop size distributions obtained using optimized parameters at 600 bar: (a) 200 bar, (b) 400 bar, (c) 800 bar.

size distribution will be achieved. Therefore, the second objective involves the full distribution:

$$\Psi_2 = \frac{\sum_{j=1}^n [n_{tar}(v_j) - n_p(v_j)]^2}{\sum_{j=1}^n [n_{tar}(v_j)]^2} \quad (6.10)$$

where  $n_{tar}$  is the target volume density and  $n_p$  is the model predicted volume density. The PBE model was spatially and temporally discretized to generate a nonlinear algebraic equation system that was posed as equality constraints in the optimization problem. The homogenization pressure was constrained to be between 100 and 1000 bar. Given a specified objective and a fixed number of homogenization passes, the problem of determining the optimal pressure at each pass was solved within AMPL using the nonlinear optimization code CONOPT.

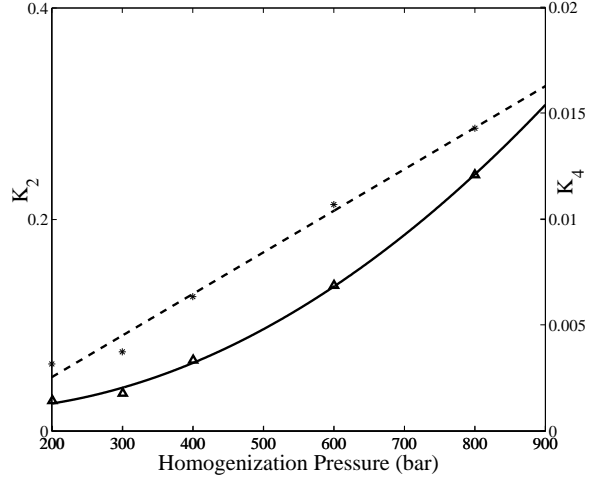


**Figure 6.3.** Interpolated model parameters using  $K_2$  (\*) and  $K_4$  ( $\Delta$ ) values obtained at four different pressures.

### 6.3.2 Results

First I considered the problem of achieving a drop size distribution with  $d_{32_{tar}} = 0.3$  mm and  $PD_{tar} = 2.0$  using 1–4 homogenization passes. Objective function values showed that at least four passes were required to achieve these targets (Table 6.2). Experimental implementation of the optimal solution for four passes showed very good agreement with the predicted results.

**Table 6.2.** Model predicted and experimental results for the target  $d_{32} = 0.3$  and  $PD = 2$

Pressure (bar)				$d_{32}$	$PD$	$\Psi_1$
1 <sup>st</sup> pass	2 <sup>nd</sup> pass	3 <sup>rd</sup> pass	4 <sup>th</sup> pass			
				Model prediction		
1000	—	—	—	0.617	2.944	1.126
1000	645	—	—	0.410	2.197	0.379
1000	740	280	—	0.340	2.091	0.140
1000	846	353	234	0.308	2.033	0.031
				Experimental result		
1000	846	353	234	0.306	1.997	0.019

Specification of a target drop size distribution for minimization of the  $\Psi_2$  objective is more challenging. Our experience is that normal-like distributions are achievable when the drop size is represented in logarithmic coordinates (see Figure 6.1). Therefore, target distributions were generated from the normal distribution by specifying the mean ( $\mu$ ) and variance ( $\sigma^2$ ). First I considered the case where  $\mu = 0.5$  mm and  $\sigma^2 = 0.8$  mm<sup>2</sup>. Based on the objective function values, a minimum of four passes was required to achieve the target distribution that resulted from these specifications (Table 6.3). Experimental implementation of the optimal solution for four passes produced very good agreement with the target distribution (Figure 6.4).

**Table 6.3.** Model predicted and experimental results for the target  $\mu = 0.5$  and  $\sigma^2 = 0.8$

Pressure (bar)					$\Psi_2$	
1 <sup>st</sup> pass	2 <sup>nd</sup> pass	3 <sup>rd</sup> pass	4 <sup>th</sup> pass	5 <sup>th</sup> pass	Model predicted	Experimental
1000	—	—	—	—	0.253	—
1000	414	—	—	—	0.047	—
1000	356	332	—	—	0.012	—
1000	112	269	357	—	0.008	0.009
656	107	113	241	419	0.008	—

Finally I considered the case where  $\mu = 0.8$  mm and  $\sigma^2 = 0.8$  mm<sup>2</sup>. Because the target mean drop size was relatively large, only two passes were required to achieve the resulting target distribution (Table 6.4). Although some model error was evident, experimental implementation of the optimal solution for two passes produced acceptable agreement with the target distribution (Figure 6.5).

## 6.4 Conclusions

A population balance equation (PBE) model that accounts for drop breakage and coalescence in high pressure homogenization was used for emulsion product design. Mechanistic functions allowed PBE model to have predictive capability over range of

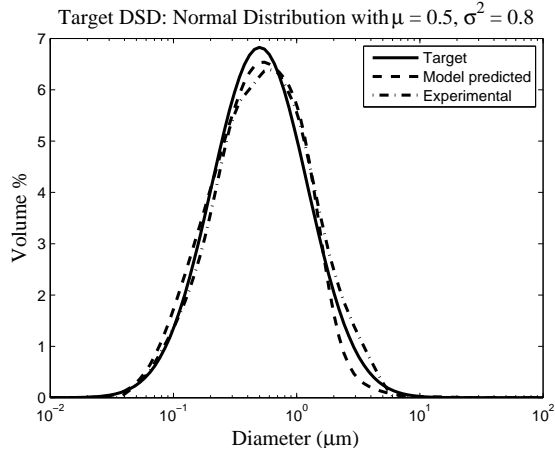


**Figure 6.4.** Model predicted and experimental distributions obtained with four optimized homogenization passes for the target  $\mu = 0.5$  and  $\sigma^2 = 0.8$ .

**Table 6.4.** Model predicted and experimental results for the target  $\mu = 0.8$  and  $\sigma^2 = 0.8$

Pressure (bar)			$\Psi_2$	
1 <sup>st</sup> pass	2 <sup>nd</sup> pass	3 <sup>rd</sup> pass	Model predicted	Experimental
1000	—	—	0.034	—
203	711	—	0.010	0.021
100	100	650	0.013	—

processing conditions. Six adjustable parameters were estimated by nonlinear optimization from measured drop volume distribution at specified base case condition. The values of parameters  $K_2$  and  $K_4$  were interpolated to generate improved results over broad range of homogenization pressure. Two optimization objectives that differ with respect to the distribution specifications were formulated. Using PBE model, number of homogenization passes and optimal pressure corresponding to each pass were obtained for different target drop size distribution. After experimentally implementing the optimal solutions, I found that experimental results showed very good agreement with target distribution properties.

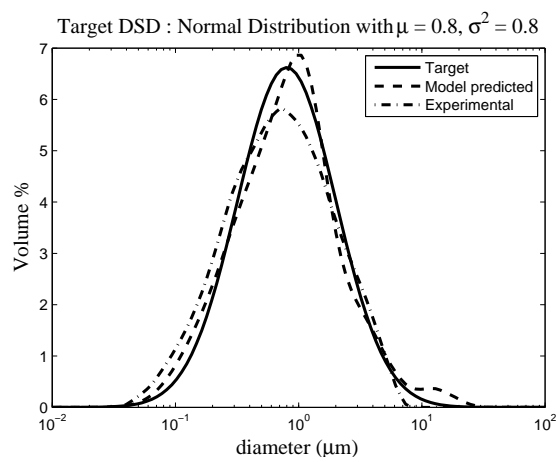


**Figure 6.5.** Model predicted and experimental distributions obtained with two optimized homogenization passes for the target  $\mu = 0.8$  and  $\sigma^2 = 0.8$ .

## CHAPTER 7

### CONCLUSIONS AND FUTURE WORK

#### 7.1 Summary

I have developed population balance equation (PBE) models of emulsification processes to predict the drop size distribution. I have demonstrated that incorporating the drop coalescence functions into breakage-only PBE model significantly improves the model predictions for emulsions with high oil-to-surfactant ratios. I have extended the PBE model by incorporating the equilibrium surface coverage model. The goal of the modeling effort was to extend my previous PBE model of combined drop breakage and coalescence to predict distributions obtained with different surfactant types given adjustable model parameters estimated from drop volume distribution data collected for a single surfactant. The equilibrium surface coverage was calculated using the surfactant specific properties obtained from equilibrium interfacial tension data. The extended model was able to predict the drop size distribution of emulsions with different surfactant type without re-estimation of adjustable model parameters. I have further modified PBE model in order to make model extensible over wide range of surfactant and oil concentrations representing “surfactant limited” and “surfactant rich” regimes. I have modified the model by (1) reformulating the breakage frequency functions, (2) replacing the constant continuous phase viscosity with a calculated emulsion viscosity that increased strongly with oil content, and (3) replacing the equilibrium model of surfactant adsorption with a size independent dynamic model. Using a single set of adjustable parameters, the new PBE model was able to satisfactorily predict drop size distributions for emulsion formulations

with wide range of oil and surfactant concentrations with the exception of the most surfactant limited formulation. Furthermore, I have utilized the PBE model of high pressure homogenization for emulsion product design. Mechanistic functions allowed the PBE model to have predictive capability over range of processing conditions. Target drop size distribution was achieved using the PBE model by controlling number of homogenization passes and homogenization pressure corresponding to each pass. I have experimentally validated the optimal solutions.

I have also developed PBE model to predict drop size distributions in colloid mill emulsification. The model accounts for drop breakage due to capillary instability, and drop coalescence due to shear driven drop collision. At high dispersed phase to emulsion viscosity ratios, colloid mill produces bimodal drop size distributions, while at low viscosity ratios, it produces unimodal distributions. The model failed to predict these drop size distributions using conventional daughter drop distribution functions, which determines the number and size of the drops that result from a breakage event. I have proposed a new bimodal daughter distribution function that captured the formation of many small satellite drops and produced acceptable drop distribution predictions at high viscosity ratios. While at low viscosity ratios, I have proposed a new unimodal daughter distribution function to capture formation of more uniform daughter drops.

## **7.2 Future work**

Even though the PBE model was used for emulsion product design, only the operating conditions were used as controlling parameters. In industrial emulsified product design, apart from operating conditions, amount of surfactant is also the decision variable. It is desirable to use the least amount of surfactant to achieve target properties, due to very high cost of surfactants. Next step of work should be to extend the design methodology to minimize total surfactant amount and find the

number of homogenization passes and optimal pressure at each pass such that the target drop size distribution can be achieved. This requires model to minimize error between model prediction and target distribution as well as minimize the amount of surfactant. In order to get the target distribution, the optimization problem needs to be slightly altered. The error between model prediction and target distribution should be less than some critical value to avoid large variations in distribution. Therefore an additional constraint of this error being less than some critical value will be required.

The geometry of the emulsification device is known to have a large impact on flow conditions and the resulting DSD. Most PBE models are based on the assumption that the fluid in the emulsification zone is well mixed and therefore do not account for device geometry. The development of integrated CFD-PBE models will enable the direct incorporation of detailed geometry information into simulations of high pressure homogenizers and colloids mills. This extension will make PBE models much more device specific and should substantially improve scale-up capabilities. For example, I believe that more detailed device geometry will be critical for improving predictions for applied pressure variations in high pressure homogenizers.

## APPENDIX A

### COLINEARITY OF THE ADJUSTABLE BREAKAGE AND COALESCENCE PARAMETERS

The PBE models can be expected to be extensible to new emulsification conditions if the breakage/coalescence parameters  $K_1$ – $K_6$  can be uniquely determined from data collected at a particular condition. This requires that the parameters are not highly correlated such that their effects on measured outputs are distinct and identifiable. My experience is that parameter effects in complex process models are invariably colinear and the ability to find unique parameter estimates is determined by the degree of colinearity. My computational studies with the PBE models suggested that parameter effects were sufficiently distinct to be identifiable, as initial parameter guesses that produced converged solutions also produced unique parameter estimates. To further investigate this issue, I applied a parameter identifiability test. For analysis of parameter colinearity in the PBE models, the algorithm was adapted as follows.

1. Consider a steady-state operating point corresponding to the nominal parameters  $\bar{\theta}_j$  and the single pass objective function values  $\bar{\psi}_i$ . Introduce a small perturbation  $\Delta\theta_j = \theta_j - \bar{\theta}_j$  in the  $j$ -th parameter and denote the resulting change in the objective function value for the  $i$ -th pass as  $\Delta\psi_i = \psi_i - \bar{\psi}_i$ . Compute the dimensionless sensitivity coefficient matrix  $\tilde{S} = \{\tilde{S}_{ij}\}$ :

$$\tilde{S}_{ij} = \frac{\bar{\theta}_j}{\bar{\psi}_i} \frac{\Delta\psi_i}{\Delta\theta_j} \tag{A.1}$$

2. Compute the linear independence metric  $d_j \in [0, 1]$  for each parameter  $\theta_j$ :

$$d_j = \sin \left[ \cos^{-1} \left( \frac{\tilde{s}_j^T \tilde{s}}{\|\tilde{s}_j\| \|\tilde{s}\|} \right) \right] \quad (\text{A.2})$$

where  $\tilde{s}_j$  is the dimensionless sensitivity vector associated with  $\theta_j$  and  $\tilde{s}$  is the vector in the space spanned by the sensitivity vectors of the other five parameters which is closest to  $\tilde{s}_j$  in the Euclidean sense [43].

If the sensitivity coefficient  $\tilde{S}_{ij}$  is near zero for all passes  $i$ , then the  $j^{\text{th}}$  parameter has very little effect on the total objective function value and cannot be reliably determined by parameter estimation. Table A.2 shows the sensitivity coefficients obtained by introducing  $\pm 5\%$  perturbations in each parameter of the base model. Nominal parameter values corresponded to the base case condition of 50 wt% oil and 1 wt% PF68 (Table A.1). The parameters  $K_1$ – $K_5$  had strong effects on multiple passes, while  $K_6$  only had a moderate effect on the fifth and final pass. Sufficiently large sensitivity coefficients are a necessary but not sufficient condition for parameter identifiability. Another possible obstruction is colinearity of parameter effects, which is measured by the linear independence metric  $d_j$ . Table A.2 shows  $d_j$  values computed from the sensitivity vectors  $\tilde{s}_j$  listed in the same table. The results show that parameters  $K_1$ – $K_3$  were highly independent of the other parameters, the parameters  $K_4$  and  $K_5$  exhibited a small degree of colinearity and the parameter  $K_6$  was moderately colinear. Based on my experience with this parameter identifiability test, I concluded that the six breakage/coalescence parameters could be reliably estimated from drop volume distribution data collected after each homogenizer pass.

**Table A.1.** Optimized parameters obtained using base model.

Parameters	50 wt% oil, 0.5 wt% PF68	50 wt% oil, 1 wt% PF68	50 wt% oil, 2 wt% PF68
$K_1 \times 10^7 (kg/m^3)^{-1/3}$	3.3098	0.8916	1.1836
$K_2 (kg/m^3)^{2/3}$	1.2754	0.3075	0.2965
$K_3 \times 10^6 (kg/m^3)^{-1/2}$	2.5437	1.3042	0.7054
$K_4 \times 10^2$	7.2843	1.1213	0.9664
$K_5 \times 10^{10} (kg^{-1/3} m^{-2})$	0.9945	0.5556	0.4162
$K_6 \times 10^9 (m/kg)$	0	1.0178	1.4291

**Table A.2.** Parameter sensitivity coefficients and measure of parameter colinearity.

Parameter	Objective Function Values					Colinearity Measure
	$\psi_1$	$\psi_2$	$\psi_3$	$\psi_4$	$\psi_5$	$d_j$
$K_1$	0.6371	1.3760	0.8050	2.2828	-2.0918	0.9156
$K_2$	-0.4134	0.2159	0.7065	0.3244	2.2082	0.9991
$K_3$	-1.9889	4.3921	1.2158	0.5302	-0.8524	0.9599
$K_4$	0.2214	-0.9765	0.4069	0.9464	3.0750	0.7535
$K_5$	0.0800	-0.8405	0.2679	0.5422	6.4473	0.8155
$K_6$	0.0154	0.0162	-0.0109	0.0885	-0.1578	0.5352

## APPENDIX B

### DERIVATION OF EQUATIONS OF ADSORBED AND FREE SURFACTANT CONCENTRATION

#### Surfactant Mass Balance Equations

The total amount of surfactant at any instant of time  $t$  is the sum of the free surfactant and adsorbed surfactant,

$$C_{s_t} V_c + \Gamma_t A_t = C_{s_{t+\Delta t}} V_c + \Gamma_{t+\Delta t} A_{t+\Delta t} \quad (\text{B.1})$$

where  $C_s$  is free surfactant concentration in the continuous phase (mol/m<sup>3</sup>);  $\Gamma$  is the surface coverage (mol/m<sup>2</sup>);  $V_c$  is the volume of the continuous phase (m<sup>3</sup>); and  $A$  is the total oil-water interfacial area (m<sup>2</sup>). Dividing both sides of the equation by  $\Delta t$  and taking the limit  $\Delta t \rightarrow 0$ ,

$$\frac{C_{s_{t+\Delta t}} V_c - C_{s_t} V_c}{\Delta t} = - \frac{\Gamma_{t+\Delta t} A_{t+\Delta t} - \Gamma_t A_t}{\Delta t}$$

$$\frac{dC_s}{dt} = - \frac{1}{V_c} \frac{d}{dt} (\Gamma A) = - \frac{1}{V_c} \frac{dM}{dt} \quad (\text{B.2})$$

$$V_c = \frac{1-\phi}{\phi} \int_0^\infty N V_t dv = \frac{1-\phi}{\phi} \int_0^\infty n v dv; \quad A = \int_0^\infty n \pi d^2 dv$$

where  $M$  is total amount of adsorbed surfactant (mol),  $V_t$  is the total conserved volume of dispersed phase (m<sup>3</sup>),  $N dv$  and  $n dv$  are the volume fraction and number of drops, respectively, of size between  $v$  and  $v + dv$  and  $d$  is the diameter of a drop of size  $v$ . For the size independent surfactant adsorption model,

$$\frac{dC_s}{dt} = -\frac{\phi}{1-\phi} \frac{d}{dt} \left( \Gamma \frac{\int_0^\infty n\pi d^2 dv}{\int_0^\infty n\frac{\pi}{6} d^3 dv} \right) = -\frac{6\phi}{1-\phi} \frac{d}{dt} \left( \frac{\Gamma}{d_{32}} \right) \quad (\text{B.3})$$

For the size dependent surfactant adsorption model,

$$M = \int_0^\infty M_v dv$$

$$\frac{dC_s}{dt} = -\frac{\phi}{1-\phi} \frac{1}{\int_0^\infty NV_t dv} \int_0^\infty \frac{dM_v}{dt} dv \quad (\text{B.4})$$

where  $M_v$  is the amount of adsorbed surfactant on drops of size between  $v$ . To calculate the initial free surfactant concentration  $C_{s_{\text{init}}}$ , the following mass balance equation were solved,

$$C_{s_{\text{input}}} V_c = C_{s_{\text{init}}} V_c + \Gamma_{\text{init}} A_{\text{init}}$$

$$C_{s_{\text{input}}} = C_{s_{\text{init}}} + \frac{6\phi}{1+\phi} \frac{\Gamma_{\text{init}}}{d_{32_{\text{pre}}}}; \quad \Gamma_{\text{init}} = \Gamma_\infty \frac{C_{s_{\text{init}}}}{C_{s_{\text{init}}} + C_{1/2}}$$

$$C_{s_{\text{input}}} = C_{s_{\text{init}}} + \frac{6\phi}{1+\phi} \frac{\Gamma_\infty}{d_{32_{\text{pre}}}} \frac{C_{s_{\text{init}}}}{C_{s_{\text{init}}} + C_{1/2}} \quad (\text{B.5})$$

where  $C_{s_{\text{input}}}$  is the total surfactant concentration used to prepare the emulsion,  $\Gamma_{\text{init}}$  is the initial surface coverage,  $A_{\text{init}}$  is the total oil-water interfacial area of initial or premix distribution, and  $d_{32_{\text{pre}}}$  is Sauter mean drop size of premix distribution.

## Amount of Adsorbed Surfactant

For the size independent surfactant adsorption model, the total amount of adsorbed surfactant at any instant of time  $t$  is determined by the adsorption and desorption rates as follows,

$$\begin{aligned}
M_{t+\Delta t} &= M_t + \Delta t A (K_a (\Gamma_\infty - \Gamma) C_s - K_d \Gamma) \\
\frac{dM}{dt} &= A (K_a (\Gamma_\infty - \Gamma) C_s - K_d \Gamma)
\end{aligned} \tag{B.6}$$

This equation was rewritten in terms of the surface coverage as follows,

$$\begin{aligned}
M &= \Gamma A; \quad A = \int_0^\infty n \pi d^2 dv = \int_0^\infty \frac{6V_t N}{d} dv \\
\frac{d(\Gamma A)}{dt} &= A (K_a (\Gamma_\infty - \Gamma) C_s - K_d \Gamma) \\
A \frac{d\Gamma}{dt} &= A (K_a (\Gamma_\infty - \Gamma) C_s - K_d \Gamma) - \Gamma \frac{dA}{dt} \\
\frac{d\Gamma}{dt} &= (K_a (\Gamma_\infty - \Gamma) C_s - K_d \Gamma) - \frac{\Gamma}{\int_0^\infty \frac{N}{d} dv} \int_0^\infty \left( \frac{1}{d} \frac{\partial N}{\partial t} \right) dv
\end{aligned}$$

For the size dependent model, the equations were derived similarly,

$$\begin{aligned}
\frac{\partial M_v}{\partial t} &= A_v (K_a (\Gamma_\infty - \Gamma_v) C_s d - K_d \Gamma_v) \\
\frac{\partial M_v}{\partial t} &= 6V_t \frac{N}{d} (K_a (\Gamma_\infty - \Gamma_v) C_s d - K_d \Gamma_v) \\
\Gamma_v &= \frac{M_v}{A_v} \quad \text{if } N > 0 \\
&= 0 \quad \text{if } N = 0
\end{aligned}$$

where  $\Gamma_v$  and  $A_v$  are the surface coverage, and total surface area, respectively, of drops of size  $v$ .

## BIBLIOGRAPHY

- [1] Almeida-Rivera, Cristhian, and Bongers, Peter. Modelling and experimental validation of emulsification processes in continuous rotor–stator units. *Computers & Chemical Engineering* 34, 5 (2010), 592–597.
- [2] Alopaeus, V., Koskinen, J., and Keskinen, K.I. Simulation of the population balances for liquid-liquid systems in a nonideal stirred tank. Part 1 Description and qualitative validation of the model. *Chemical Engineering Science* 54, 24 (1999), 5887–5899.
- [3] Alopaeus, V., Koskinen, J., and Keskinen, K.I. Utilization of population balances in simulation of liquid-liquid systems in mixed tanks. *Chemical Engineering Communications* 190, 11 (2003), 1468–1484.
- [4] Alopaeus, V., Koskinen, J., Keskinen, K.I., and Majander, J. Simulation of the population balances for liquid-liquid systems in a nonideal stirred tank. Part 2 - Parameter fitting and the use of the multiblock model for dense dispersions. *Chemical Engineering Science* 57, 10 (2002), 1815–1825.
- [5] Barnes, Howard A. Rheology of emulsions A review. *Colloids and Surfaces A: Physicochemical and Engineering Aspects* 91 (1994), 89–95.
- [6] Becher, P. *Encyclopedia of Emulsion Technology, Vol I*. Marcel Dekker, New York, NY, 1983.
- [7] Becher, P. *Emulsions: Theory and Practice*. Oxford University Press, New York, NY, 2001.
- [8] Bleys, G, and Joos, P. Adsorption kinetics of bolaform surfactants at the air/water interface. *The Journal of Physical Chemistry* 89, 6 (1985), 1027–1032.
- [9] Canu, P. Prediction of multimodal distributions in breakage processes. *Industrial & Engineering Chemistry Research* 44, 8 (2005), 2649 – 2658.
- [10] Chang, CH, and Franses, EI. Adsorption dynamics of surfactants at the air/water interface: a critical review of mathematical models, data, and mechanisms. *Colloids And Surfaces A-Physicochemical And Engineering Aspects* 100 (1995), 1–45.
- [11] Chappat, M. Some applications of emulsions. *Colloids And Surfaces A-Physicochemical And Engineering Aspects* 91 (1994), 57 – 77.

- [12] Chatzi, EG, and Kiparissides, C. Drop size distributions in high holdup fraction dispersion systems: effect of the degree of hydrolysis of PVA stabilizer. *Chemical Engineering Science* 49, 24 (1994), 5039–5052.
- [13] Chen, Z, Pruss, J, and Warnecke, HJ. A population balance model for disperse systems: Drop size distribution in emulsion. *Chemical Engineering Science* 53, 5 (1998), 1059–1066.
- [14] Chen, Z., Pruss, J., and Warnecke, H.J. A population balance model for disperse systems: Drop size distribution in emulsion. *Chemical Engineering Science* 53, 5 (1998), 1059–1066.
- [15] Chesters, AK. The modelling of coalescence processes in fluid liquid dispersions - A review of current understanding. *Chemical Engineering Research and Design* 69 (1991), 259–270.
- [16] Coualoglou, C.A., and Tavlarides, L.L. Description of interaction processes in agitated liquid-liquid dispersions. *Chemical Engineering Science* 32, 11 (1977), 1289–1297.
- [17] Cristini, V, Guido, S, Alfani, A, Blawdziewicz, J, and Loewenberg, M. Drop breakup and fragment size distribution in shear flow. *Journal of Rheology* 47, 5 (2003), 1283–1298.
- [18] De Bruijn, RA. *Deformation and breakup of drops in simple shear flow*. PhD thesis, Eindhoven university of Technology, The Netherlands, 1989.
- [19] Derkach, Svetlana R. Rheology of emulsions. *Advances in colloid and interface science* 151, 1 (2009), 1–23.
- [20] Desnoyer, C, Masbernat, O, and Gourdon, C. Experimental study of drop size distributions at high phase ratio in liquid–liquid dispersions. *Chemical Engineering Science* 58, 7 (2003), 1353–1363.
- [21] Dhingra, D. Feasible drop sizes in laminar emulsification systems. Master’s thesis, University of Massachusetts Amherst, 2001.
- [22] Diemer, R.B., and Olson, J.H. A moment methodology for coagulation and breakage problems: Part 3 - generalized daughter distribution functions. *Chemical Engineering Science* 57, 19 (2002), 4187 – 4198.
- [23] Drud, AS. CONOPT – a large-scale GRG code. *ORSA Journal on Computing* 6, 2 (1994), 207–216.
- [24] Drumm, Christian, Attarakih, Menwer M, and Bart, Hans-Jörg. Coupling of CFD with DPBM for an RDC extractor. *Chemical Engineering Science* 64, 4 (2009), 721–732.

- [25] Fourer, R., Gay, D. M., and Kernighan, B. W. *AMPL: A Modeling Language for Mathematical Programming*. Brooks/Cole Publishing Company, Pacific Grove, CA, 2003.
- [26] Ghaouar, N, Henda, M Ben, Aschi, A, and Gharbi, A. Study of PEO-PPO-PEO copolymers conformational changes: Viscosity and dynamic light scattering measurements. *Journal of Macromolecular Science, Part B* 50, 11 (2011), 2150–2164.
- [27] Gupta, S. Structured liquid products: Emulsification process design for viscoelastic liquids. Master’s thesis, University of Massachusetts Amherst, 2004.
- [28] Hakansson, A, Tragardh, C, and Bergenstahl, B. Dynamic simulation of emulsion formation in a high pressure homogenizer. *Chemical Engineering Science* 64, 12 (2009), 2915 – 2925.
- [29] Hakansson, A, Tragardh, C, and Bergenstahl, B. Studying the effects of adsorption, recoalescence and fragmentation in a high pressure homogenizer using a dynamic simulation model. *Food Hydrocolloids* 23, 4 (2009), 1177–1183.
- [30] Håkansson, Andreas, Innings, Fredrik, Trägårdh, Christian, and Bergenståhl, Björn. A high-pressure homogenization emulsification modelimproved emulsifier transport and hydrodynamic coupling. *Chemical Engineering Science* 91 (2013), 44–53.
- [31] Hill, P.J., and Ng, K.M. Statistics of multiple particle breakage. *AIChE Journal* 42, 6 (1996), 1600 – 1611.
- [32] Israelachvili, J. The science and applications of emulsions - An overview. *Colloids And Surfaces A-Physicochemical And Engineering Aspects* 91 (1994), 1 – 8.
- [33] Jansen, KMB, Agterof, WGM, and Mellema, J. Viscosity of surfactant stabilized emulsions. *Journal of Rheology* 45 (2001), 1359–1371.
- [34] Janssen, JJM, Boon, A, and Agterof, WGM. Droplet break-up in simple shear flow in the presence of emulsifiers. *Colloids and Surfaces A: Physicochemical and Engineering Aspects* 91 (1994), 141–148.
- [35] Joos, P, Bleys, G, and Petre, G. Adsorption-kinetics of nonanediol and nonane dicarbonic acid at the air water interface. *Journal de Chimie Physique et de Physico-Chimie Biologique* 79, 4 (1982), 387–393.
- [36] Kelly, W.J., and Muske, K.R. Optimal operation of high-pressure homogenization for intracellular product recovery. *Bioprocess And Biosystems Engineering* 27, 1 (2004), 25–37.
- [37] Khakpay, Amir, Abolghasemi, Hossein, and Salimi-Khorshidi, Ali. The effects of a surfactant on mean drop size in a mixer-settler extractor. *Chemical Engineering and Processing: Process Intensification* 48, 6 (2009), 1105–1111.

- [38] Klink, IM, Phillips, RJ, and Dungan, SR. Effect of emulsion drop-size distribution upon coalescence in simple shear flow: A population balance study. *Journal of Colloid and Interface Science* 353 (2011), 467–475.
- [39] Kostoglou, M, and Karabelas, AJ. A contribution towards predicting the evolution of droplet size distribution in flowing dilute liquid/liquid dispersions. *Chemical Engineering Science* 56, 14 (2001), 4283–4292.
- [40] Kumar, S., and Ramkrishna, D. On the solution of population balance equations by discretization 1. A fixed pivot technique. *Chemical Engineering Science* 51, 8 (1996), 1311–1332.
- [41] Kumar, S., and Ramkrishna, D. On the solution of population balance equations by discretization 2. A moving pivot technique. *Chemical Engineering Science* 51, 8 (1996), 1333–1342.
- [42] Li, Qiu-Shu, Wen, Pu, and Xu, Lan-Xi. Transition to Taylor vortex flow between rotating conical cylinders. *Journal of Hydrodynamics, Ser. B* 22, 2 (2010), 241–245.
- [43] Li, R, Henson, MA, and Kurtz, MJ. Selection of model parameters for off-line parameter estimation. *IEEE transactions on control systems technology* 12, 3 (2004), 402–412.
- [44] Liao, Yixiang, and Lucas, Dirk. A literature review of theoretical models for drop and bubble breakup in turbulent dispersions. *Chemical Engineering Science* 64, 15 (2009), 3389–3406.
- [45] Liao, Yixiang, and Lucas, Dirk. A literature review on mechanisms and models for the coalescence process of fluid particles. *Chemical Engineering Science* 65, 10 (2010), 2851–2864.
- [46] Maguire, L.A., Zhang, H., and Shamlou, P.A. Preparation of small unilamellar vesicles (SUV) and biophysical characterization of their complexes with poly-L-lysine-condensed plasmid DNA. *Biotechnology And Applied Biochemistry* 37 (2003), 73–81.
- [47] Mahoney, A.W., Doyle, F.J., and Ramkrishna, D. Inverse problems in population balances: Growth and nucleation from dynamic data. *AIChE Journal* 48, 5 (2002), 981–990.
- [48] Maindarkar, S, Dubbelboer, A, Meuldijk, J, Hoogland, H, and Henson, M. Prediction of emulsion drop size distributions in colloid mills. *Chemical Engineering Science* 118 (2014), 114 – 125.
- [49] Maindarkar, S, Raikar, N, and Henson, M. Incorporating emulsion drop coalescence into population balance equation models of high pressure homogenization. *Colloids And Surfaces A-Physicochemical And Engineering Aspects* 396 (2012), 63–73.

- [50] Maindarkar, Shashank N, Bongers, Peter, and Henson, Michael A. Predicting the effects of surfactant coverage on drop size distributions of homogenized emulsions. *Chemical Engineering Science* 89 (2012), 102–114.
- [51] McClements, D. J. *Food Emulsions : Principles, Practice, and Techniques*. CRC Press, Boca Raton, FL, 2005.
- [52] Narsimhan, G., Neffelt, G., and Ramkrishna, D. Breakage functions for droplets in agitated liquid-liquid dispersions. *AIChE Journal* 30, 3 (1984), 457–467.
- [53] Narsimhan, G., Ramkrishna, D., and Gupta, J.P. Analysis of drop size distributions in lean liquid-liquid dispersions. *AIChE Journal* 26, 6 (1980), 991–1000.
- [54] Narsimhan, Ganesan. Model for drop coalescence in a locally isotropic turbulent flow field. *Journal of Colloid and Interface Science* 272, 1 (2004), 197–209.
- [55] Nilsson, Lars, and Bergenståhl, Björn. Adsorption of hydrophobically modified starch at oil/water interfaces during emulsification. *Langmuir* 22, 21 (2006), 8770–8776.
- [56] Pal, Rajinder. Novel viscosity equations for emulsions of two immiscible liquids. *Journal of Rheology* 45 (2001), 509.
- [57] Pandolfe, WD. Emulsion and dispersion generation – A look at homogenizers, colloid mills and mixer/emulsifiers. *Chemical Processing* 59 (1996), 59–65.
- [58] Qian, Cheng, and McClements, David Julian. Formation of nanoemulsions stabilized by model food-grade emulsifiers using high-pressure homogenization: Factors affecting particle size. *Food Hydrocolloids* 25, 5 (2011), 1000–1008.
- [59] Raikar, NB, Bhatia, SR, Malone, MF, Almeida-Rivera, C, Bongers, P, McClements, DJ, and Henson, MA. Prediction of emulsion drop size distributions with population balance equation models of multiple drop breakage. *Colloids and Surfaces A: Physicochemical and Engineering Aspects* 361, 1 (2010).
- [60] Raikar, NB, Bhatia, SR, Malone, MF, and Henson, MA. Experimental studies and population balance equation models for breakage prediction of emulsion drop size distributions. *Chemical Engineering Science* 64, 10 (2009), 2433–2447.
- [61] Rallison, J.M. The deformation of small viscous drops and bubbles in shear flows. *Annual Review Of Fluid Mechanics* 16 (1984), 45 – 66.
- [62] Ramkrishna, D. Drop-breakage in agitated liquid-liquid dispersions. *Chemical Engineering Science* 29, 4 (1974), 987–992.
- [63] Ramkrishna, D. *Population Balances: Theory and Applications to Particulate Processes in Engineering*. Academic Press, New York, NY, 2000.
- [64] Ramkrishna, D., Sathyagal, A., and Narsimhan, G. Analysis of dispersed-phase systems - fresh perspective. *AIChE Journal* 41, 1 (1995), 35–44.

- [65] Rimmer, D. P., Gregoli, A. A., Hamshar, J. A., and Yildirim, E. *Pipeline Emulsion Transportation for Heavy Oils*, in *Emulsions: Fundamentals and Applications in the Petroleum Industry*. American Chemical Society, Washington, DC, 1992.
- [66] Ruiz, M.C., Lermenda, P., and Padilla, R. Drop size distribution in a batch mixer under breakage conditions. *Hydrometallurgy* 63, 1 (2002), 65–74.
- [67] Ruiz, M.C., and Padilla, R. Analysis of breakage functions for liquid-liquid dispersions. *Hydrometallurgy* 72, 3-4 (2004), 245 – 258.
- [68] Saniere, A., Henaut, I., and Argillier, J.F. Pipeline transportation of heavy oils, a strategic, economic and technological challenge. *Oil And Gas Science And Technology-Revue De L Institut Francais Du Petrole* 59, 5 (2004), 455 – 466.
- [69] Sathyagal, A.N., and Ramkrishna, D. Droplet breakage in stirred dispersions: Breakage functions from experimental drop-size distributions. *Chemical Engineering Science* 51, 9 (1996), 1377–1391.
- [70] Sathyagal, A.N., Ramkrishna, D., and Narsimhan, G. Solution of inverse problems in population balances 2: Particle break-up. *Computers and Chemical Engineering* 19, 4 (1995), 437–451.
- [71] Schramm, L. L. *Petroleum Emulsions: Basic Principles in Emulsions: Fundamentals and Applications in the Petroleum Industry*. American Chemical Society, Washington, DC, 1992.
- [72] Simon, M., Schmidt, S.A., and Bart, H.J. The droplet population balance model - Estimation of breakage and coalescence. *Chemical Engineering & Technology* 26, 7 (2003), 745–750.
- [73] Sis, H, Kelbaliyev, G, and Chander, S. Kinetics of drop breakage in stirred vessels under turbulent conditions. *Journal of Dispersion Science and Technology* 26, 5 (2005), 565–573.
- [74] Soon, S.Y., Harbidge, J., Titchener-Hooker, N.J., and Shamlou, P.A. Prediction of drop breakage in an ultra high velocity jet homogenizer. *Journal of Chemical Engineering of Japan* 34, 5 (2001), 640–646.
- [75] Sovova, H. Breakage and coalescence of drops in a batch stirred vessel .2. Comparison of model and experiments. *Chemical Engineering Science* 36, 9 (1981), 1567–1573.
- [76] Sovova, H, and Prochazka, J. Breakage and coalescence of drops in a batch stirred vessel .1. Comparison of continuous and discrete models. *Chemical Engineering Science* 36, 1 (1981), 163–171.
- [77] Stone, H.A. Dynamics of drop deformation and breakup in viscous fluids. *Annual Review Of Fluid Mechanics* 26 (1994), 65 – 102.

- [78] Tabor, RF, Eastoe, J, and Dowding, P. Adsorption and desorption of nonionic surfactants on silica from toluene studied by atr-ftir. *Langmuir* 25, 17 (2009), 9785 – 9791.
- [79] Tcholakova, Slavka, Denkov, Nikolai D, and Danner, Thomas. Role of surfactant type and concentration for the mean drop size during emulsification in turbulent flow. *Langmuir* 20, 18 (2004), 7444–7458.
- [80] Tcholakova, Slavka, Denkov, Nikolai D, Sidzhakova, Doroteya, Ivanov, Ivan B, and Campbell, Bruce. Interrelation between drop size and protein adsorption at various emulsification conditions. *Langmuir* 19, 14 (2003), 5640–5649.
- [81] Tcholakova, Slavka, Lesov, Ivan, Golemanov, Konstantin, Denkov, Nikolai D, Judat, Sonja, Engel, Robert, and Danner, Thomas. Efficient emulsification of viscous oils at high drop volume fraction. *Langmuir* 27, 24 (2011), 14783–14796.
- [82] Torn, LH, Koopal, LK, Keizer, A, and Lyklema, J. Adsorption of nonionic surfactants on cellulose surfaces: Adsorbed amounts and kinetics. *Langmuir* 21, 17 (2005), 7768–7775.
- [83] Vankova, N., Tcholakova, S., Denkov, N.D., Ivanov, I.B., Vulchev, V.D., and Danner, T. Emulsification in turbulent flow - 1. Mean and maximum drop diameters in inertial and viscous regimes. *Journal of Colloid and Interface Science* 312, 2 (2007), 363 – 380.
- [84] Vankova, N., Tcholakova, S., Denkov, N.D., Vulchev, V.D., and Danner, T. Emulsification in turbulent flow 2. Breakage rate constants. *Journal of Colloid and Interface Science* 313, 2 (2007), 612 – 629.
- [85] Walstra, P. Principles of emulsion formation. *Chemical Engineering Science* 48, 2 (1993), 333–349.
- [86] Wang, L., Marchisio, D.L., Vigil, R.D., and Fox, R.O. CFD simulation of aggregation and breakage processes in laminar Taylor-Couette flow. *Journal of Colloid and Interface Science* 282, 2 (2005), 380 – 396.
- [87] Wang, T.F., Wang, J.F., and Jin, Y. A CFD-PBM coupled model for gas-liquid flows. *AIChE Journal* 52, 1 (2006), 125–140.
- [88] Wieringa, JA, Vandieren, F, Janssen, JJM, and Agterof, WGM. Droplet breakup mechanisms during emulsification in colloid mills at high dispersed phase volume fraction. *Chemical Engineering Research & Design* 74 (1996), 554 – 562.
- [89] Wu, Q, Kim, S, Ishii, M, and Beus, SG. One-group interfacial area transport in vertical bubbly flow. *International Journal of Heat and Mass Transfer* 41, 8 (1998), 1103–1112.
- [90] Yaghi, B.M., and Al-Bemani, A. Heavy crude oil viscosity reduction for pipeline transportation. *Energy Sources* 24, 2 (2002), 93 – 102.

- [91] Zaccone, A., Gabler, A., Maass, S., Marchisio, D., and Kraume, M. Drop breakage in liquid-liquid stirred dispersions: Modelling of single drop breakage. *Chemical Engineering Science* 62, 22 (2007), 6297 – 6307.
- [92] Zhang, Hu, Zhang, Kai, and Fan, Shengdi. CFD simulation coupled with population balance equations for aerated stirred bioreactors. *Engineering in Life Sciences* 9, 6 (2009), 421–430.
- [93] Zhao, X. Drop breakup in dilute Newtonian emulsions in simple shear flow: New drop breakup mechanisms. *Journal of Rheology* 51, 3 (2007), 367–392.
- [94] Zhao, X., and Goveas, J.L. Size selection in viscoelastic emulsions under shear. 3788 – 3791.